Astronomical calibration of upper Campanian–Maastrichtian carbon isotope events and calcareous plankton biostratigraphy in the Indian Ocean (ODP Hole 762C): implication for the age of the Campanian–Maastrichtian boundary

Nicolas Thibault[a*], Dorothée Husson[b], Rikke Harlou[a], Silvia Gardin[c], Bruno Galbrun[b], Emilia Huret[d], Fabrice Minoletti[b]

[a] Department of Geography and Geology, University of Copenhagen, Øster Voldgade 10, 1350 Copenhagen C., Denmark.

[b] Institut des Sciences de la Terre de Paris, UMR CNRS 7193, Université Pierre et Marie Curie Paris 06, 4, place Jussieu, 75252 Paris cedex 05, France.

[c] « Paléobiodiversité et Paléoenvironnements », UMR CNRS 5143, Université Pierre et Marie Curie Paris 06, 4, place Jussieu, 75252 Paris cedex 05, France.

[d] Andra, 1/7, rue Jean-Monnet, Parc de la Croix Blanche, 92298 Chatenay-Malabry cedex, France.

* corresponding author, present address, nt@geo.ku.dk

Abstract

An integrated framework of magnetostratigraphy, calcareous microfossil bio-events, cyclostratigraphy and $\delta^{13}C$ stratigraphy is established for the upper Campanian–Maastrichtian of ODP Hole 762C (Exmouth Plateau, Northwestern Australian margin). Bulk-carbonate $\delta^{13}C$ events and nannofossil bio-events have been recorded and plotted against magnetostratigraphy, and provided absolute ages using the results of the cyclostratigraphic study and the recent astronomical calibration of the Maastrichtian. Thirteen carbon-isotope events and 40 nannofossil bio-events are recognized and calibrated with cyclostratigraphy, as well as 14 previously published foraminifer events, thus constituting a solid basis for large-scale correlations. Results show that this site is characterized by a nearly continuous sedimentation from the upper Campanian to the K-Pg boundary, except for a 500 kyr gap in magnetochron C31n. Correlation of the age-calibrated $\delta^{13}C$ profile of ODP Hole 762C to the $\delta^{13}C$ profile of the Tercis les Bains section, Global Stratotype Section and Point of the Campanian–Maastrichtian boundary (CMB), allowed a precise recognition and dating of this stage boundary at 72.15±0.05 Ma. This accounts for a total duration of 6.15±0.05 Ma for the Maastrichtian stage. Correlation of the boundary level with northwest Germany shows that the CMB as defined at the GSSP is ~800 kyr younger than the CMB as defined by Belemnite zonation in the Boreal realm. ODP Hole 762C is the first section to bear at the same time an excellent recovery of sediments throughout the upper Campanian–Maastrichtian, a precise and well-defined magnetostratigraphy, a high-resolution record of carbon isotope events and calcareous plankton biostratigraphy, and a cyclostratigraphic study tied to the La2010a astronomical solution. This section is thus proposed as an excellent reference for the upper Campanian–Maastrichtian in the Indian Ocean.

Keywords: Late Cretaceous; calcareous nannofossils; planktic foraminifera; biostratigraphy; $\delta^{13}C$ stratigraphy, cyclostratigraphy

1. Introduction

The Maastrichtian stage has been intensively studied the past 15 years after the identification of several distinct climatic episodes (Barrera and Savin, 1999; Li and Keller, 1999) that impacted several biotic groups in the marine realm : Inoceramid bivalves (MacLeod et al., 1996), rudist bivalves (Johnson et al., 1996), planktic foraminifera (Li and Keller, 1998a, 1998b; Olsson et al., 2001; Abramovich and Keller, 2002, 2003) and calcareous nannofossils (Friedrich et al., 2005, Thibault and Gardin, 2006, 2007, 2010). In the pelagic realm, the correlation of these climatic episodes and associated biotic events mainly relies on the confidence in planktic foraminifera and calcareous nannofossil biozonations, along with magnetostratigraphy. Because polarity reversals are geologically rapid events that are potentially recorded simultaneously in rocks all over the world, the use of magnetostratigraphic divisions is the most reliable correlation tool, contrary to lithostratigraphic and biostratigraphic divisions which are often time-transgressive. In Late Cretaceous carbonates, magnetic properties are poorly recorded and good magnetostratigraphic records along with calcareous microfossil events are only available for a limited number of sections (Bralower et al., 1995 and references therein).

The climatic evolution of the latest Cretaceous is characterised by a long-term global cooling trend that started in the late Campanian and led to increased bioprovinciality of calcareous microfossil assemblages into distinct Tethyan, Intermediate (Transitional is rather adopted here), Boreal and Austral Provinces that persisted to the end of the Maastrichtian (Shafik, 1990; Huber, 1992a; Huber and Watkins, 1992; Burnett, 1998; Lees, 2002). This seriously complicates the application of available biostratigraphical zonation schemes. Two distinct Late Cretaceous Austral and Tethyan biozonal schemes exist for Planktic foraminiferal assemblages (Premoli-Silva and Sliter, 1994; Huber, 1992b) whereas 3 distinct biozonal schemes (TP for Intermediate and Tethyan provinces, BP for the Boreal Province and AP for the Austral Province) were proposed by Burnett (1998) for Late Cretaceous calcareous nannofossils. The BP and TP schemes have different nannofossil subzones but similar zones.

Throughout the Campanian-Maastrichtian interval, Northwestern Australia was part of the Transitional Province (Huber, 1992a, Huber and Watkins, 1992). Microfossil assemblages from this region show affinities to the warm Tethyan Province and to the cool Austral Province (Shafik, 1990; Howe et al., 2003, Campbell et al., 2004). Several authors noted the difficulties in applying standard planktic foraminiferal and nannofossil Tethyan biostratigraphical zonal schemes to the Campanian-Maastrichtian interval of northwestern Australia due to the absence of key markers or to variations in the ranges of these species (Apthorpe, 1979; Wonders, 1992; Bralower and Siesser, 1992; Shafik, 1998; Petrizzo, 2000; Howe et al, 2003). Petroleum companies that operate in northwestern Australia use the regional KCCM (Cretaceous Composite Calcareous Microfossil) zonation which integrates nannofossil, planktonic foraminiferal and benthic foraminiferal bio-events. This zonation was succesfully applied to numerous sites of Western Australian phanerozoic basins (Howe et al., 2003; Campbell et al., 2004). The example of the North Australian margin shows that possible diachronism of key calcareous microfossil bio-events across latitudes needs to be properly tested and eventually quantified in order to improve the correlation between AP, TP and BP schemes.

In addition, high-resolution bulk carbonate $\delta^{13}C$ reference curves have started to be generated for the Maastrichtian stage (Voigt et al., 2010; Thibault et al., 2012, Voigt et al., 2012) but have not been tied to cyclostratigraphy so far. Because $\delta^{13}C$ is not dependent to temperature and more robust than $\delta^{18}O$ to diagenesis, the use of carbon stable-isotope profiles calibrated with detailed biostratigraphies have proved to be a powerful tool for correlating and dating Cretaceous strata on a global scale (Gale et al., 1993; Jenkyns et al., 1994; Voigt, 2000; Jarvis et al., 2002; Föllmi et al., 2006).

This paper presents new results on calcareous nannofossil biostratigraphy, carbon stable isotopes and cyclostratigraphy throughout the upper Campanian–Maastrichtian section of Hole 762C (Northwestern Australian margin) for which magnetostratigraphy was well established (Galbrun, 1992) and recently updated (Husson et al., 2011, 2012). Using the results obtained with the cyclostratigraphic study and the recent astronomical calibration of the Maastrichtian (Husson et al., 2011), we calibrate all carbon isotopic and biotic events in age and propose a new chronostratigraphic reference for the Indian Ocean. The calibrated chronostratigraphic framework is then correlated and compared to reference sites in the Tethyan and Boreal realms and allows a focus on the correlation and age of the Campanian–Maastrichtian boundary at the global scale.

2. Exmouth Plateau : setting and previous work

ODP Hole 762C (19°53.24'S, 112°15.24'E) was drilled at a water depth of 1360 m in the western part of the central Exmouth Plateau, off NW Australia in the eastern Indian Ocean (Fig. 1). Sediments were deposited in an upper bathyal setting (Zepeda, 1998). The estimated palaeolatitude of this site is 43°S using Ocean Drilling Stratigraphic Network (ODSN) plate tectonics reconstruction (Based on Hay et al., 1999). The studied interval almost spans the whole Maastrichtian stage from the K-Pg boundary to magnetochron C33n downhole (Fig. 2). This interval recovers Subunit IVA and the upper part of Subunit IVB which correspond to nannofossil chalks with varying amounts of clays and foraminifers (Haq et al., 1992). Sediments consist of white to very light green-gray nannofossil chalk (light beds) alternating with intervals of light green-gray clayey nannofossil chalk (dark beds). These cyclic color changes of light and dark beds without distinct limits reflect the relative abundance of clay and calcium carbonate (Haq et al., 1992). These cycles were deposited under a Milankovitch control (Golovchenko et al., 1992; Huang et al., 1992). The biostratigraphy of planktonic foraminifera was first established by Wonders (1992) and revised by Zepeda (1998). The biostratigraphy of calcareous nannofossils was established by Bralower & Siesser (1992) and refined in this study with a higher resolution. Howe et al. (2003) and Campbell et al. (2004) provided a detailed regional, composite biostratigraphic zonation of this site using numerous calcareous nannofossil, planktic and benthic foraminiferal bio-events. The magnetostratigraphy was first established by Galbrun (1992) and refined in Husson et al. (2011, 2012). All the magnetochrons of the standard magnetic polarity time scale (Gradstein et al., 2004) have been retrieved with a high precision and very few uncertainties across boundary reversals (Appendix 1). Hole 762C bears one of the best defined magnetostratigraphic signals throughout the upper Campanian–Maastrichtian along with Site 525A in the South Atlantic (Chave, 1984) and the Bottaccione and Contessa sections in central Italy (Gardin et al., 2012). The lower half of the astronomical calibration of the Maastrichtian also relies on this site (Husson et al., 2011) and the detailed cyclostratigraphic analysis of this section is presented here. ODP Hole 762C thus constitutes the only section that bears at the same time (1) an excellent recovery of sediments throughout the upper Campanian–Maastrichtian, (2) a very precise and well-defined magnetostratigraphy with all magnetochrons and subchrons of this period identified, (3) a record of calcareous nannofossil and planktonic foraminifera bio-events and (4) a high potential for a cyclostratigraphic study tied to the recent astronomical calibration of the Maastrichtian.

Figure 1 about here: format one column, 8 cm wide

Figure 2 about here: format landscape on full page

3. Materials and methods

3.1. Micropaleontological analysis

167 samples of ODP Hole 762C were processed as follows : sediments were gently disaggregated in a mortar and 50 mg of dried sediment were weighed and dispersed in 50 ml of distilled water. The suspension was ultrasonicated for 15 sec and homogenized with a magnetic stirrer. Then 1mL of this suspension was extracted with a finnpipette and homogeneously dropped on a microscopic slide. Particles are therefore evenly distributed on the slide.

Semi-quantitative counts were performed on key and other potential additional stratigraphic markers (Appendix 2) at a magnification of x1600 (x100 oil objective with a x1.6 additional lense). Counts were determined in the following fashion: a species was determined as abundant (A) if, on average, more than 10 specimens could be observed in a field of view; common (C) if one to 10 specimens could be observed in each field; few (F) if one specimen or more could be observed in every 10 fields of view, rare (R) if, on average, only one specimen could be observed in 11 to 100 fields, single (S) if only one specimen was observed during the investigation. Preservation of nannofossils ranges from moderate (M) to poor (P) in the investigated section.

The biozonation of Burnett (1998) was applied. Calcareous nannofossil species considered in this paper followed taxonomic concepts of Perch-Nielsen (1985) and Young & Bown (1997). Bibliographic references for the determined taxa are given in Perch-Nielsen (1985), Bown (1998) and Howe et al. (2003).

3.2. Cyclostratigraphic analysis

As many of Deep Sea Drilling Project (DSDP) and ancient Ocean Drilling Program (ODP) sections, Hole 762C lacks high-resolution geophysical measurements that could be used for a cyclostratigraphic analysis. However, it has been shown that high-resolution core photographs can be used for such a purpose (Cramer, 2001). A Gray-scale log was generated on core photographs from the upper Campanian–Maastrichtian interval of this hole, available on the ODP website (http://www-odp.tamu.edu/publications/122_IR/122TOC.HTM). Each photograph displays one ODP core, with sections of the core arranged parallel to one another (Fig. 3). For each section, gray-scales logs were processed using the free open-source software Image-J (http://rsb.info.nih.gov/ij/) with a scaling of 2100 pixels for each 1.5 m long section (Fig. 3). Gray-scale logs reflect the values of pixels along a line traced in the centre of each section with a corresponding sampling interval of about 0.7 mm. Gray-scale values were then smoothed and resampled at 1 cm intervals (Appendix 4).

Contrary to Cramer (2001) who adjusted core depths by removing all voids and contracting cores for which the measured length was longer than the drilled length, we chose to consider intervals of no recovery which can either represent a void or loss of recovered material, and to keep additional lengths, in order not to potentially contract sedimentary cycles. Adjusted depths were generated and are given in 'ambsf' units.

Fractures present on the core photographs, characterized by very low gray-level values, close to 0, were removed from the original signal using a MATLAB script as explained in Husson et al. (2011).

The effects of lighting on the photographs were treated by the recognition and filtering of cycles with a period of 1.5 m (length of a section), 6.5 and 8.5 to 9.5 m (lengths of distinct cores).

The resulting data were then analyzed via spectral analysis using the multitaper method (MTM, Thomson, 1982). More detailed methodology for the cyclostratigraphic analysis is given in Husson et al. (2011).

Figure 3 about here: format one column, 8 cm wide

3.3. Stable isotope analysis

A total of 200 stable isotope analyses has been performed throughout the late Campanian–Maastrichtian of ODP Hole 762C. Oxygen and carbon isotopic composition of bulk carbonates were measured with a mass spectrometer Finnigan Delta E on 87 samples at the Laboratoire Biominéralisations et Paléoenvironnements (Université Pierre et Marie Curie, Paris 6, France) in 2007. The extraction of CO_2 was done by reaction with anhydrous orthophosphoric acid at 50°C. Additional analyses were performed with a micromass isoprime spectrometer on 113 bulk carbonates at the Department of Geography and Geology, University of Copenhagen in 2009. The extraction of CO_2 was done by reaction with anhydrous orthophosphoric acid at 70°C. The oxygen and carbon isotope values are expressed in per mil relative to the V-PDB standard reference. The analytical precision is estimated at 0.1‰ for oxygen and 0.05‰ for carbon for both laboratories. Common samples and samples from the same stratigraphic intervals show a constant offset of -0.25‰ for $\delta^{18}O$ values and -0.2‰ for $\delta^{13}C$ values between measurements from 2009 and those from 2007, likely due to the different methods and apparatus. Values of 2007 were thus adequately corrected for standardization. Inter-laboratory offsets of 0.1 to 0.2 per mil can commonly occur when laboratories use single-point anchoring with one certified internal standard. Inter-laboratory normalization producing minimal errors <0.1 per mil is possible only when laboratories use anchoring with two or more certified internal standards (Debajyoti et al., 2007).

4. Results

4.1. Calcareous microfossil biochronology

Foraminifera bio-events recorded in Howe et al. (2003) and Campbell et al. (2004) are reported here along with magnetostratigraphy, carbon-isotope stratigraphy and nannofossil biostratigraphy refined in this study (Fig. 2). The resolution of the nannofossil analysis is ca. 1 m across the studied interval and below 0.5 m in the interval between 620 and 595 mbsf where a large number of bio-events were recorded (Fig. 2). In addition to the record of typical first (FO) and last occurences (LO) of taxa, few particular features are proposed here as bio-events. A transition in the abundance of *Watznaueria manivitae* sensu lato was observed with abundances shifting from common to frequent at 649.63 mbsf (Chron C33n, upper Campanian) (Fig. 2). As in Lees and Bown (2005), two different forms of *Uniplanarius trifidus* with distinct stratigraphic levels of extinction were observed, a medium-rayed and a short-rayed form (Fig. 2). Three species also exhibit intervals of acmes: *Cribrocorona gallica* (561.4 to 559.08 mbsf), *Micula murus* (564.14 to 556.33 mbsf) and *Lithraphidites* spp. (573.6 to 561.4 mbsf) (Fig. 2). This provides a total record of 18 foraminifer bio-events, 40 nannofossil bio-events and 4 additional nannofossil events based on obvious changes of abundances correlated to carbon-isotope stratigraphy (Fig. 2 and Table 1).

Table 1 about here: format portrait

4.2. Cyclostratigraphy

4.2.1. Spectral analysis and amplitude spectrogram

The respective thickness of magnetochrons C31r and C30n relative to their duration, according to the Geologic Time Scale 2004 (GTS2004, Gradstein et al., 2004), suggest variations of the sedimentation rate. To ascertain these variations, spectral analyses have been performed on two different intervals: the upper Campanian–lower Maastrichtian interval, from 593 to 638 ambsf, and the upper Maastrichtian from 550 to 593 ambsf. The study of the lower Maastrichtian periodogram highlights cycles with wavelength ranging from 0.26 to 4.1 m, with low frequency cycles presenting the highest power and the best individualisation (Fig. 4). Comparison of their period ratios with the ratio of orbital parameters periods has permitted their attribution to a forcing by the 405 kyr eccentricity (2.15 to 4.1 m cycles), 100 kyr eccentricity (0.58 m to 0.75 m cycles), and obliquity (0.26 m) variations (Fig. 4). The identification of groups of cycles rather than distinct periods is linked to sedimentation rate variation within the studied interval, which modifies the thickness of the cycles (Herbert, 1994).

The spectral analysis performed between 550 and 593 ambsf (upper Maastrichtian) detects cycles with a wavelength ranging from 0.40 to 7.46 m (Fig. 4). The periodogram shows numerous low frequency cycles and less expressed high frequencies variations. The frequency ratios method applied to the periodogram indicates a forcing of the sedimentation by obliquity, 100 kyr eccentricity, and 405 kyr eccentricity (Fig. 4). Colour variations in the upper Maastrichtian have less amplitude, and the power of 405 kyr cycles is attenuated in the frequency spectrum of the 550-593 ambsf interval as compared to the interval below (Fig. 4). This strong attenuation and a disturbance due to the presence of numerous cracks in the "strange" interval between 576 and 588 ambsf hindered the recognition of clear 405 kyr cycles in the amplitude spectrograms of the upper Maastrichtian (Fig. 4). In addition, apart from one interval in core 48X between 604 and 610 ambsf (Figs. 3–4), precession cycles are not very well defined on the periodograms and in amplitude spectrograms. The studied intervals may be too large to highlight high frequency cycles with accuracy. A strong shift of the cycles toward lower frequencies can be observed between the two periodograms. It characterises an increase of the sedimentation rate in the upper Maastrichtian.

Figure 4 about here: format portrait full page

Amplitude spectrograms characterize shifts in the frequency of Milankovith cycles and variations of the sedimentation rate. Well-defined trends present on the entire record are related to the evolution of 100 kyr and 405 kyr eccentricity cycles by comparison to the results of the spectral analysis (Fig. 4). Obliquity is well characterised in the upper Campanian and is also recorded during the lower Maastrichtian, though its amplitude is lower (Fig. 4). Eccentricity is disturbed between 612.5 and 607.5, due once again to important core cracks in this interval (Fig. 4). This interval also corresponds to decreasing sedimentation rates. Sedimentation rates are much higher in the upper Maastrichtian as suggested by the shift of 100 kyr eccentricity cycles toward lower frequencies after the "strange" disturbed interval (Fig. 4). Perturbations of the analysis in the higher frequencies, due to the remaining cracks in the cores, prevent a good identification of precession and obliquity variations. For the upper Maastrichtian, only a filtering of 100 kyr eccentricity cycles could be performed because doubts remained on the identification of 405 kyr cycles attenuated in the frequency cpectrum and hindered in the amplitude spectrograms. For the upper Campanian and lower Maastrichtian, a filter output of the 405 kyr eccentricity was performed from the lowermost part of Chron C31n down to the upper part of Chron C33n. This filter output was already presented in Husson et al. (2011) and calibrated to the La2010a astronomical solution (Laskar et al., 2011).

The identification of 100 kyr and 405 kyr eccentricity cycles allows estimation of durations by cycle counting. The counting is performed considering that minima in grey values (darker colours) might correspond to maxima of insolation. Indeed, darker sediments have higher terrigenous content which seem to reliably reflect enhanced weathering during periods of higher insolation throughout the Cenozoic and Cretaceous period (Pälike et al., 2006, Westerhold et al., 2008, Batenburg et al., 2012).

When precession cycles are well defined, the resolution in the cycle counting can be down to 20 kyr (Fig. 3). Cycle counting was performed on a 5 points moving average smoothed grey scale signal and relies on the 100 kyr filter output (Fig. 5). 100 kyr and 405 kyr eccentricity cycles have been numbered downhole with the Cretaceous/Paleogene (K-Pg) boundary as starting point. Filtering can induce phase-shifts and create a misleading impression of regular cyclicity where grey level variations are important (Weedon, 2003). This effect has been limited by using a very large bandwidth.

Figure 5 about here: Format portrait full page

4.2.2. Downhole 100 kyr numbering and age-calibration of calcareous plankton bio-events

The position of the boundary between chrons C30n and C29r has been revised here and is given a much larger uncertainty than in Galbrun (1992). Indeed, most of the samples of core 43X2 to core 43X5 analysed by Galbrun (1992) could not be demagnetized at high steps, given their weakness in NRM intensity. As a consequence, these samples showed a weak negative inclination which was previously interpreted as a normal polarity (Galbrun, 1992). However the sub-jacent well-magnetized sample 44X1-132 (565.32 mbsf), shows a strong positive inclination, interpreted as a short interval of reversed polarity (Galbrun, 1992) and is then followed by numerous well-magnetized samples of normal polarity. Thus, the base of C29r which was previously placed at 556.5 mbsf could also be placed downhole at 565.32 mbsf. Moreover, according to Henriksson (1993) whose study focused on the biochronology of *Micula prinsii* biozone on a large number of sites, the FO of this taxon is synchronous throughout the tethyan and transitional realms and lies very close to the base of magnetochron C29r. In our study, the FO of this taxon is recorded at 560.46 mbsf (Fig. 2 and Table 1). A downhole position of the base of C29r may thus be expected. The interval of no recovery at the base of core 43X further complicates the precise identification of the boundary between C29r and C30n. As a consequence, the whole uncertainty (between 556.5 and 565.32 mbsf) is taken into account and the C29r/C30n boundary is rather placed at 560.91 +/- 4.41 mbsf (Table 2a, Fig. 2). This new position results in a duration of 397 +/- 221 kyr for the Cretaceous part of C29r which is consistent with the estimation provided in Husson et al. (2011). However, the latter provided a much more precise and reliable estimation of the duration of the Cretaceous part of chron C29r which is rather adopted here.

The duration and ages of biostratigraphic events and carbon-isotope trends rely precisely on the downhole numbering of 100 kyr cycles (Fig. 5). This numbering is based on the cycles identified according to the results of spectral analyses and can be followed on Figure 5 along the 100 kyr filter output. The numbering also remains in accordance with the astronomical calibration of the Maastrichtian tied to the La2010a astronomical solution (Husson et al., 2011). The following reasoning has been followed for the different gaps of the record: (1) Consistency in the thickness of the cycles has been assumed for all the intervals of no recovery, except for the interval centered around 592 ambsf (Fig. 5). (2) Cyclostratigraphic interpretations at Sites 1267B and 525A showed that chron C30r partly covers 100 kyr eccentricity cycles e_{100}23 and e_{100}24 (Husson et al., 2011, Figure 3). Two samples clearly indicated a reverse polarity around 595 ambsf (Appendix 1) and a total uncertainty of 4.3 m is accounted for the boundary between chrons C30n and C30r (Fig. 2 and Table 2a). Therefore, we have assigned the interval of no recovery between 591 and 594 ambsf as well as a short part of the filter output between 594 and 594.6 ambsf to e_{100}23 and the following cycle to e_{100}24, ending around 596.5 ambsf (Fig. 5). (3) A maximum of four 100 kyr eccentricity cycles can be identified in the interval between 596.5 and 599.5 ambsf corresponding to Chron C31n (Fig. 5). This contrasts with Herbert et al. (1999) and Husson et al. (2011) who showed an average duration of this chron of 900 kyr. Therefore, a gap of ca. 500 kyr can be accounted here and likely placed around 597 ambsf, where a neat change in the sedimentation rate can be observed while comparing the thickness of e_{100}23 and e_{100}24 with the underlying cycles (Fig. 5). This gap corresponds to the darkest interval of core 47X which could suggest a much lower carbonate input to the sea-floor responsible for very low sedimentation rates. Downhole numbering of the following cycles takes into account this 500 kyr gap and further remains consistent with the numbering of 100 kyr eccentricity cycles at Sites 525A and 1258A with an average assignment to the base of e_{100}33 for the base of Chron C31n (Fig. 5, Husson et al., 2011, Figure 3) and with the calibration of these three sites to the La2010a astronomical solution (Husson et al., 2011, Figure 5). Uncertainties are low for the boundaries of the following magnetochrons of the lower Maastrichtian and upper Campanian (Tables 2a and 2b).

Foraminifera and calcareous nannofossil bio-events recorded in Hole 762C are calibrated in ages using the results of the cyclostratigraphic study (Table 1). Age uncertainties on the ages of bio-events are calculated by taking into account the uncertainty between top and bottom depths as well as the uncertainty on the ages of the K/Pg boundary (0.07 Ma, Husson et al., 2011). An age of 66 Ma for the K-Pg was chosen based on the recent results on radiometric dating and astronomical calibrations of the Paleocene (Kuiper et al., 2008; Westerhold et al., 2008; Hilgen et al., 2010; Renne et al., 2010). This provides a robust stratigraphic framework that can be used as a reference for the Indian Ocean and also provides a base for large-scale correlations and testing in the future of potential synchronism/diachronism of planktonic microfossil bio-events between the different provinces of the southern hemisphere.

Table 2a and 2b about here

4.3. Carbon stable isotopes

A cross-plot of carbon- and oxygen-isotope values (Fig. 6) shows no significant trends and lacks the pronounced covariance seen in many mixing lines produced by the addition of variable quantities of isotopically homogeneous diagenetic cement to isotopically homogeneous skeletal calcite (Jenkyns et al., 1995; Mitchell et al., 1997). The pattern of $\delta^{13}C$ values generally conforms to trends observed in bulk stable isotopes of a number of reference sites (Figs. 7–10). Given that chalk sediments of Hole 762C are mainly composed of calcareous nannofossils, the characteristic form of this curve likely reflects primary sea-surface water values with minimal diagenetic effects affecting the section in generally consistent manner.

Due to the higher ratio of oxygen in interstitial fluids with respect to oxygen in carbonate as compared to similar ratio of carbon, and due to their thermo-dependence, oxygen isotopes are far more sensitive to post-depositional processes which increase with the porosity of the sediment (Schrag et al., 1995). In chalks of ODP Hole 762C, oxygen isotope values are highly variable which may reflect the Milankovitch control on the sedimentation enhanced by diagenesis. No clear long-term trends or trends conformed to previously published planktic foraminifera $\delta^{18}O$ profiles worldwide (Barrera and Savin, 1999) were observed in our analysis. Diagenetic overprint may have altered primary $\delta^{18}O$ values which are thus not presented here.

Carbon isotope values range between 2.35 and 3.1‰ and do not display any significant difference with respect to colour alternations (Fig. 2). The carbon isotope profile exhibits several positive and negative excursions and inflection points which are calibrated in age using the cyclostratigraphic results from the K-Pg boundary to 645 ambsf (642.65 mbsf) downhole. The rest of the profile was calibrated in age considering an average sedimentation rate of 14.5 m/Ma similar to the interval above between 634 and 644 ambsf (Figs. 7–11).

Despite some local expressions probably due to changing sedimentation rates and occurrence of stratigraphical gaps, the patterns of $\delta^{13}C$ values found at Site 762C well conforms to trends observed in bulk stable isotopes of a number of sites of the same age. The pattern of $\delta^{13}C$ values conforms to trends observed in bulk stable isotopes of Tercis les Bains (Fig. 7), of the Gubbio composite curve (Fig. 7), of the Lägerdorf – Kronsmoor – Hemmoor (LKH) section in Northwest Germany (Fig. 8), in stable isotopes of planktic and benthic foraminifera in South Atlantic DSDP Hole 525A (Fig. 9) and in the Indian Ocean ODP Hole 761 (Barrera and Savin, 1999). The most prominent $\delta^{13}C$ events identified in common in the nearby Indian Ocean Site 761 and in other reference sites fall within the same magnetochrons and, approximately, within the same subparts of magnetochrons, thus making a high degree of reliability (Figs. 7–9).

Figure 6 about here: format one column,~ 8 cm wide

These correlations helped to define 13 isotopic events in ODP Hole 762C whose description is given below (Figs. 7–10 and Table 3).

A short negative excursion (C1-) is identified in the uppermost Campanian right at the base of chron C32n2n above the LO of *Eiffelithus eximius* (Fig. 2). This excursion is characterized by a sharp 0.25‰ negative shift, a small rebound and another 0.1‰ negative shift (Figs. 7–8). This event is poorly defined in Hole 762C, where values do not come back to pre-excursion levels at the top of the event as observed in Tercis les Bains, LKH or Gubbio (Figs. 7–8). C1- event, also identified at the base of C32n2n at Gubbio (Fig. 7) has an estimated duration of ~300 kyr in Hole 762C (Table 4), which matches the 405 kyr filtering in LKH (Fig. 8).

The three-step negative shift of the Campanian – Maastrichtian boundary defined as CMB a, CMB b and CMB c (Thibault et al., 2012) is identified within chron C32n2n in Hole 762C, in accordance with the results of Tercis les Bains and Gubbio (Fig. 7). The LOs of *Uniplanarius trifidus* and *U. gothicus* are recorded within CMB c in Hole 762C and above this event at Tercis les Bains (Fig. 7). In addition, the LO of *T. stemmerikii* is recorded within CMB c both in Hole 762C and in Stevns-1 (Fig. 8).

Nearly all Maastrichtian δ^{13}C events defined in Stevns-1 (Thibault et al., 2012) can be identified in Hole 762C and in the LKH section, resulting in a precise correlation between the three sections (Fig. 8). One exception concerns the identification of M3-(b), a small and short-lived negative excursion in Stevns-1 and LKH and well-defined event named MME for Mid-Maastrichtian event in the Gubbio curve (Fig. 7, Voigt et al., 2012). This event falls into the identified gap in Hole 762C (Figs. 7–8).

A 0.4‰ positive excursion between M3-(b) and M4-(a) occurs in the lower half of chron C30n in Hole 762C (Fig. 7). This excursion is also observed in the same chron at ODP Hole 761, another site of the Exmouth Plateau in the Indian Ocean (Barrera and Savin, 1999,

Fig. 6B) as well as at Site 1210B in the Pacific Ocean (Voigt et al., 2012). This positive excursion, not observed in Stevns-1, is more evident in LKH and better expressed at Gubbio composite curve (Figs. 8–9). However, the fairly large extent of this event, that we named as Exmouth Plateau event (Figs. 7–10), rather points to a regional peculiarity (+0.4‰ in Hole 762C versus 0.1‰ at Gubbio) (Fig. 7) .

Figure 7 about here: format portrait full page width

Figure 8 about here: format landscape on full page

Figure 9 about here: format landscape on full page

Table 3 about here: format portrait full page width

Table 4 about here

5. Discussion

5.1. Early Maastrichtian disconformity or diachronism of microfossil bio-events ?

Howe et al. (2003) identified an early Maastrichtian disconformity in sites from the Exmouth Plateau (Hole 762C and 761B) within biozones KPF3/KPF2c (nannofossil zone UC18, Fig. 2) based on the stratigraphic order of nannofossil and foraminifera bio-events which differs from Tethyan stratigraphic frameworks. This assumption is mainly based on the last co-occurrence of *Broinsonia parca constricta* and *Reinhardtites levis* and the very close first occurrence of *Abathomphalus mayaroensis* (Fig. 2). Apthorpe (1979) previously suggested that this early Maastrichtian disconformity is widespread on the western Australian margin as she was unable to identify foraminifer biozone C12 in 45 of 52 wells from this area. This disconformity would thus lie within chron C31r in Hole 762C (Fig. 2). No hiatus can be characterized in the amplitude spectrograms of Hole 762C within chron C31r (Fig. 4). Moreover, the obtained duration estimated in this section for chron C31r matches almost perfectly those obtained at the Contessa highway section, central Italy (Husson et al., 2012), as well as at Hole 1258A, Demerara Rise, central Atlantic (Husson et al., 2011). This result differs from the duration provided in the GTS2004 by only 160 kyr (Table 2b). These results do not suggest such a disconformity in Hole 762C. During the late Campanian and Maastrichtian, the Perth and Carnarvon basins in the south of the western Australian margin were shown to have Austral affinities whereas the northwestern margin where the Exmouth Plateau is situated had Transitional affinities between Austral and Tethyan assemblages (Rexilius, 1984; Shafik, 1990 ; Huber, 1992a; Huber and Watkins, 1992) (Fig. 1). Diachronism of Late Cretaceous planktic foraminifer and nannofossil datums with respect to paleolatitude in the Southern Ocean was discussed by Huber and Watkins (1992) and Petrizzo (2003). Gardin et al. (2012) also discussed calcareous plankton diachronism and the difficult applicability of the available “standard” calcareous nannofossil biozonations for the the late Campanian–Maastrichtian. In the latest Cretaceous, during times of climatic cooling, standard Tethyan zonations are difficult to apply because some index species are absent or have different age ranges (Bralower and Siesser, 1992; Wonders, 1992; Petrizzo, 2000, 2003; Howe et al., 2003; Campbell et al., 2004). Barrera and Savin (1999) and Li and Keller (1999) showed that a global climatic cooling occurred right before the C32n/C31r transition and was followed by warming in the topmost part of chron C31r. These climatic changes were mainly deciphered through the oxygen isotope ratios of benthic foraminifera but also affected surface waters as expressed by changes in calcareous nannofossil assemblages (Thibault and Gardin, 2006, 2007, Thibault et al., 2011). Therefore, the different order of nannofossil and foraminifera bio-events observed in Hole 762C within chron C31r are rather the expression of diachronism between Transitional and Tethyan provinces due to these climatic changes than the evidence of a disconformity.

5.2. Age of the Campanian–Maastrichtian boundary

Before the ratification of the GSSP boundary at Tercis les Bains, the base of the Maastrichtian stage was assigned to the first occurrence of belemnite *Belemnella lanceolata* with reference to the chalk section of Kronsmoor, North Germany (Birkelund et al., 1984; Schönfeld et al., 1996). However, this marker has a biogeographic distribution which is limited to the Boreal realm (Odin, 1996). The Maastrichtian Working Group chose to identify the base of the Maastrichtian by the first occurrence of ammonoid *Pachydiscus neubergicus* (Odin, 1996), which has a much wider geographical distribution (Hancock, 1991), on the basis of indirect correlations and comparison of strontium isotope stratigraphy with the U.S. Western Interior (McArthur et al., 1992; Landman and Waage, 1993; Schönfeld et al., 1996). Subsequently, the Campanian–Maastrichtian GSSP boundary was defined and ratified at Tercis les Bains close to the first occurrence of ammonoid *P. neubergicus* (the preferred guide event, Odin and Lamaurelle, 2001) and as the arithmetical mean of 12 distinct biohorizons in order to get the best precise definition. This combination of criteria ensures more secure correlation of the boundary level at the global scale (Odin and Lamaurelle, 2001) than just the ammonite bio-horizon only. Based on a large array of paleontological, paleomagnetic and radiometric considerations, the GSSP boundary was considered nearly contemporaneous to the FO of *B. lanceolata* in the Boreal realm (lan in LKH section, Fig. 8), lies close to the middle or in the upper part of chron C32n2n, and was assigned an age of 72.0 +/- 0.5 Ma (Barchi et al., 1997; Lewy and Odin, 2001; Odin and Lamaurelle, 2001). In the GTS2004, two distinct ages are proposed. (1) A first approximate age of 70.6 Ma is based on the supposed last occurrence of nannofossil *Uniplanarius trifidus* at the top of belemnite *Belemnella obtusa* zone in northwest Germany, calibrated with the strontium isotope curve of McArthur et al. (1994) at ca. 69.9 Ma. This estimate is ~0.75 Myr younger than the boundary level at Tercis les Bains, by assuming a constant sedimentation rate on this section. However, *U. trifidus* is actually inconsistent in Germany because this species is mainly restricted to low latitudes (Schönfeld et al., 1996; Burnett, 1998) and the strontium isotope age calibration method has an uncertainty comprised between 0.8 and 1.5 Ma (McArthur et al., 1994). (2) A second estimate at 71.3 Ma is given, based on a strontium isotope age projection of the FO of *B. lanceolata* (Schönfeld et al., 1996) on the curve of McArthur et al. (1994).

None of these two estimates actually match the biohorizon criteria provided for the GSSP boundary and they do not take into account the large uncertainty of the strontium isotope age calibration. In Husson et al. (2011), the LO of *U. trifidus* was considered to be ca. 0.75 Myr younger than the CMB at Tercis les Bains, assuming an obliquity-driven metric rhythm of the sedimentation (40 kyr/m, Odin and Amorosi, 2001). The LO of *U. trifidus* is identified with great precision in ODP Hole 762C (614.06 +/-0.06 mbsf), allowing a cyclostratigraphic assignment to the top of $Ca_{405}1$ (616.09 ambsf, Fig. 5, $Ma_{405}16$ in Husson et al., 2011). Consequently, the CMB was previously placed in the lowermost part of $Ca_{405}2$ (corresponding to $Ma_{405}17$ in Husson et al., 2011), within the middle of 100 kyr eccentricity cycle $e_{100}68$. However, uncertainties remain for the position of the CMB because the LO of *U. trifidus* at ODP Hole 762C falls within the interval of reduced sedimentation rates (Fig. 10) and because a reasonable diachronism of this bio-event between the Tethyan and Transitional Provinces can not be completely ruled out.

The correlation of $\delta^{13}C$ events CMBa, CMBb and CMBc between Stevns-1, Tercis les Bains, LKH, Gubbio and Hole 762C (Figs. 7–9) calls for a revision of the placement and subsequent age of the CMB. The boundary as defined in Tercis les Bains lies within CMBc

(Fig. 7), thus leading to a much more precise correlation of the boundary and a location at 615.4 mbsf (617.37 ambsf) in Hole 762C, i.e. within $Ca_{405}1$ and $e_{100}62$, in the uppermost part of chron C32n2n (Fig. 5). A precise age of 72.15±0.05 Ma can thus be proposed for the CMB, considering an average age of 66 Ma for the K-Pg boundary (Kuiper et al., 2008; Westerhold et al., 2008; Hilgen et al., 2010; Renne et al. 2010). An independent approach to estimate the age of the CMB has been recently documented in Voigt et al. (2012) based on macrofossil biostratigraphic correlations of Inoceramids between Tercis les Bains and the Western Interior Basin. Revised $^{40}Ar/^{39}Ar$ ages of two bentonites, bracketing ammonite zones tied to Inoceramid zonation across the Campanian–Maastrichtian boundary interval of the Western Interior Basin, gives an age of 72.2±0.2 Ma for the CMB.

In addition, the correlation of Hole 762C, Stevns-1 and LKH sections shows that the CMB falls exactly at the base of the *Belemnella obtusa* zone in northwest Germany (Fig. 8). The base of the *B. lanceolata* zone in the Boreal realm corresponds to the base of $\delta^{13}C$ event CMBa and is approximately two 405 kyr cycles older than the identified level for the CMB (Fig. 8). Consequently, the CMB as defined by the Belemnite zonation in the Boreal realm is ~800 kyr older than the CMB as defined in the GSSP of Tercis les Bains. This duration is slightly greater than the 500 kyr discrepancy already estimated by Niebuhr and Esser (2003). Gradstein et al. (2004) already proposed a projection of the base of the Maastrichtian stage as defined in Tercis les Bains approximately at the base of the *Belemnella obtusa* zone of northwest Germany and consequently estimated a 700 kyr discrepancy between the GSSP and the base of *B. lanceolata*.

5.3. Variations of the sedimentation rate

Variations of the sedimentation rate can be precisely estimated at the scale of 100 kyr and 405 kyr eccentricity cycles (Fig. 10). The resulting curves agree with the trends delineated on the amplitude spectrograms and show a drop of sedimentation rates from ~1.5 cm/kyr in C33n/C32r to very low values around 0.6 cm/kyr throughout the top of C32n2n to C31n. The sedimentation rate suddenly increases to ~1.3 cm/kyr close to the transition between chrons C31n and C30r, right after the identified 500 kyr gap. A second increase in the middle part of chron C30n results in a average value of the sedimentation rate of 1.9 cm/kyr (Fig. 10).

Figure 10 about here: format landscape full page

An interesting issue is the comparison of the variations of the sedimentation rate with $\delta^{13}C$ variations at Hole 762C and with the sea-level record (Fig. 10). Kominz et al. (2008) recently provided an updated sea-level record for the last 108 Ma through the backstripping of corehole data from the New Jersey and Delaware Coastal Plains. The temporal resolution of the sea level curve is quite low for comparison at the scale of one single stage (+/-1Ma for the Late Cretaceous) and still bears large uncertainties (Fig. 10). The three sea-levels curves of Miller et al. (2005), Kominz et al. (2008) and Haq et al. (1987) are rather different for this time interval (Fig. 10). Taking into account age uncertainties of these sea-level curves, a late Campanian–early Maastrichtian 3rd order regression can be observed in the three records and may correlate to the large interval of lower $\delta^{13}C$ values between events CMBa and M3+ (Fig. 10). This interval is also marked by low values of the sedimentation rate in Hole 762C (Fig. 10).

Several hypothesis may explain the variations of the sedimentation rate such as variations in pelagic carbonate productivity, changes in accommodation by variations of subsidence or detrital supply, dissolution at the sea-floor and winnowing. At Site 762C, variations of the sedimentation rate may actually reflect a change in the strength and chemistry of bottom currents along the northwestern Australian margin. The early Maastrichtian 3rd order regression was correlated to an episode of accelerated cooling associated to an inferred reversal of the thermohaline circulation (Barrera et al., 1997). The coincidence between this 3rd order regression and this episode of accelerated cooling suggests a glacio-eustatic mechanism (Miller et al., 1999). These authors argued for the development of a moderate Antarctic ice-sheet at that time. Such a short early Maastrichtian ice-age would have intensified high-latitude formation of cooler and oxygenated bottom-waters and increased latitudinal temperature gradients (Barrera et al., 1997; Barrera and Savin, 1999). The Southern and Indian Oceans were isolated by geographical barriers between Antarctica and South America and in the central Atlantic, which inhibited the free circulation of intermediate to deep-waters. As a result, bottom-waters generated around Antarctica would have flowed north past the northwestern Australian margin into the Tethys Ocean (Howe et al., 2003). These cooler and well-oxygenated bottom waters may have been slightly more corrosive. Alternatively, stronger bottom currents could have resulted in displacing the pelagic rain further north of the site of deposition of Site 762C at that time. These bottom waters could also have resulted into higher winnowing of the sea-floor. No sign of erosion, condensation or winnowing was noticed in the original description of cores 47X to 49X which correspond to this interval of reduced sedimentation rates (Haq et al., 1990) but this interpretation calls for a more detailed examination of these cores. Nethertheless, any of these processes would have been associated to this paleoceanographic reorganization and may account for lower sedimentation rates within this interval. At the early-late Maastrichtian transition (topmost part of chron C31r), the geographical barrier formed by the Rio Grande Rise and Walvis Ridge in the Atlantic Ocean was breached by sea-floor spreading on the

Mid-Atlantic Ridge, allowing free circulation of bottom-waters between the North Atlantic and Indian Oceans (Frank and Arthur, 1999). Such a return of warmer, less corrosive and less powerful bottom-waters might eventually explain the following increase of the sedimentation rate in the remaining part of the Maastrichtian (Fig. 10).

5.4. Correlations and paleoenvironmental interpretation of carbon-isotope signals

Li and Keller (1998a, 1998b) and Barrera and Savin (1999) described carbon isotope trends on separated planktic and benthic foraminifera from a large number of deep-sea sites in the Atlantic, Pacific, Indian and Southern Oceans using time control on paleomagnetic reversal stratigraphy and/or Sr isotopes calibrated on paleomagnetic reversal stratigraphy. Their absolute ages were therefore based on Cande and Kent (1995) for magnetochronology. These ages have been revised in the GTS2004, in particular for the K-Pg boundary whose calibration shifted from 65 to 65.5 Ma and recently to 66 Ma (Kuiper et al., 2008; Westerhold et al., 2008; Renne et al. 2010). This led to discrepant late Maastrichtian ages of isotopic events presented here and those described by previous authors. However, the bulk $\delta^{13}C$ profile of the Maastrichtian of Hole 762C resembles previous $\delta^{13}C$ profiles acquired on separated foraminifera (Li and Keller, 1998a,1998b; Barrera and Savin, 1999), though several additional events are recorded here, likely due to the higher-resolution dataset of our study or to the localized expression of some events. As discussed above, correlation of major $\delta^{13}C$ events can be achieved throughout the Indian Ocean, the Tethys, the South Atlantic and the Boreal realm (Figs. 7–9).

Changes in the $\delta^{13}C$ record of marine carbonates are generally interpreted as a reflect of changes in the ratio of burial fluxes of isotopically light C of organic matter to C in the carbonates (Scholle and Arthur, 1980; Arthur et al., 1988; Weissert, 1989; Weissert et al., 1998). Additional factors that can influence this record are the addition into the marine realm of various external carbon species, such as terrestrial (through weathering), platform-derived C_{org} and dissolved inorganic carbon (platform drowning), atmospheric CO_2, or methane-derived carbon from the dissociation of clathrates (Cerlings et al., 1993; Dickens et al., 1995; Hesselbo et al., 2000; Kump and Arthur, 1999; Immenhauser et al., 2003; Weissert and Erba, 2004; Swart and Eberli, 2005; Panchuk et al., 2005, 2006, Föllmi et al., 2006). However, processes generally associated to large (>1.5‰) $\delta^{13}C$ excursions during oceanic anoxic events (OAEs) in the Jurassic, early and mid-Cretaceous can hardly be applied to Campanian-Maastrichtian records because no black shales were deposited on a large-scale during this interval and because carbon-isotope excursions recorded here in bulk carbonates are either much smaller (≤0.4‰) and/or are not short-lived episodes (for instance, the overall negative trend regrouping CMBa-c accounts for a total duration of 1 Ma, Table 4).

Barrera and Savin (1999) noted that the $\delta^{13}C$ negative excursion of the lower Maastrichtian is seen most markedly at southern polar Sites 689, 690 and 750. These authors proposed two distinct mechanisms to explain this excursion : (1) at the global scale, an increased ratio of organic to inorganic carbon in the input to the oceans driven by increased weathering of organic-rich sediments exposed on continental shelves during the sea-level drop, (2) in the southern ocean, a deepening of the oxygen minimum zone would reflect increased oxidation of organic matter and an associated production of ^{13}C-depleted bicarbonate which would have resulted in more pronounced negative values as observed in the benthic foraminiferal profiles. However, these authors noted that a second sea-level drop recorded in C30n (Haq et al., 1987 and Kominz et al., 2008) did not affect this ratio as inferred from their $\delta^{13}C$ values in that interval. In the Late Cretaceous (Cenomanian to Campanian), Jarvis et al. (2002, 2006) noted that the carbon-isotope reference curve for the English Chalk was remarkably similar in shape to supposedly eustatic sea-level curves. They concluded that both long-term and short-term $\delta^{13}C$ changes were controlled by sea-level throughout these stages with increasing $\delta^{13}C$ values accompanying sea-level rise and transgression, and decreasing $\delta^{13}C$ values characterizing sea-level fall and regression. This relationship is explained by variations in epicontinental sea area affecting organic-matter burial fluxes.

When taking into account the large uncertainty of the age-scale of the sea-level curve for the Late Cretaceous (+/- 1Ma, Kominz et al., 2008), it is not currently possible to confirm or infirm Jarvis' hypothesis on the relationship between variations of the sea-level and variations of $\delta^{13}C$ in the Late Cretaceous (Fig. 10). More work is needed to reduce these uncertainties and establish the evolution of regional sea-level changes.

Friedrich et al. (2009) interpreted the large carbon isotope perturbations of the CMB and early Maastrichtian as a weakening of surface water stratification and increased productivity in the southern high latitudes caused by ongoing cooling during the Late Cretaceous. This would have led to the strengthening contribution of intermediate- to deep-water production in the high southern latitudes.

Climate change might have also contributed to some of the observed $\delta^{13}C$ excursions. In particular, in the late Maastrichtian, M4-(b) is coincident with the last occurrence of the high-fertility species *Biscutum constans* (Fig. 9). This bio-event, which was also recorded in the Tropical Atlantic and Pacific Oceans (Thibault and Gardin, 2010) could suggest a decrease of surface-water fertility by the end of the Maastrichtian. In addition, M4-(b) occurs during the acme of nannofossil warm-water species *Micula murus* which has been interpreted as the expression of the end-Maastrichtian Deccan warming (Thibault and Gardin, 2006, 2007, 2010). This warming event has not been associated so far with any stratification of the ocean and the pulse of volcanically derived CO_2 ($\delta^{13}C \approx -5‰$) associated with Deccan volcanism would have contributed only to very small changes in the isotopic composition of the oceans (Kump and Arthur, 1999). However, this global warming event might have significantly reduced photosymbiotic activity (Abramovich and Keller, 2003) and caused an ecological stress (Li and Keller, 1998a, 1998b; Abramovich and Keller, 2003), resulting in a decrease of surface ocean productivity. Thus, the negative excursion M4-(b) may be the expression of a global decrease in surface ocean productivity.

6. Conclusions

1) Combined calcareous plankton biostratigraphy, $\delta^{13}C$ stratigraphy, magneto- and cyclostratigraphy of ODP Hole 762C has been established and shows that this site had a nearly continuous sedimentation all along the upper Campanian–Maastrichtian apart from a ~500 kyr gap identified in Chron C31n.
2) There is no disconformity in the lower Maastrichtian of the Exmouth Plateau contrary to what stated in Howe et al. (2003). The observed higher-than-expected extinctions of lower Maastrichtian nannofossil species, and the different stratigraphic orders of nannofossil and foraminifera events as compared to “standard” Tethyan zonations, are rather the result of diachronism and migration patterns between the Tethyan, Transitional and Austral realms. These migration patterns could well be caused by paleoceanographic reorganizations triggered by the prominent climatic changes of the Campanian–Maastrichtian.
3) Results of the cyclostratigraphic approach tied to the astronomical calibration of the Maastrichtian allowed a precise age-calibration of biostratigraphic events and of the carbon-isotope profile.
4) Reduced sedimentation rates in the early Maastrichtian may be the response to either reduced pelagic carbonate productivity, or either major global reorganizations of

bottom-currents leading to reduced sedimentation rates along the northwestern margin of Australia.

5) Correlation of the calibrated $\delta^{13}C$ profile of Hole 762C to that of the Tercis section, GSSP of the Campanian–Maastrichtian boundary, allows proposal of a precise age of 72.15±0.05 Ma for this boundary considering an age of 66 Ma for the K-Pg boundary. The total duration of the Maastrichtian stage is 6.15±0.05 Ma.

6) The original CMB as defined by the base of the Boreal Belemnite zone *Belemnella lanceolata* in northwest Germany is ~800 kyr older than the CMB as defined in the GSSP of Tercis les Bains, which, in turn lies at the base of the *Belemnella obtusa* zone.

7) The obtained chronostratigraphic framework of ODP Hole 762C is proposed as a robust reference for the Indian Ocean and can serve as a basis for large-scale correlation of $\delta^{13}C$ profiles and to test synchronism/diachronism of microfossil bio-events throughout the Boreal, Tethyan, Transitional and Austral realms.

Plate 1 and Plate 2 around here: format portrait full page

Acknowledgements

We are grateful to Nathalie Labourdette, Damien Huygues and Vincent Gressier for technical support and analytical help. Kipis to Julien Moreau. This research used samples provided by the Ocean Drilling Program (ODP). ODP is sponsored by the US National Science Foundation (NSF) and participating countries under the management of Joint Oceanographic Institutions (JOI), Inc. Funding for this study was provided by Eclipse II Program, the Danish National Foundation (FNU) and the Carlsberg Foundation. We warmly thank Silke Voigt and

Andy Gale for numerous fruitful discussions on Campanian–Maastrichtian stratigraphy as well as Jim Ogg and an anonymous reviewer for their insightful and constructive reviews.

References

Abramovich, S., Keller, G., 2002. High stress late Maastrichtian paleoenvironment: inference from planktonic foraminifera in Tunisia. Palaeogeogr. Palaeoclimat. Palaeoecol. 178, 145–164.

Abramovich, S., Keller, G., 2003. Planktonic foraminiferal response to the latest Maastrichtian abrupt warm event: a case study from South Atlantic DSDP Site 525A. Mar. Micropaleontol. 48, 225–249.

Apthorpe, M.C., 1979. Depositional history of the Upper Cretaceous of the Northwest shelf, based upon Foraminifera. The APPEA Journal 19, 74–89.

Arthur, M. A., Dean, W.E., Pratt, L.M. 1988. Geochemical and climatic effects of increased marine organic carbon burial at the Cenomanian/Turonian boundary, Nature 35, 714– 717.

Barchi, P., Bonnemaison, M., Galbrun, B., Renard, M., 1997. Tercis (Landes, Sud-Ouest France) : point stratotypique de la limite Campanien-Maastrichtien. Résultats magnétostratigraphiques et premières données sur la nannoflore calcaire. Bull. Soc. Géol. France 168, 133–142.

Barrera, E., Savin, S.M., 1999. Evolution of Campanian–Maastrichtian marine climates and oceans. In: Barrera, E., Johnson, C.C. (Eds.), Evolution of the Cretaceous Ocean-Climate System. Geol. Soc. Am. Spec. Paper, vol. 332, pp. 245–282.

Barrera, E., Savin, S.M., Thomas, E., Jones, C.E., 1997. Evidence for thermohaline-circulation reversals controlled by sea level change in the latest Cretaceous. Geology 25, 715–718.

Batenburg, S.J., Sprovieri, M., Gale, A.S., Hilgen, F.J., Hüsing, S., Laskar, J., Liebrand, D., Lirer, F., Orue-Etxebarria, X., Pelosi, N., Smit, J., 2012. Cyclostratigraphy and astronomical tuning of the Maastrichtian at Zumaia (Basque country, Northern Spain). Earth Planet. Sci. Lett., in press.

Birkelund, T., Hancock, J.M., Hart, M.B., Rawson, P.F., Remane, J., Robaszynski, F., Schmid, F., and Surlyk, F. 1984. Cretaceous stage boundaries Proposals. Bulletin of the Geological Society of Denmark 33, 3–20.

Bown, P.R., 1998. Calcareous Nannofossil Biostratigraphy. British Micropaleontology Society Publication Series. Chapman & Hall/Kluwer Academic Publishers, London, 328 pp.

Bralower, T.J., Siesser, W., 1992. Cretaceous calcareous nannofossil biostratigraphy of Sites 761, 762 and 763, Exmouth and Wombat Plateaus, northwest Australia. Proc. ODP Sci. Results 122, 529-556.

Bralower, T.J., Leckie, R.M., Sliter, W.V., Thierstein, H.R., 1995. An integrated Cretaceous microfossil biostratigraphy. In: Berggren, W.A., Kent, D.V., Aubry, M.-P., Hardenbol, J. (Eds.), Geochronology, Timescales and Global Stratigraphic Correlations. SEPM Special Publication 54, Tulsa, pp. 65–79.

Burnett, J.A. with contributions from Gallagher, L.T. & Hampton, M.J. 1998. Upper Cretaceous. In: P.R. Bown (Ed.). Calcareous Nannofossil Biostratigraphy. British Micropalaeontological Society Series. Chapman & Hall/Kluwer Academic Publishers, London: 132–199.

Campbell, R.J., Howe, R.W., Rexilius, J.P., 2004. Middle Campanian–lowermost Maastrichtian nannofossil and foraminiferal biostratigraphy of the northwestern Australian margin. Cretaceous Res. 25, 827–864.

Cande, S.C., Kent, D.V., 1995. Revised calibration of the geomagnetic polarity timescale for the late Cretaceous and Cenozoic. J. Geophys. Res. 100, 6093–6095.

Cerlings, T. E., Y. Wang, Quade, J., 1993. Expansion of C4 ecosystems as an indicator of global ecological change in the late Miocene. Nature 361, 344– 345.

Chave, A.D., 1984, Lower Paleocene-Upper Cretaceous magnetostratigraphy, Sites 525, 527, 528, and 529, Deep Sea Drilling Project Leg 74, Init. Rep. DSDP 74, 525–531.

Cramer, B.S., 2001. Latest Palaeocene-earliest Eocene cyclostratigraphy: using core photographs for reconnaissance geophysical logging. Earth Planet. Sci. Lett. 186, 231–244.

Debajyoti, P., Skrzypek, G., Forizs, I., 2007. Normalization of measured stable isotopic compositions to isotope reference scales – a review. Rapid Commun. Mass Spectrom. 21, 3006–3014.

Dickens, G.R., O'Neil, J.R., Rea, D.K., Owen, R.M., 1995. Dissociation of oceanic methane hydrate as a cause of the carbon isotope excursion at the end of the Paleocene. Paleoceanography 10, 965–971.

Föllmi, K.B., Godet, A., Bodin, S., Linder, P., 2006. Interactions between environmental change and shallow water carbonate buildup along the northern Tethyan margin and their impact on the Early Cretaceous carbon isotope record. Paleoceanography 21, PA4211, doi:10.1029/2006PA001313.

Frank, T.D., Arthur, M.A., 1999. Tectonic forcings of Maastrichtian ocean-climate evolution. Paleoceanography 14, 103-117.

Friedrich, O., Herrle, J.O., Hemleben, C., 2005. Climatic changes in the Late Campanian–Early Maastrichtian: Micropaleontological and stable isotopic evidence from an epicontinental sea. J. Foraminiferal Res. 35, 228–247.

Friedrich, O., Herrle, J.O., Wilson, P.A., Cooper, M.J., Erbacher, J., Hemleben, C., 2009. Early Maastrichtian carbon cycle perturbation and cooling event: Implications from the South Atlantic Ocean. Paleoceanography 24, PA2211, doi:10.1029/2008PA001654.

Galbrun, B., 1992. Magnetostratigraphy of Upper Cretaceous and lower Tertiary sediments, Sites 761 and 762, Exmouth Plateau, northwest Australia. Proc. ODP Sci. Results 122, 699–716.

Gale, A.S., Jenkyns, H.C., Kennedy, W.J., Corfield, R.M., 1993. Chemostratigraphy versus biostratigraphy: data from around the Cenomanian–Turonian boundary. J. Geol. Soc. London 150, 29–32.

Gardin, S., Monechi, S., 2001. Calcareous Nannofossil distribution in the Tercis geological site (Landes, SW France) around the Campanian-Maastrichtian boundary, in: Odin G.S. (Ed.), The Campanian–Maastrichtian stage boundary. Characterization at Tercis les Bains (France) and correlation with Europe and other continents. Developments in Palaeontology and Stratigraphy 19, pp. 272–284.

Gardin, S., Odin, G.S., Bonnemaison, M., Melinte, M., Monechi, S., von Salis, K., 2001. Results of the cooperative study on the calcareous nannofossils across the Campanian-Maastrichtian boundary at Tercis les Bains (Landes, France), in: Odin G.S. (Ed.), The Campanian–Maastrichtian stage boundary. Characterization at Tercis les Bains (France) and correlation with Europe and other continents. Developments in Palaeontology and Stratigraphy 19, pp. 293–309.

Gardin, S., Galbrun, B., Thibault, N., Coccioni, R., Premoli Silva, I., 2012. Bio-magnetochronology for the upper Campanian - Maastrichtian from the Gubbio area, Italy: new results from the Contessa Highway and Bottaccione sections. Newsl. Stratigr. 45, in press.

Golovchenko, X., Borella, P.E., O'Connell, S., 1992. Sedimentary cycles on the Exmouth Plateau. Proc. ODP Sci. Results 122, 279–294.

Gradstein, F.M., Ogg, J.G., Smith, A.G., 2004. A Geologic Time Scale 2004, Cambridge University Press, Cambridge, U.K., 500 pp.

Hancock, J.M., 1991. Ammonite time scales for the Cretaceous. Cretaceous Res. 12, 259–291.

Haq, B.U., Hardenbol, J., Vail, P.R., 1987. Chronology of fluctuating Sea levels Since the Triassic. Science 235, 1156–1167.

Haq et al., 1992. Site 762, Shipboard Scientific Party. Proc. ODP Init. Rep. 122, 213–288.

Hay, W.H., DeConto, R.M., Wold, C.N., Wilson, K.N., Voigt, S., Schulz, M., Rossby Wold, A., Dullo, W.-C., Ronov, A.B., Balukhovsky, A.N., Söding, E., 1999. Alternative global Cretaceous paleogeography. In: Barrera, E., Johnson, C. C. (Eds.), Evolution of the Cretaceous Ocean-Climate System: Boulder, Colorado, Geol. Soc. Am. Spec. Paper 332, 1–47.

Henriksson, A.S., 1993. Biochronology of the terminal Cretaceous calcareous nannofossil Zone of *Micula prinsii*. Cretaceous Res. 14, 59–68.

Hesselbo, S. P., Gröcke, D.R., Jenkyns, H.C., Bjerrum, C.J., Farrimond, P., Bell, H.S.M., Green, O.R., 2000. Massive dissociation of gas hydrate during a Jurassic oceanic anoxic event. Nature 406, 392–395.

Hilgen, F. J., Kuiper, K. F., and Lourens, L. J. (2010). Evaluation of the astronomical time scale for the Paleocene and earliest Eocene. Earth Planet. Sci. Lett. 300, 139–151.

Howe, R.W., Campbell, R.J., Rexilius, J.P., 2003. Integrated uppermost Campanian–Maastrichtian calcareous nannofossil and foraminiferal biostratigraphic zonation of the northwestern margin of Australia. Journal of Micropalaeontology 22, 29–62.

Huang, Z., Boyd, R., O'Connell, S., 1992. Upper Cretaceous cyclic sediments from Hole 762C, Exmouth Plateau, northwest Australia. Proc. ODP Sci. Results 122, 259–278.

Huber, B.T., 1992a. Paleobiogeography of Campanian–Maastrichtian foraminifera in the southern high latitudes. Palaeogeogr. Palaeoclimatol. Palaeoecol. 92, 325–360.

Huber, B.T., 1992b. Upper Cretaceous planktic foraminiferal zonation for the Austral Realm. Mar. Micropaleontol. 20, 107–128

Huber, B.T., Watkins, D.K., 1992. Biogeography of Campanian–Maastrichtian calcareous plankton in the region of the Southern Ocean: Paleogeographic and Paleoclimatic implications. In: Kennett, J.P., Warnke, D.A. (Eds.), The Antarctic Paleoenvironment: A Perspective on Global Change. American Geophysical Union, Antarctic Research Series 56, Washington, pp. 31–60.

Husson, D., Galbrun, B., Laskar, J., Hinnov, L., Thibault, N., Gardin, S., Locklair, R.E., 2011. Astronomical calibration of the Maastrichtian (late Cretaceous). Earth Planet. Sci. Lett. 305, 328–340.

Husson, D., Galbrun, B., Thibault, N., Gardin, S., Huret, E., Coccioni, R., 2012. Astronomical duration of polarity Chron C31r (Lower Maastrichtian): cyclostratigraphy of ODP Site 762 (Indian Ocean) and the Contessa Highway section (Gubbio, Italy). Geol. Mag. 149, 345–351.

Immenhauser, A., Della Porta, G. Kenter, J. A. M., Bahamonde, J.R., 2003. An alternative model for positive shifts in shallow-marine carbonate $\delta^{13}C$ and $\delta^{18}O$. Sedimentology 50, 953– 959.

Ion, J., Odin, G.S., 2001. Planktonic foraminifera from the Campanian-Maastrichtian at Tercis les Bains (Landes, France). In: Odin, G.S. (Ed.), The Campanian-Maastrichtian stage boundary: characterisation at Tercis les Bains (France): correlation with Europe and other continents. Developments in Palaeontology and Stratigraphy Series 19, Elsevier Sciences Publ. Amsterdam, 349-378.

Jarvis, I., Mabrouk, A., Moody, R.T.J., de Cabrera, S., 2002. Late Cretaceous (Campanian) carbon isotope events, sea-level change and correlation of the Tethyan and Boreal realms. Palaeogeogr. Palaeoclimatol. Palaeoecol. 188, 215–248.

Jarvis, I., Gale, A.S., Jenkyns, H.C., Pearce, M.A., 2006. Secular variation in Late Cretaceous carbon isotopes: a new $\delta^{13}C$ carbonate reference curve for the Cenomanian–Campanian (99.6–70.6 Ma). Geol. Mag. 143, 561–608.

Jenkyns, H.C., Gale, A.S., Corfield, R.M., 1994. Carbon- and oxygen-isotope stratigraphy of the English Chalk and Italian Scalia and its palaeoclimatic significance. Geol. Mag. 131, 1–34.

Jenkyns, H.C., Mutterlose, J., Sliter, W.V., 1995. Upper Cretaceous carbon- and oxygen-isotope stratigraphy of deep-water sediments from the North-Central Pacific (Site 869, Flank of Pikini-Wodejebato, Marshall Islands). Proc. ODP Sci. Results 143, 105-108.

Johnson, C.C., Barron, E.J., Kauffman, E.G., Arthur, M.A., Fawcett, P.J., Yasuda, M.K., 1996. Middle Cretaceous reef collapse linked to ocean heat transport. Geology 24, 376–380.

Kominz, M.A., Browning, J.V., Miller, K.G., Sugarman, P.J., Mizintsevaw, S., Scotese, C.R., 2008. Late Cretaceous to Miocene sea-level estimates from the New Jersey and Delaware coastal plain coreholes: an error analysis. Basin Res. 20, 211–226.

Kuiper, K.F., Deino, A. Hilgen, F.J., Krijgsman, W., Renne, P.R., and Wijbrans, J.R., 2008. Synchronizing rock clocks of earth history. Science 320, 500-504.

Kump, L. R., Arthur, M.A., 1999. Interpreting carbon-isotope excursions: Carbonates and organic matter. Chem. Geol. 161, 181– 198.

Laskar, J., Fienga, A., Gastineau, M., Manche, H., 2011. La2010: a new orbital solution for the long-term motion of the Earth. Astronomy and Astrophysics 532, A89, 1–15, DOI: http://dx.doi.org/10.1051/0004-6361/201116836.

Landman, N.H., Waage, K.M., 1993. Scaphitid ammonites of the Upper Cretaceous (Maastrichtian) Fox Hills formation in South Dakota and Wyoming, Bulletin of the American Museum of National History 215, 1–257.

Lees, J.A., 2002. Calcareous nannofossils biogeography illustrates palaeoclimate change in the Late Cretaceous Indian Ocean. Cretaceous Res. 23, 537–634.

Lees, J.A., Bown, P.R., 2005. Upper Cretaceous calcareous nannofossil biostratigraphy, ODP Leg 198 (Shatsky Rise, northwest Pacific Ocean). Proc. Ocean Drill. Program Sci. Results 198, 1–60. doi:10.2973/odp.proc.sr.198.114.2005.

Lewy, Z., Odin, G.S., 2001. Magnetostratigraphy across the Campanian-Maastrichtian boundary at Tercis les Bains in comparison with northern Germany, the Apennines (Central Italy) and North America; biostratigraphical and Central Italy) and North America; biostratigraphical and geochronological constraints. In: Odin, G.S. (Ed.), The Campanian-Maastrichtian stage boundary: characterisation at Tercis les Bains (France): correlation with Europe and other continents. Developments in Palaeontology and Stratigraphy Series 19, Elsevier Sciences Publ. Amsterdam, 175-183.

Li, L., Keller, G., 1998a. Maastrichtian climate, productivity and faunal turnovers in planktic foraminifera in South Atlantic DSDP sites 525A and 21. Mar. Micropaleontol. 33, 55–86.

Li, L., Keller, G., 1998b. Abrupt deep-sea warming at the end of the Cretaceous. Geology 26, 995–998.

Li, L., Keller, G., 1999. Variability in Late Cretaceous and deep waters: evidence from stable isotopes. Mar. geol. 161, 171–190.

MacLeod, K.G., Huber, B.T., Ward, P.D., 1996. The biostratigraphy and paleobiogeography of Maastrichtian inoceramids. In: Ryder, G., Fastovsky, D., Gartner, S. (Eds.), The Cretaceous–Tertiary Event and Other Catastrophes in Earth History. Geol. Soc. Am. Spec. Paper 307, Boulder, pp. 361–373.

Manivit, H., 1984. Paleogene and Upper Cretaceous calcareous nannofossils from Deep Sea Drilling Project Leg 74. Init. Rep. Deep Sea Drill. Proj. 74, 475–499.

McArthur, J.M., Kennedy, W.J., Gale, A.S., Thirlwall, M.F., Chen, M., Burnett, J., Hancock, J.M., 1992. Strontium isotope stratigraphy in the Late Cretaceous: intercontinental correlation of the Campanian/Maastrichtian boundary. Terra Nova 4, 385–393.

McArthur, J.M., Kennedy, W.J., Chen, M., Thirlwall and M.F. Gale, A.S., 1994. Strontium isotope stratigraphy for Late Cretaceous time: Direct numerical calibration of the Sr isotope curve based on the US Western Interior. Palaeogeogr. Palaeoclimatol. Palaeoecol. 108, 95–119.

Miller, K.G., Barrera, E., Olsson, R.K., Sugarman, P.J. and Savin, S.M., 1999. Does ice drive early Maastrichtian eustasy? Geology 27, 783-786.

Mitchell, S.F., Ball, J.D., Crowley, S.F., Marshall, J.D., Paul, C.R.C., Veltkamp, C.J., Samir, A., 1997. Isotope data from cretaceous chalks and foraminifera: Environmental or diagenetic signals? Geology 25, 691–694.

Niebuhr, B., Esser, K., 2003. Late Campanian and Early Maastrichtian ammonites from the white chalk of Kronsmoor (northern Germany) – taxonomy and stratigraphy. Acta Geol. Pol. 53, 257–281.

Odin, G.S., 1996, Observations stratigraphiques sur le Maastrichtien. Arguments pour la localisation et la corrélation du Point Stratotype Global de la limite Campanien-Maastrichtien, Bull. Soc. Géol. France 167, 637–643.

Odin, G.S., 2001. The Campanian-Maastrichtian stage boundary: characterisation at Tercis les Bains (France): correlation with Europe and other continents. Developments in Palaeontology and Stratigraphy Series 19, Elsevier Sciences Publ. Amsterdam, 910 p.

Odin, G.S., and Amorosi, A., 2001. Interpretative reading of the Campanian-Maastrichtian deposits at Tercis les Bains: sedimentary breaks, rhythms, accumulation rate, sequences. In: Odin, G.S. (Ed.), The Campanian-Maastrichtian stage boundary: characterisation at Tercis les Bains (France): correlation with Europe and other continents. Developments in Palaeontology and Stratigraphy Series 19, Elsevier Sciences Publ. Amsterdam, 125-135.

Odin, G.S. and Lamaurelle, M.A., 2001. The global Campanian-Maastrichtian stage boundary. Episodes 24, 229–237.

Olsson, R.K., Wright, J.D., Miller, K.G., 2001. Paleobiogeography of Pseudotextularia elegans during the latest Maastrichtian global warming event. J. Foraminiferal Res. 31, 275–282.

Pälike, H., Norris, R.D., Herrle, J.O., Wilson, P.A., Coxall, H.K., Lear, C.H., Shackleton, N.J., Tripati, A.K., Wade, B.S., 2006. The heartbeat of the Oligocene climate system. Science 314, 1894–1898.

Panchuk, K. M., Holmden, C., Kump, L.R., 2005. Sensitivity of the epeiric sea carbon isotope record to local-scale carbon cycle processes: Tales from the Mohawkian Sea, Palaeogeogr. Palaeoclimat. Palaeoecol. 228, 320–337.

Panchuk, K. M., C. E. Holmden, Leslie, S.A., 2006. Local controls on carbon cycling in the Ordovician midcontinent region of North America, with implications for carbon isotope secular curves. J. Sediment. Res. 76, 200– 211.

Perch-Nielsen, K., 1985. Mesozoic calcareous nannofossils. In: Bolli, H., S et al. (Editors), Plankton Stratigraphy. Cambridge University Press, pp. 329–426.

Petrizzo, M.R., 2000. Upper Turonian–lower Campanian planktonic foraminifera from southern mid-high latitudes (Exmouth Plateau, NW Australia): biostratigraphy and taxonomic notes. Cretaceous Res. 21, 479–505.

Petrizzo, M.R., 2003. Late Cretaceous planktonic foraminiferal bioevents in the Tethys and in the Southern Ocean: an overview. J. Foraminiferal Res. 33, 330–337.

Premoli Silva, I., Sliter, W.V., 1994. Cretaceous planktonic foraminiferal biostratigraphy and evolutionary trends from the Bottaccione section, Gubbio, Italy. Palaeontogr. Ital. 82, 1–89.

Renne, P.R., Mundil, R., Balco, G., Min, K., Kudwig, K.R., 2010. Joint determination of ^{40}K decay constants and ^{40}Ar*/^{40}Ar for the Fish Canyon sanidine standard, and improved accuracy for ^{40}Ar/^{39}Ar geochronology. Geochim. Cosmochim. Acta., doi: 10.1016/j.gca.2010.06.017.

Rexilius, J.P., 1984. Late Cretaceous foraminiferal and calcareous nannoplankton biostratigraphy, Southwestern Australian Margin. PhD Thesis. Department of Geology and Geophysics, The University of Western Australia, 291p.

Scholle, P. A., Arthur, M.A., 1980. Carbon isotope fluctuations in Cretaceous pelagic limestones: Potential stratigraphic and petroleum exploration tool. Am. Assoc. Petrol. Geol. Bull. 64, 67–87.

Schönfeld, J., Schulz, M.-G., Arthur, M.A., Burnett, J., Gale, A.S., Hambach, U., Hansen, H.J., Kennedy, W.J., Rasmussen, K.L., Thirlwall, M.F., Wray, D.S., 1996. New results on biostratigraphy, paleomagnetism, geochemistry and correlation from the standard section for the Upper Cretaceous white chalk of northern Germany (Lägerdorf-Kronsmoor-Hemmoor). Mitteilungen des Geologisch-Paläontologischen Institutes der Universität Hamburg 77, 545–575.

Schrag, D.P., DePaolo, D.J., Richter, F.M, 1995. Reconstructing past sea surface temperatures: correcting for diagenesis of bulk marine carbon. Geochim. Cosmochim. Ac. 59, 2265–2278.

Shafik, S., 1990. Late Cretaceous nannofossil biostratigraphy and biogeography of the Australian western margin. Bureau of Mineral Resources, Geology and Geophysics, Report 295, 1–164.

Shafik, S., 1998. Problems with the Cretaceous biostratigraphic system of Australia: time for a review. Australian Geological Survey Organisation Research Newsletter 28, 12–14.

Swart, P. K., Eberli, G., 2005. The nature of the $\delta^{13}C$ of periplatform sediments: Implications for stratigraphy and the global carbon cycle, Sedim. Geol. 175, 115– 129.

Thibault, N., Gardin, S., 2006. Maastrichtian calcareous nannofossil biostratigraphy and paleoecology in the Equatorial Atlantic (Demerara Rise, ODP Leg 207 Hole 1258A). Rev. Micropaleontol. 49, 199–214.

Thibault, N., Gardin, S., 2007. The late Maastrichtian nannofossil record of climate change in the South Atlantic DSDP Hole 525A. Mar. Micropaleontol. 65, 163–184.

Thibault, N., Gardin, S., Galbrun, B., 2010. Latitudinal migration of calcareous nannofossil *Micula murus* in the Maastrichtian: Implications for global climate change. Geology 38, 203–206.

Thibault, N., Schovsbo, N., Harlou, R., Stemmerik, L., Surlyk, F., 2011. An age-calibrated record of upper Campanian – Maastrichtian climate change in the Boreal Realm. Abstract, 2011 Fall Meeting, AGU, San Francisco, Calif., 5-9 Dec.

Thibault, N., Harlou, R., Schovsbo, N., Schiøler, P., Minoletti, F., Galbrun, B., Lauridsen, B.W., Sheldon, E., Stemmerik, L., Surlyk, F., 2012. Upper Campanian–Maastrichtian nannofossil biostratigraphy and high-resolution carbon-isotope stratigraphy of the Danish Basin: towards a standard $\delta^{13}C$ curve fot the Boreal Realm. Cretaceous Res. 33, 72–90.

Thomson, D.J., 1982. Spectrum estimation and harmonic analysis. Inst. Electr. And Electron. Eng. Proc. 70, 1055–1096.

Voigt, S., 2000. Cenomanian–Turonian composite $\delta^{13}C$ curve for Western and Central Europe: the role of organic and inorganic carbon fluxes. Palaeogeogr. Palaeoclimatol. Palaeoecol. 160, 91–104.

Voigt, S., Schönfeld, J., 2010. Cyclostratigraphy of the standard section for the Cretaceous white chalk of northern Germany, Lägerdorf-Kronsmoor: a late Campanian – early Maastrichtian orbital time scale. Palaeogeogr. Palaeoclimatol. Palaeoecol. 287, 67–80.

Voigt, S., Friedrich, O., Norris, R.D., Schönfeld, J., 2010. Campanian – Maastrichtian carbon isotope stratigraphy: shelf–ocean correlation between the European shelf sea and the tropical Pacific Ocean. Newsl. Stratigr. 44, 57–72.

Voigt, S., Gale, A.S., Jung., C., Jenkyns, H.C., 2012. Global correlation of Upper Campanian–Maastrichtian successions using carbon-isotope stratigraphy: development of a new Maastrichtian timescale. Newsl. Stratigr. 45, in press.

Weedon, G.P., 2003. Time series analysis and cyclostratigraphy: Examining stratigraphic records of environmental cycles: Cambridge, UK Cambridge University Press, 259 p.

Weissert, H., 1989. C-isotope stratigraphy, a monitor of paleoenvironmental change: a case study from the Early Cretaceous. Surv. Geophys. 10, 1-61.

Weissert, H., Erba, E., 2004. Volcanism, CO2 and palaeoclimate: A late Jurassic-early Cretaceous carbon and oxygen isotope record. Journ. Geol. Soc. London 161, 695– 702.

Weissert, H., Lini, A., Föllmi, K.B., Kuhn, O., 1998. Correlation of Early Cretaceous carbon isotope stratigraphy and platform drowning events: A possible link? Palaeogeogr., Palaeoclimat., Palaeoecol. 137, 189–203.

Westerhold, T., Röhl, U., Raffi, I., Fornaciari, E., Monechi, S., Reale, V., Bowles, J., Evans, H.F., 2008. Astronomical calibration of the Paleocene time. Palaeogeogr. Palaeoclimatol., Palaeoecol. 257, 377–403.

Wonders, A.A.H., 1992. Cretaceous planktonic foraminiferal biostratigraphy, Leg 122, Exmouth Plateau, Australia. Proc. ODP, Sci. Results 122, 587-600.

Young, J.R., Bown, P.R., 1997. Higher classification of calcareous nannoplankton. J. Nannoplankton Res. 19, 15-20.

Zepeda, M.A., 1998. Planktonic foraminiferal diversity, equitability and biostratigraphy of the uppermost Campanian-Maastrichtian, ODP Leg 122, Hole 762C, Exmouth Plateau, NW Australia, eastern Indian Ocean. Cretaceous Res. 19, 117–152.

Captions to figures

Figure 1 : A. Palaeogeographic reconstruction of the Southern Hemisphere for the upper Campanian-lower Maastrichtian showing the location of ODP Hole 762C, DSDP Hole 525A, and the inferred palaeobiogeographical boundaries between the Austral, Transitional and Tethyan provinces (from Huber, 1992a). B. Map of Europe showing other important locations of Campanian-Maastrichtian sections. G: Gubbio, LKH: Lägerdorf – Kronsmoor – Hemmoor, M: Maastricht, N: Norfolk, R: Rørdal, S: Stevns-1, T: Tercis les Bains.

Figure 2 : Magnetostratigraphy, bulk-carbonate $\delta^{13}C$ profile, planktic foraminifer and nannofossil bio-events in ODP Hole 762C, with inferred biozonations of Howe et al. (2003) and Campbell et al. (2004) for planktic foraminifera and Burnett (1998) for calcareous nannofossils. (a) Revised in this study from data published by Galbrun (1992). (b) Planktic foraminifer transitional biozonation from Zepeda (1998). (c) Data from Howe et al. (2003).

(d) This study. (e) Data from Campbell et al. (2004). C/F: sudden change of abundance from common to frequent only.

Figure 3 : Illustration of an ODP core photograph (core 48X) from the early Maastrichtian of Hole 762C. One hundred kyr eccentricity cycles e_{100}39 to e_{100}55 are identified on the core and bracketed between the “X”. A few obvious precession cycles are shown (P). These precession cycles are also expressed on the amplitude spectrograms of Figure 4 in the interval between 604 and 610 ambsf.

Figure 4 : (a) Gray scale log reflectance. The presented signal has been filtered for cracks and lighting effects. (b) MTM power spectra of the gray scale log for the stratigraphical intervals 550-593 ambsf and 593-638 ambsf. (c) Amplitude spectrograms for the studied interval. The shaded area corresponds to a “strange” interval with disturbance (D.) caused by numerous cracks in the cores which hinder the identification of clear 405 kyr eccentricity cycles.

Figure 5 : Cyclostratigraphic age-model for the upper Campanian-Maastrichtian of ODP Hole 762C. The counting of 100 and 405 kyr eccentricity cycles is here based on the 100 kyr filter output extracted from the original gray-scale log reflectance. 405 kyr cycles are thus hand-counted by regroupment of 100 kyr cycles. From the base of C31n to the top of C33n, this counting corresponds fairly well to the extracted 405 kyr filter output (Figs. 7–10). The identified Campanian–Maastrichtian boundary level lies within 100 kyr eccentricity cycle e_{100}62 which provides an age of 72.15±0.05 Ma for the CMB (with a K-Pg boundary at 66 Ma) and a total duration of 6.15±0.05 Ma for the Maastrichtian stage.

Figure 6 : Cross-plot of carbon- and oxygen-isotope ratios for bulk samples analyzed from the Maastrichtian section of ODP Hole 762C. There is no significant correlation between the two sets of values.

Figure 7: Correlation of the age-calibrated $\delta^{13}C$ profile of ODP Hole 762C with the $\delta^{13}C$ profile of Tercis les Bains, GSSP of the Campanian–Maastrichtian boundary, and the Gubbio composite section. (a) This study. PF datums are in bold and PF zones correspond to the transitional biozonation of Zepeda (1998). (b) All references on planktic foraminiferal (PF) and nannofossil biostratigraphic datums of Tercis les Bains can be found in Voigt et al. (2012). The first occurrences of planktic foraminifers *C. contusa* and *T. scotti* reported for the Tercis les Bains section are not reliable and thus not presented here (I. Premoli Silva in Gardin et al., 2012). (c) The Gubbio composite presented here was built using the $\delta^{13}C$ records of the Bottaccione and Contessa sections presented in Voigt et al. (2012) and corresponding biostratigraphic datums of Gardin et al. (2012). (d) 405 kyr filter after Husson et al. (2011). Only the 100 kyr filtering could be used for magnetochrons C29r to C30r in Hole 762C, 405 kyr eccentricity cycles of this interval (in grey) are thus hand counted by regroupment of four 100 kyr cycles.

Figure 8: Correlation of $\delta^{13}C$ profiles between ODP Hole 762C (Indian Ocean), Stevns-1 (Danish Basin), and Lägerdorf – Kronsmoor – Hemmoor composite section (LKH, Northwest Germany). (a) This study. (b) After Husson et al. (2011). Only the 100 kyr filtering could be used for magnetochrons C29r to C30r in Hole 762C, 405 kyr eccentricity cycles of this interval (in grey) are thus hand counted by regroupment of four 100 kyr cycles. (c) Thibault et al. (2012). (d) Voigt et al. (2010). (e) 405 kyr filter of $CaCO_3$ data and corresponding numbering of cycles for Boreal Campanian and Maastrichtian stages after Voigt and

Schönfeld (2010). (f) Nannofossil datums by Burnett in Schönfeld et al. (1996). Belemnite zones are: polypl = *polyplucum*, gri/gra = *grimmenis/granulosis*, lan = *lanceolata*, p = *pseudoobtusa*, obt = *obtusa*, cimb = *cimbrica*, fas = *fastigata*, teg/jun = *tegulatus/junior*, arg/jun = *argentea/junior*, da = *danica*, ba/da = *baltica/danica*. The Boreal CMB as defined by belemnite zones in LKH section corresponds to the base of $\delta^{13}C$ event CMBa and thus shows a discrepancy of ca. two 405 kyr cycles with the CMB as defined in ODP Hole 762C within $\delta^{13}C$ event CMBc by comparison with the GSSP of Tercis les Bains.

Figure 9: Correlation of $\delta^{13}C$ profiles between ODP Hole 762C (Indian Ocean) and DSDP Hole 525A (South Atlantic). (a) Husson et al. (2011), (b) Thibault and Gardin (2007), (c) Manivit (1984), (d) Li and Keller (1998a).

Figure 10: Age-calibrated bulk-carbonate $\delta^{13}C$ profile and variations of the sedimentation rate in ODP Hole 762C vs variations of the sea-level as estimated in Miller et al. (2005), Kominz et al. (2008) and Haq et al. (1987).

Table 1: Top depths, sub-bottom depths, estimated absolute ages and error margins of calcareous nannofossil, planktic and benthic foraminifera bio-events in ODP Hole 762C. (a) calcareous nannofossil bio-events, this study. (b) planktic foraminiferal bio-events, Howe et al. (2003). (c) benthic foraminiferal bio-events, Howe et al. (2003). (d) planktic foraminiferal bio-events, Campbell et al. (2004). (e) calcareous nannofossil bio-events, Campbell et al. (2004).

Table 2: Depth and estimated ages (2a), and mean durations (2b) of uppermost Cretaceous magnetochrons in ODP Hole 762C and comparison with the standard Geological Time Scale

(Gradstein et al., 2004). Table 2a modified after Husson et al. (2011). Note that the durations of C29r to C30n at ODP Hole 762C (2b) are consistent with the astronomical calibration of Husson et al. (2011). (*) The duration of chron C30r is doubtful because the base of this chron falls very near the identified 500 kyr gap and the cyclostratigraphic signal is distorted here (Fig. 5). Magnetochron durations and ages of upper Maastrichtian chron boundaries provided in Husson et al. (2011) are more precise with lower uncertainties and are rather adopted here for the chronostratigraphic framework of Figures 7-10. Magnetochron durations and ages of upper Campanian–lower Maastrichtian chron boundaries are based on Hole 762C in Husson et al. (2011). Comparison of these durations with the standard marine magnetic model is discussed in Husson et al. (2011).

Table 3: Description, top and bottom depths of $\delta^{13}C$ events in ODP Hole 762C. CMB: Campanian–Maastrichtian boundary.

Table 4: Top depths, sub-bottom depths, estimated absolute ages and durations of $\delta^{13}C$ events in ODP Hole 762C.

Plate 1: Calcareous nannofossils from the upper Campanian–Maastrichtian of ODP Hole 762C. 1, *Ahmuellerella octoradiata*, 53X-7, 1–2 cm. 2, *Amphizygus brooksii*, 49X-1, 61–62 cm. 3, *Biscutum coronum*, 44X-7, 14–15 cm. 4, *Biscutum constans*, 44X-4, 110–111 cm. 5, *Biscutum magnum*, 49X-1, 61–62 cm. 6, *Broinsonia parca constricta*, 49X-5, 124–125 cm. 7, *Broinsonia parca parca*, 55X-1, 66–67 cm. 8, *Calculites obscurus*, 51X-4, 11–12 cm. 9, *Ceratolithoides aculeus*, 50X-4, 101–102 cm. 10, *Ceratolithoides indiensis*, 43X-1, 33–34 cm. 11, *Ceratolithoides kamptneri*, 44X-3, 108–109 cm. 12 *Cribrocorona gallica*, 43X-1, 33–34 cm. 13, *Cribrosphaerella daniae*, 43X-1, 33–34 cm. 14, *Discorhabdus ignotus*, 49X-5, 35–

36 cm. 15, *Eiffellithus angustus*, 52X-3, 77–78 cm. 16, *Eiffellithus eximius*, 54X-7, 20–21 cm. 17, *Lithraphidites praequadratus*, 43X-1, 33–34 cm. 18, *Lithraphidites quadratus*, 44X-4, 110–111 cm. 19, *Micula murus*, 43X-2, 33–34 cm. 20, *Micula praemurus*, 43X-2, 83–84 cm. 21, *Micula prinsii*, 43X-2, 33–34 cm. 22, *Micula prinsii*, 43X-1, 33–34 cm. 23, *Monomarginatus quaternarius*, 49X-2, 82–83 cm. 24, *Nephrolithus frequens*, 43X-1, 33–34 cm. 25, *Petrarhabdus copulatus*, 49X-1, 9–10 cm. 26 and 27, *Petrarhabdus copulatus* (same specimen), 49X-5, 35–36 cm. 28, *Petrarhabdus vietus* 48X-4, 54–55 cm. 29, *Prediscosphaera mgayae*, 49X-1, 9–10 cm. 30, *Pseudomicula quadrata*, 43X-3, 66–67 cm. 31, *Quadrum gartneri*, 50X-2, 11–12 cm. 32, *Quadrum svabenickae*, 51X-4, 11–12 cm. 33, *Reinhardtites anthophorus*, 54X-6, 60–62 cm. 34, *Reinhardtites elegans*, 51X-6, 35–36 cm.

Plate 2: Calcareous nannofossils from the upper Campanian–Maastrichtian of ODP Hole 762C. 1, *Reinhardtites levis*, 51X-4, 11–12 cm. 2, *Rotelapillus laffittei*, 49X-1, 61–62 cm. 3, *Stoverius* cf. *S. achylosus*, 48X-6, 104–105 cm. 4, *Stoverius coangustatus*, 49X-2, 82–83 cm. 5, *Stoverius coangustatus*, 50X-4, 101–102 cm. 6, *Tortolithus hallii*, 53X-3, 101–102 cm. 7, *Tortolithus hallii*, 54X-7, 20–21 cm. 8, *Tranolithus orionatus*, 49X-4, 105–106 cm. 9, *Tranolithus orionatus*, 55X-1, 66–67 cm. 10, *Tranolithus stemmerikii*, 50X-5, 100–101 cm. 11, *Tranolithus stemmerikii*, 55X-1, 66–67 cm. 12, *Uniplanarius gothicus*, 49X-5, 35–36 cm. 13, *Uniplanarius gothicus*, 49X-3, 104–105 cm. 14, *Uniplanarius sissinghii* (very rare), 50X-3, 10–11 cm. 15, *Uniplanarius sissinghii*, 52X-3, 77–78 cm. 16, *Uniplanarius trifidus* short-rayed, 51X-3, 10–11 cm. 17, *Uniplanarius trifidus* medium-rayed, 49X-3, 89–90 cm. 18, *Uniplanarius trifidus* long-rayed (very rare), 52X-3, 77–78 cm. 19, *Watznaueria manivitiae* sensu stricto, 55X-1, 66–67 cm. 20, *Watznaueria manivitiae* sensu lato, 49X-4, 105–106 cm. 21, *Zeugrhabdotus bicrescenticus* (big form), 52X-6, 83–85 cm. 22, *Zeugrhabdotus bicrescenticus* (small form), 54X-1, 138–139 cm. 23, *Zeugrhabdotus diplogrammus*, 50X-1,

10–11 cm. 24, *Zeugrhabdotus diplogrammus*, 49X-3, 104–105 cm. 25, *Zeugrhabdotus erectus*, 49X-3, 38–39 cm. 26, curved spine, 53X-1, 12–13 cm. 27, curved spine, 52X-2, 112–113 cm.

Appendix 1: Values of inclination, paleomagnetic interpretation and additional remarks for the upper Campanian–Maastrichtian of ODP Hole 762C.

Appendix 2: Stratigraphic distribution of key and potential stratigraphic calcareous nannofossil markers in the upper Campanian-Maastrichtian of ODP Hole 762C. M: moderate preservation, P: poor preservation.

Appendix 3: Alphabetical list of calcareous nannofossil species considered in this study.

Appendix 4: Grey level values obtained for core photographs used for cyclostratigraphy. These data correspond to a resampling at a step of 1 cm. Adjusted depths (ambsf) and equivalent original depths (mbsf) are given along with cores, sections and identified 100 kyr and 405 kyr eccentricity cycles.

Appendix 5: Measured and standardized bulk carbonate $\delta^{13}C$ values for ODP Hole 762C with depths (mbsf), adjusted depths (ambsf) and calibrated absolute ages (Ma).

Appendix 6: Age-depth plot for ODP Hole 762C. Horizontal axis shows standard tropical/subtropical planktonic foraminiferal and calcareous nannofossil biozones correlated to the Gradstein and others (2004) Geologic Time Scale. A line of correlation is drawn through each of the counted 100 kyr cycles below the K-Pg boundary (numbers 1 to 83). Nine average calculated sedimentation rates (cm/kyr) are shown for each significant change in slope of the line of correlation. Grey-shaded squares represent the uncertainties of magnetic polarity reversals.

Appendix 7: Exmouth Plateau age model based on Hole 762C versus a conventional age model based on Gradstein et al. (2004) and Huber et al. (2008) (Huber, B.T., MacLeod, K.G., Tur, N.A., 2008. Chronostratigraphic framework for upper Campanian-Maastrichtian sediments on the Blake Nose (Subtropical North Atlantic). J. Foraminiferal Res. 38, 162–182). FO of *M. murus* at mid-latitudes (1) and low-latitudes (2) after Thibault et al. (2010). Thick grey lines of correlation indicate reliable biostratigraphic datums. Calcareous plankton diachronism is compelling.

Figure1

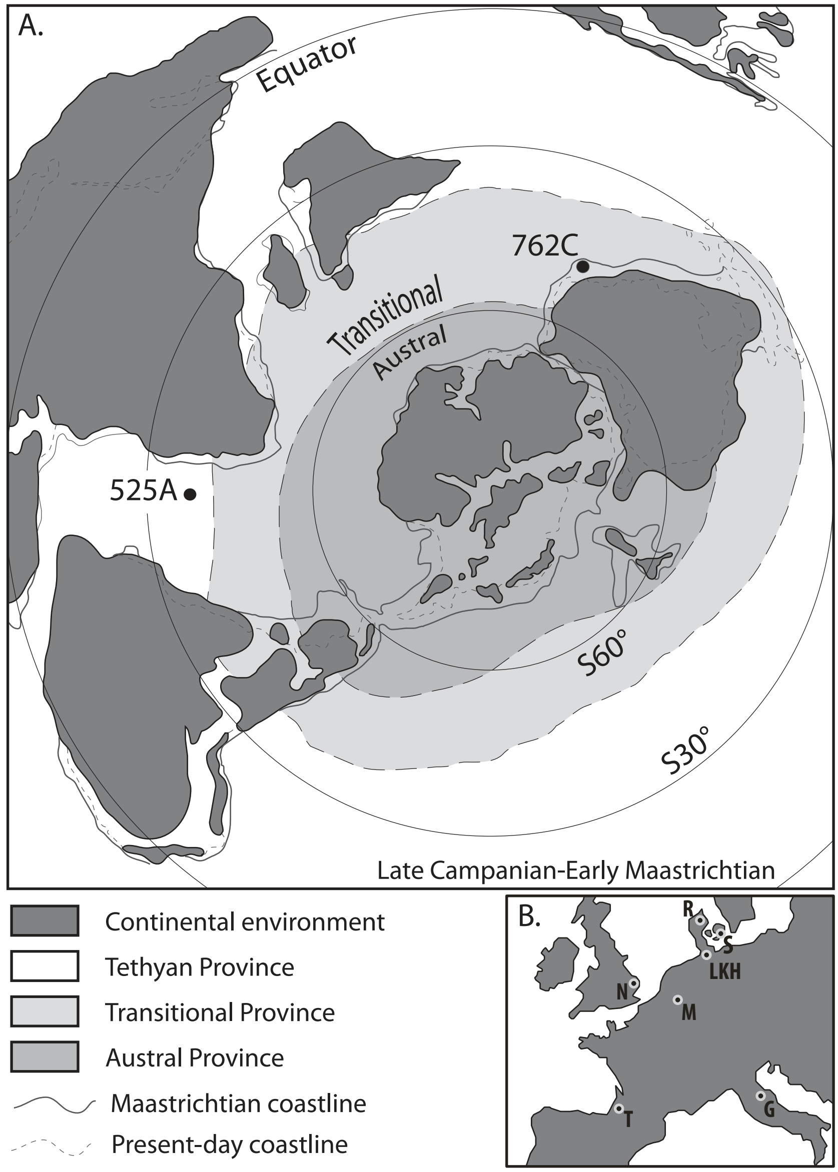

Figure 1 : A. Palaeogeographic reconstruction of the Southern Hemisphere for the upper Campanian-lower Maastrichtian showing the location of ODP Hole 762C, DSDP Hole 525A, and the inferred palaeobiogeographical boundaries between the Austral, Transitional and Tethyan provinces (from Huber, 1992a). B. Map of Europe showing other important locations of Campanian-Maastrichtian sections. G: Gubbio, LKH: Lägerdorf – Kronsmoor – Hemmoor, M: Maastricht, N: Norfolk, R: Rørdal, S: Stevns-1, T: Tercis les Bains.

Figure2

Click here to download high resolution image

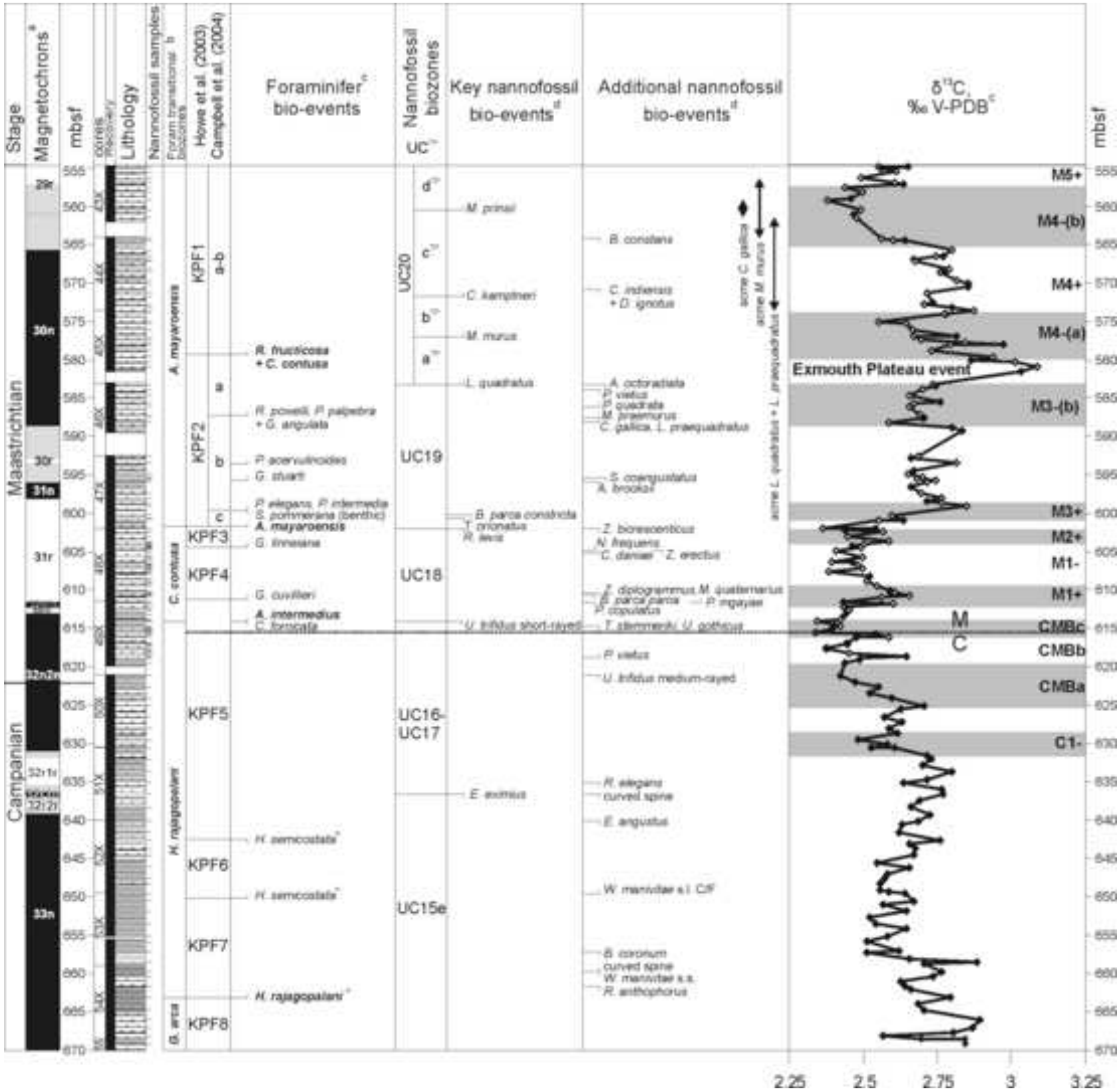

Figure3

Click here to download high resolution image

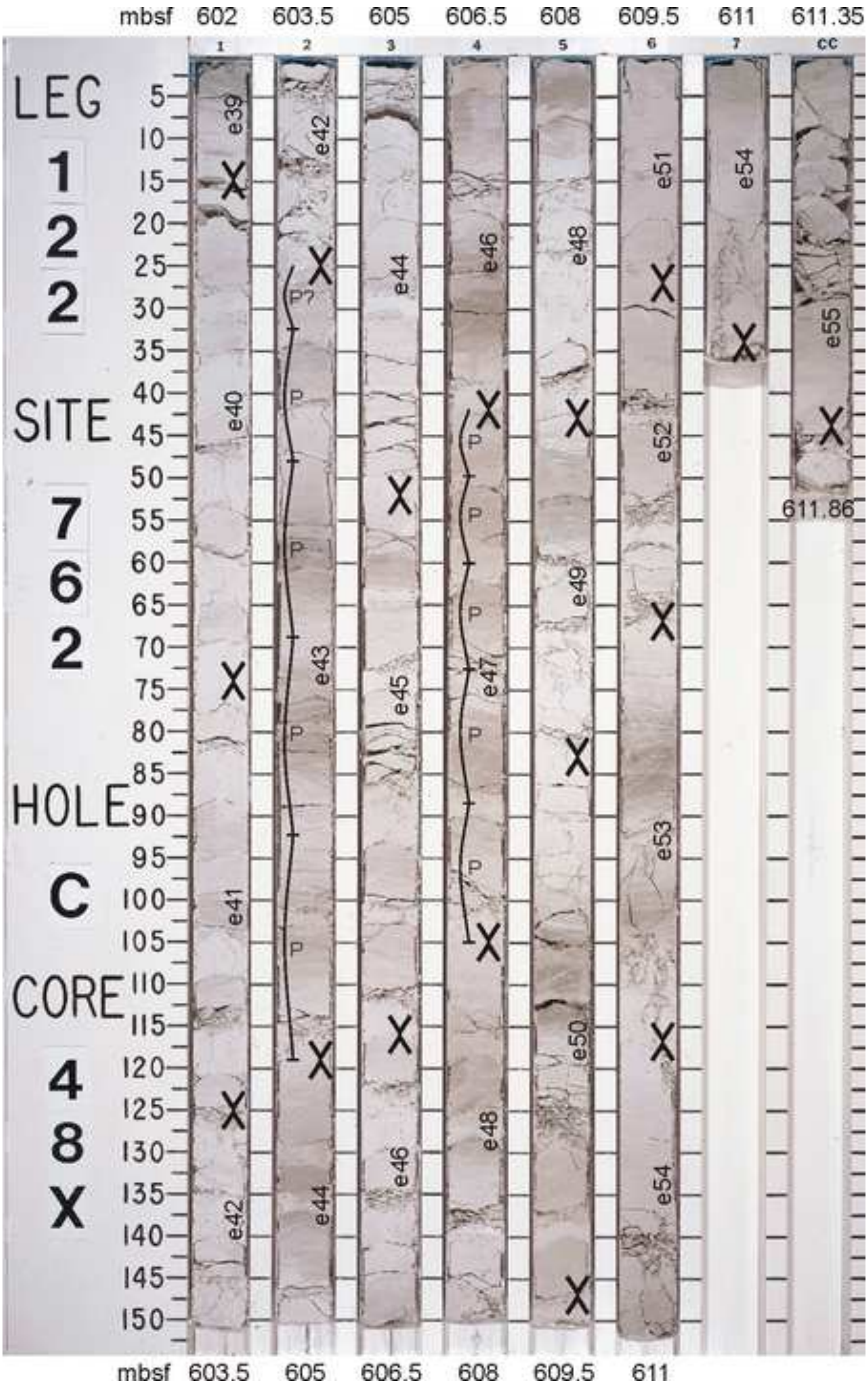

Figure3BW

Click here to download high resolution image

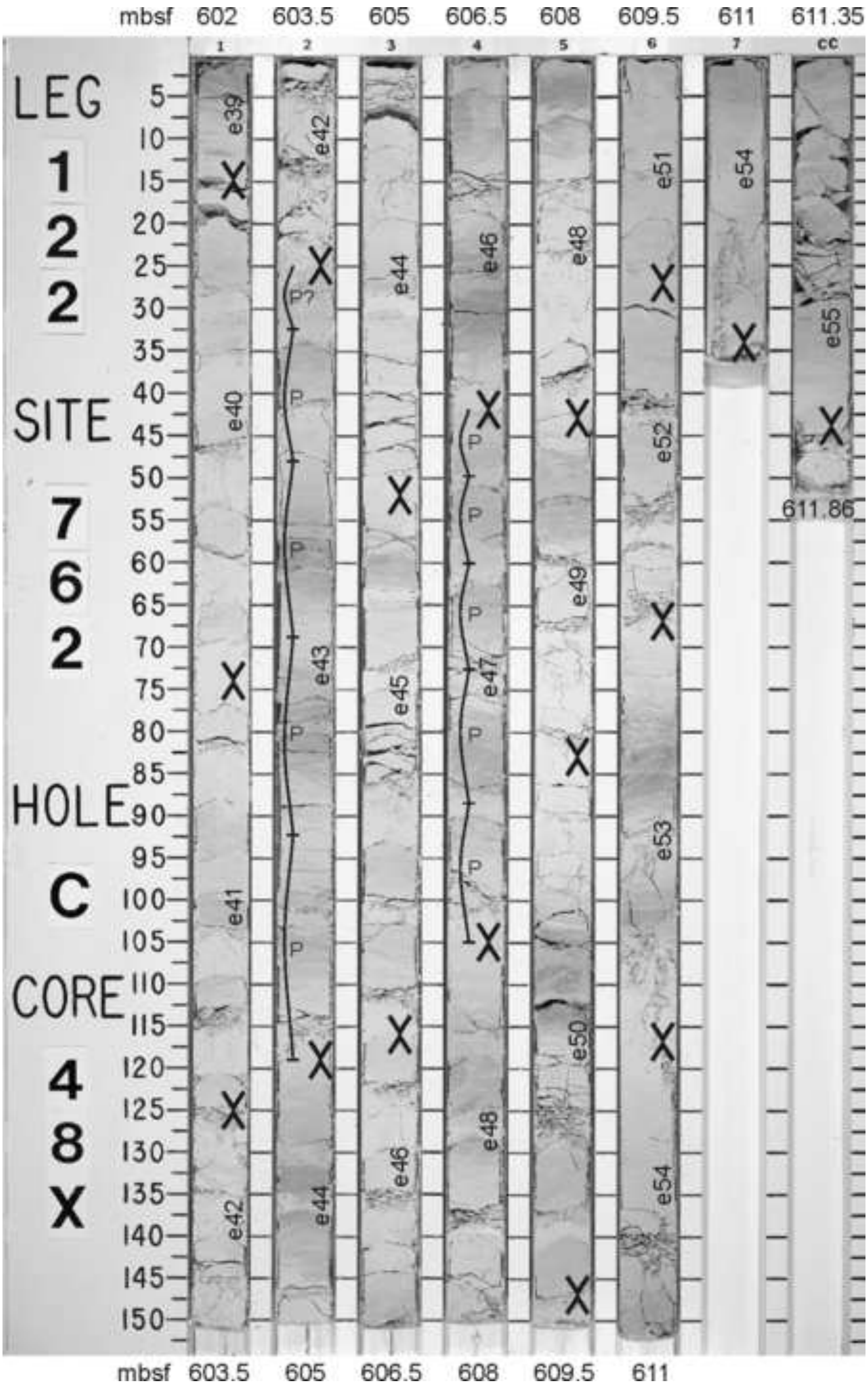

Figure4

Click here to download high resolution image

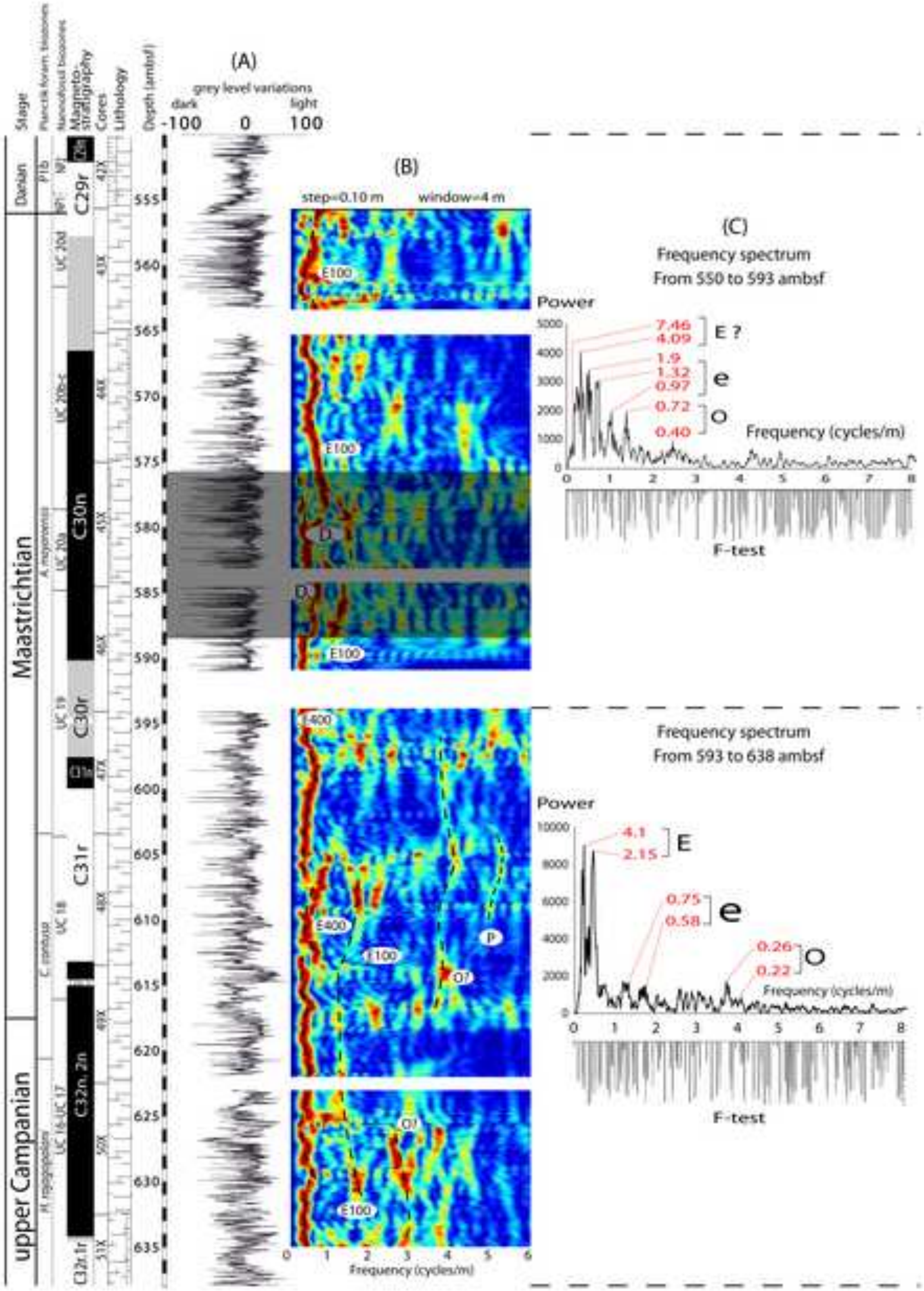

Figure4BW
Click here to download high resolution image

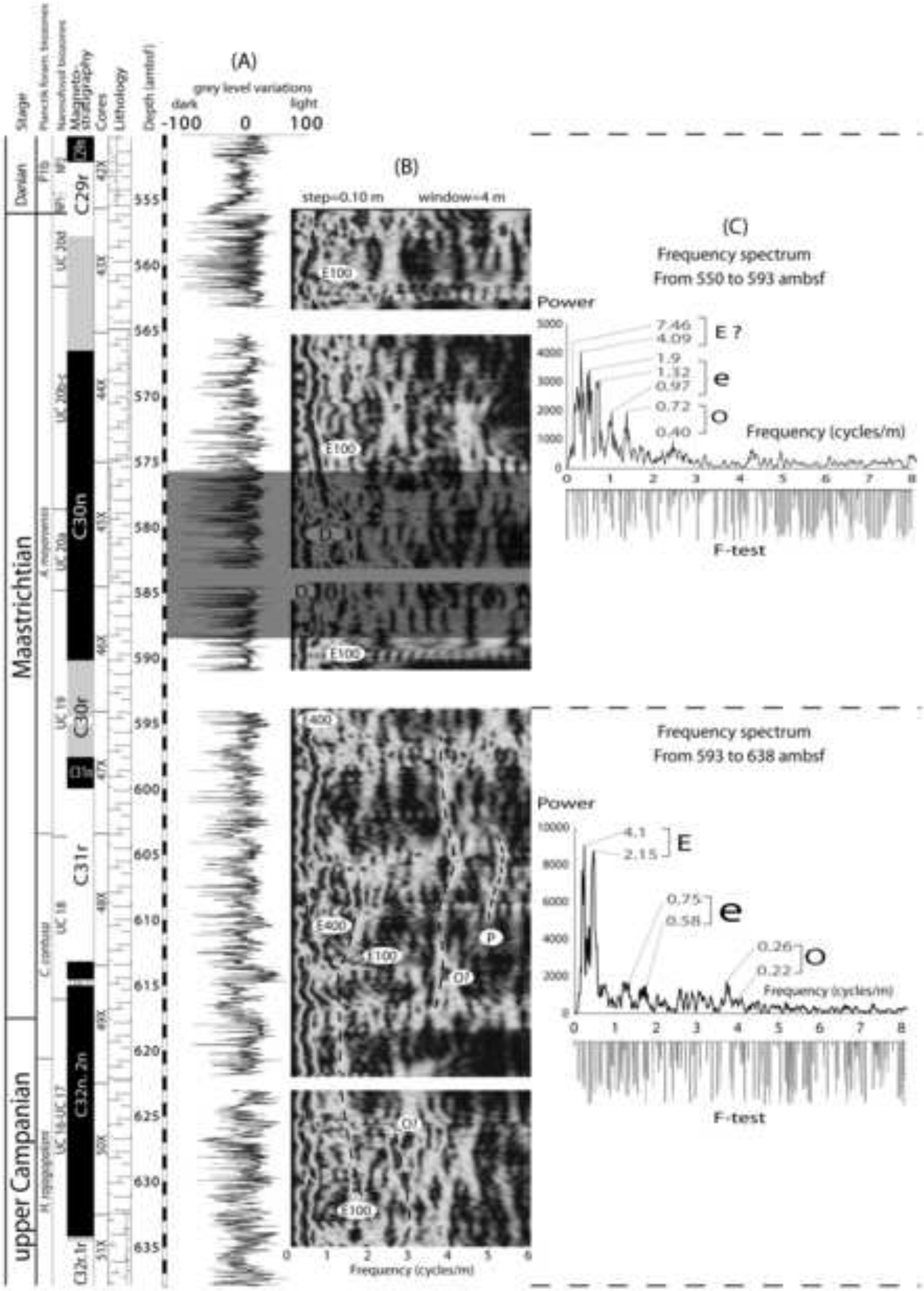

Figure 5

Click here to download high resolution image

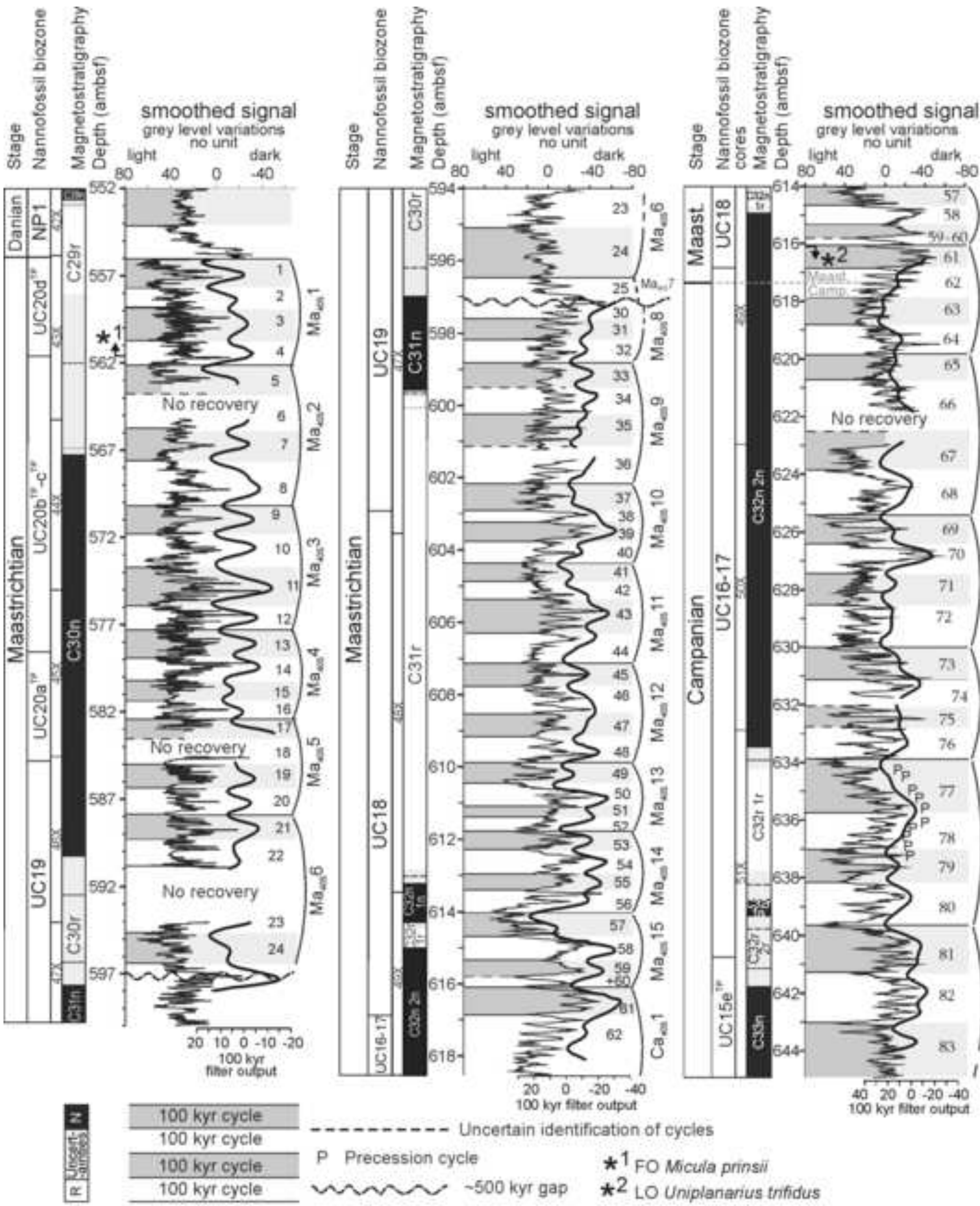

Figure6
Click here to download high resolution image

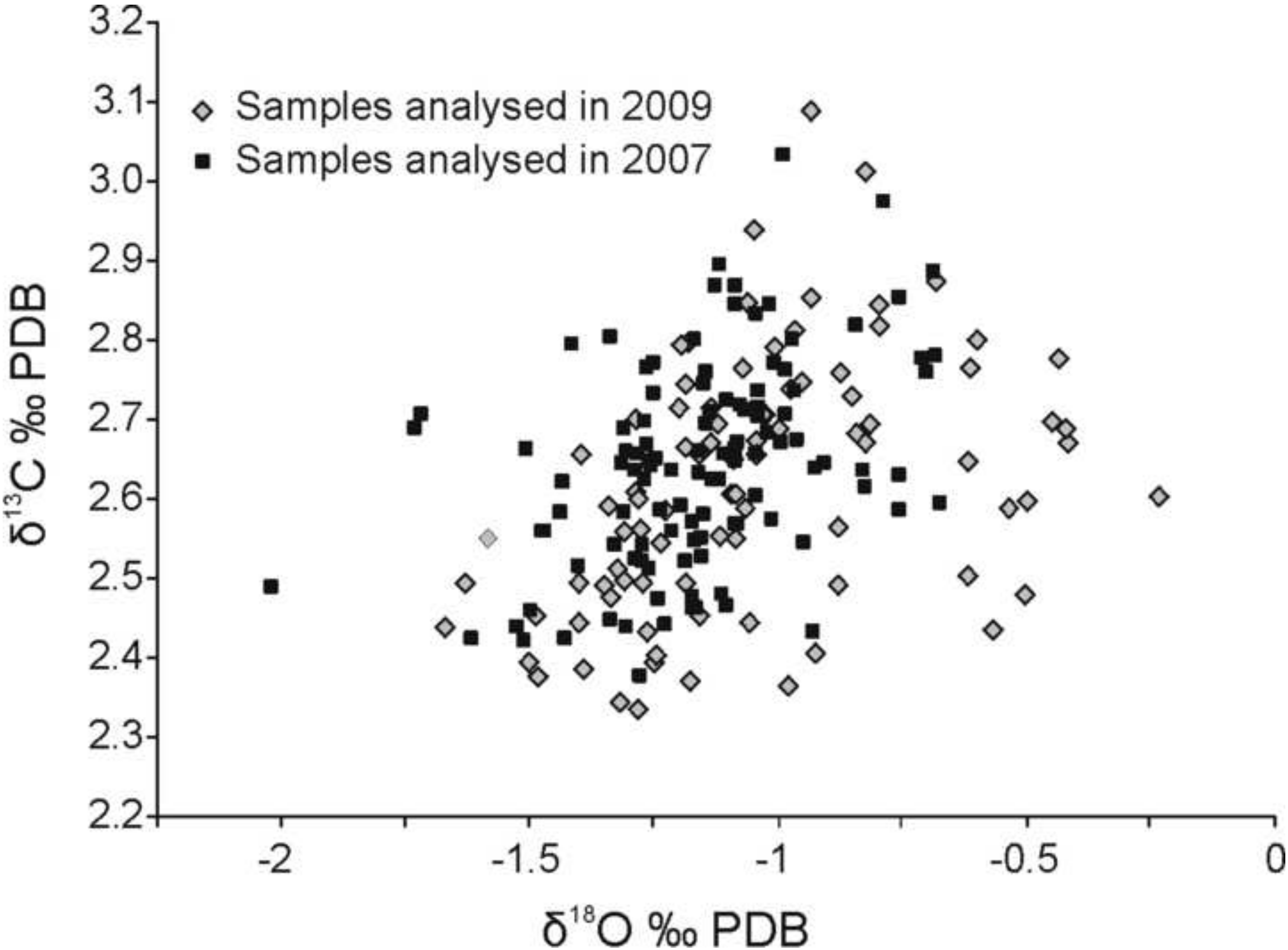

Figure7

Click here to download high resolution image

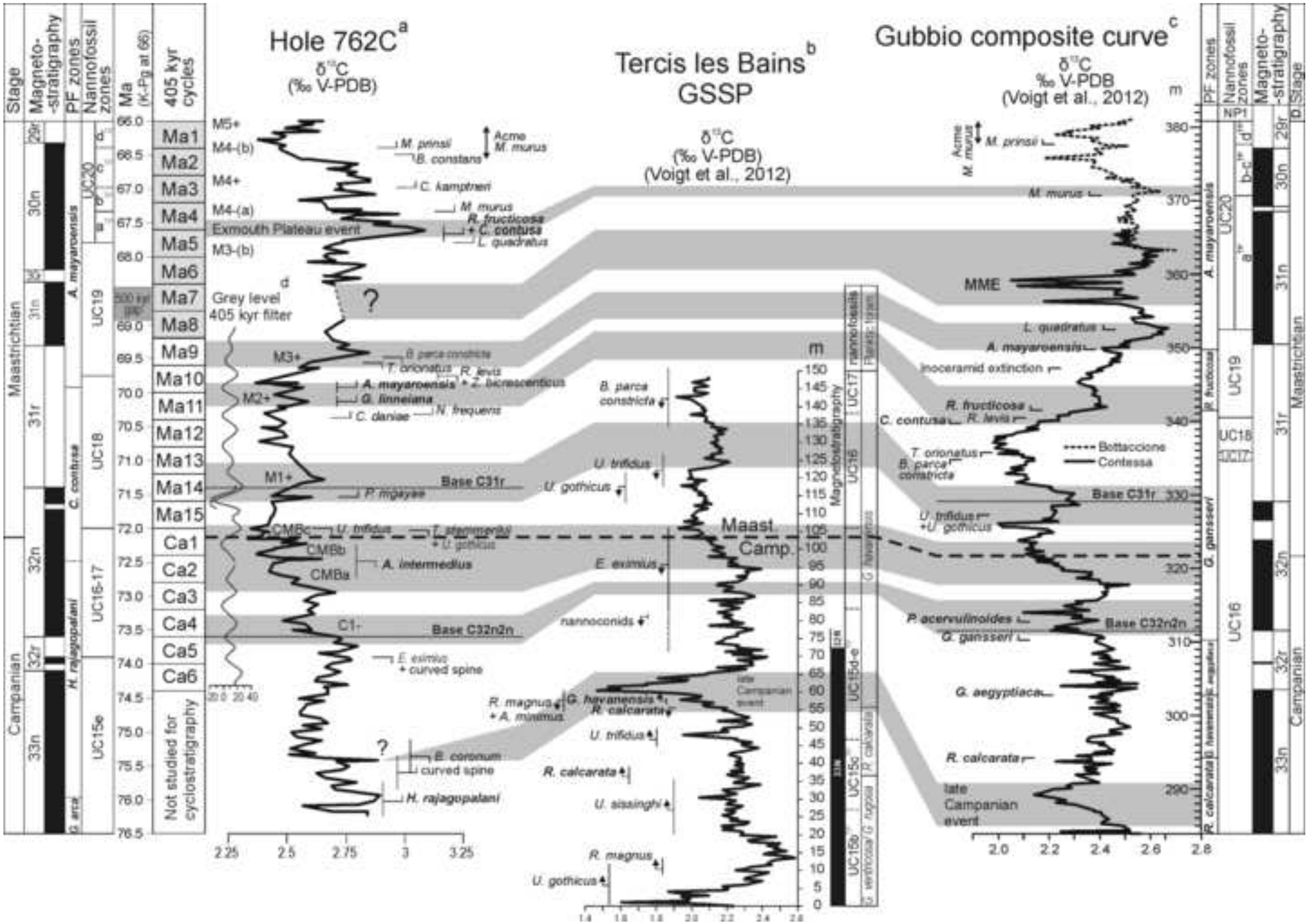

Figure 8
Click here to download high resolution image

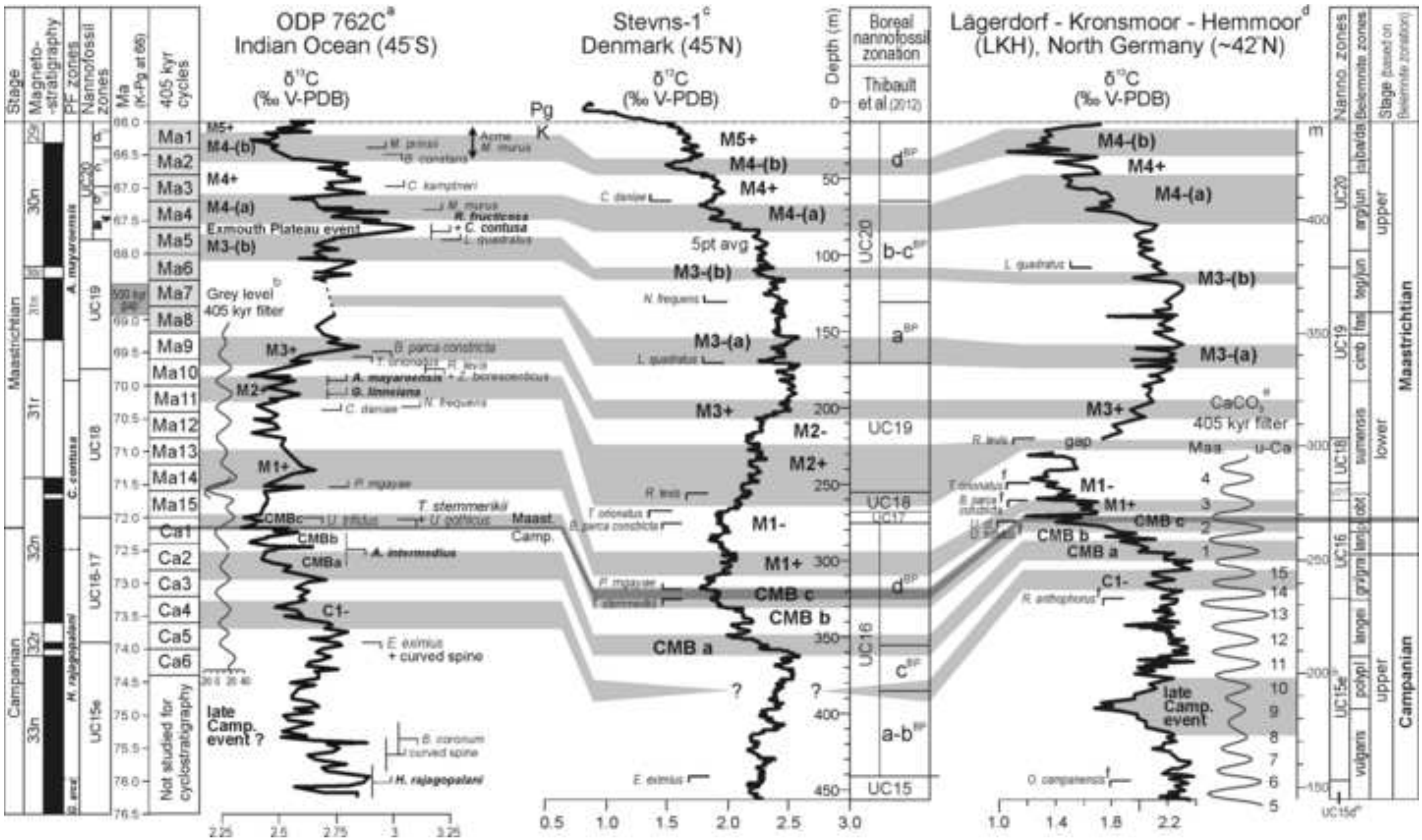

Figure 9

Click here to download high resolution image

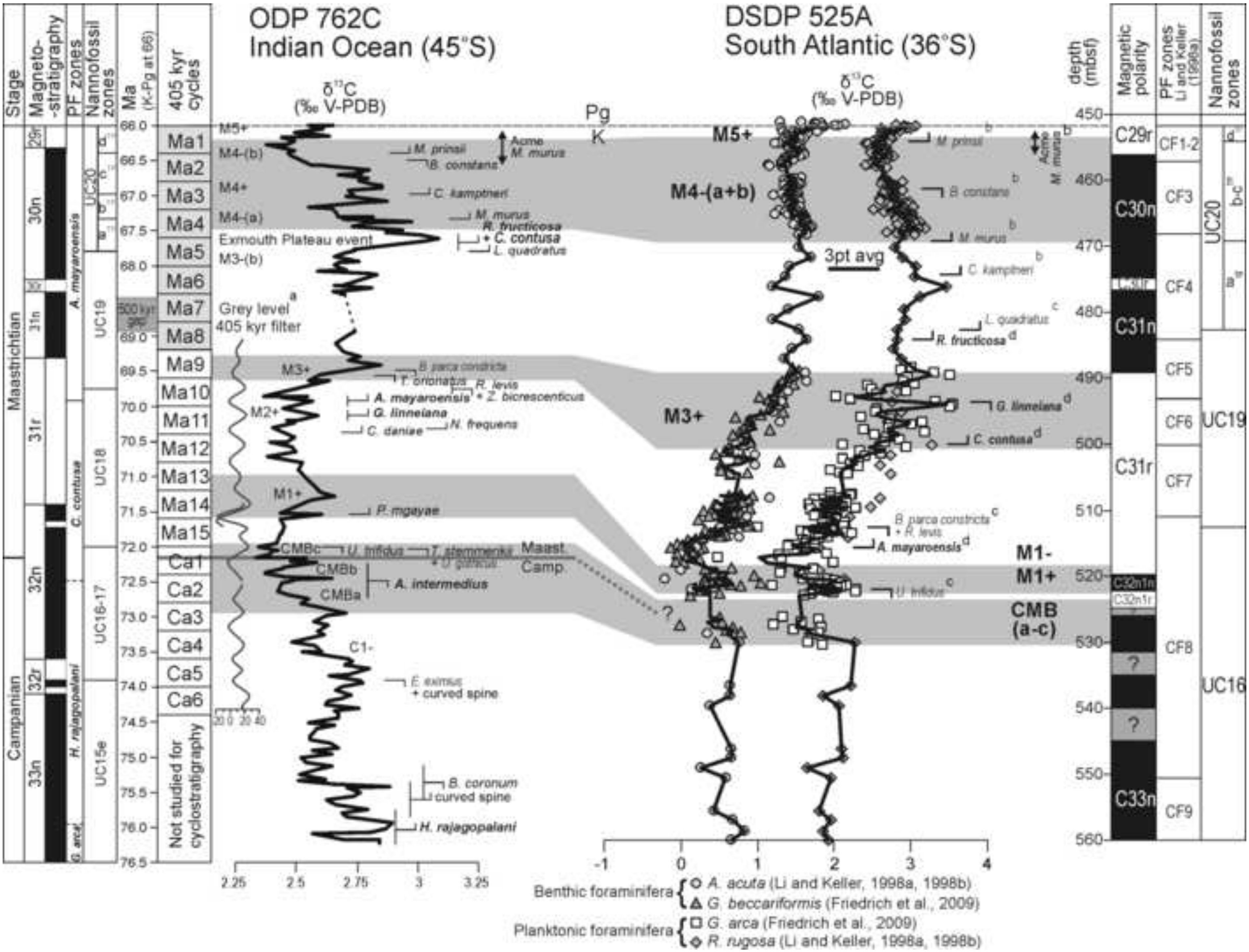

Figure 10

Click here to download high resolution image

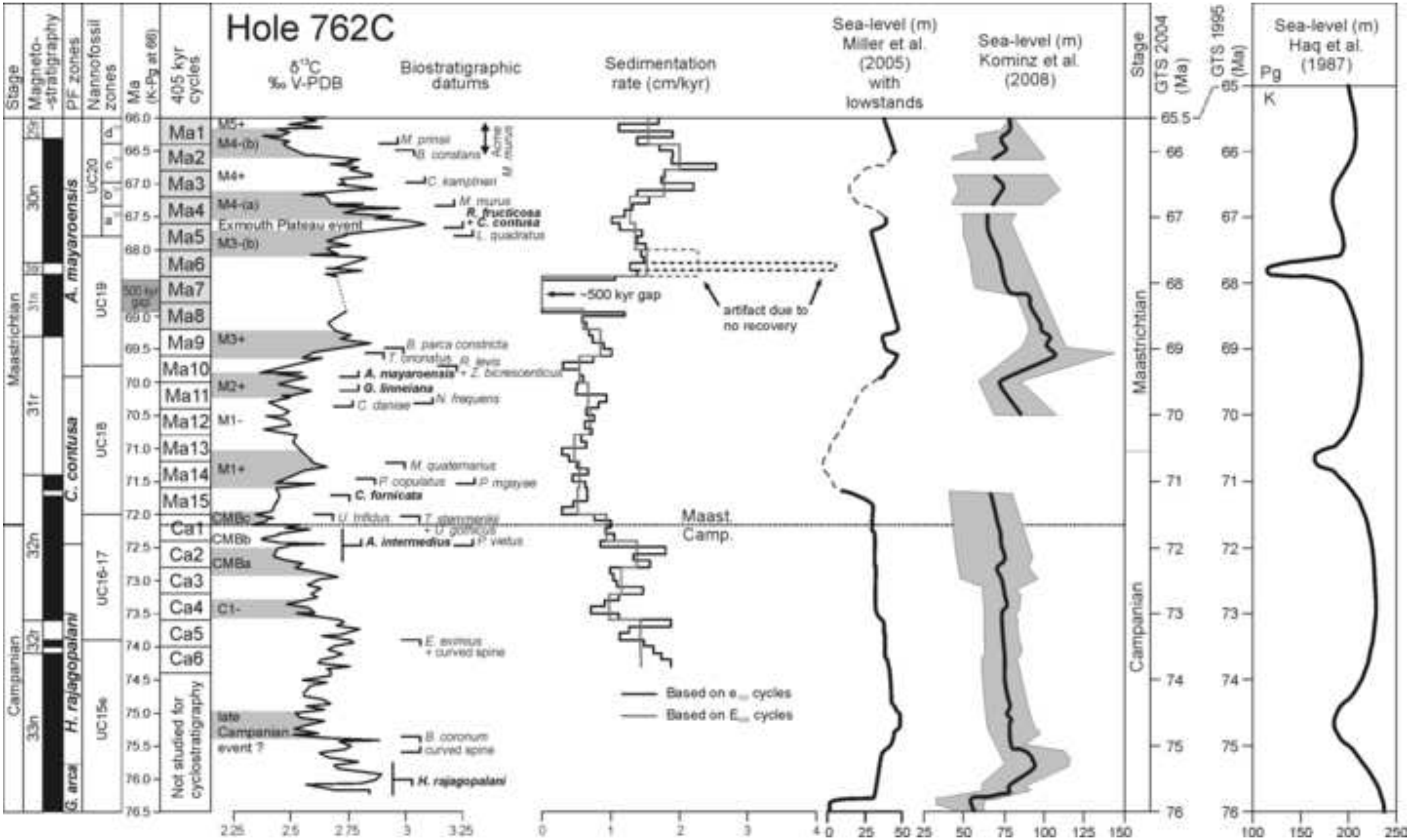

Plate1

Click here to download high resolution image

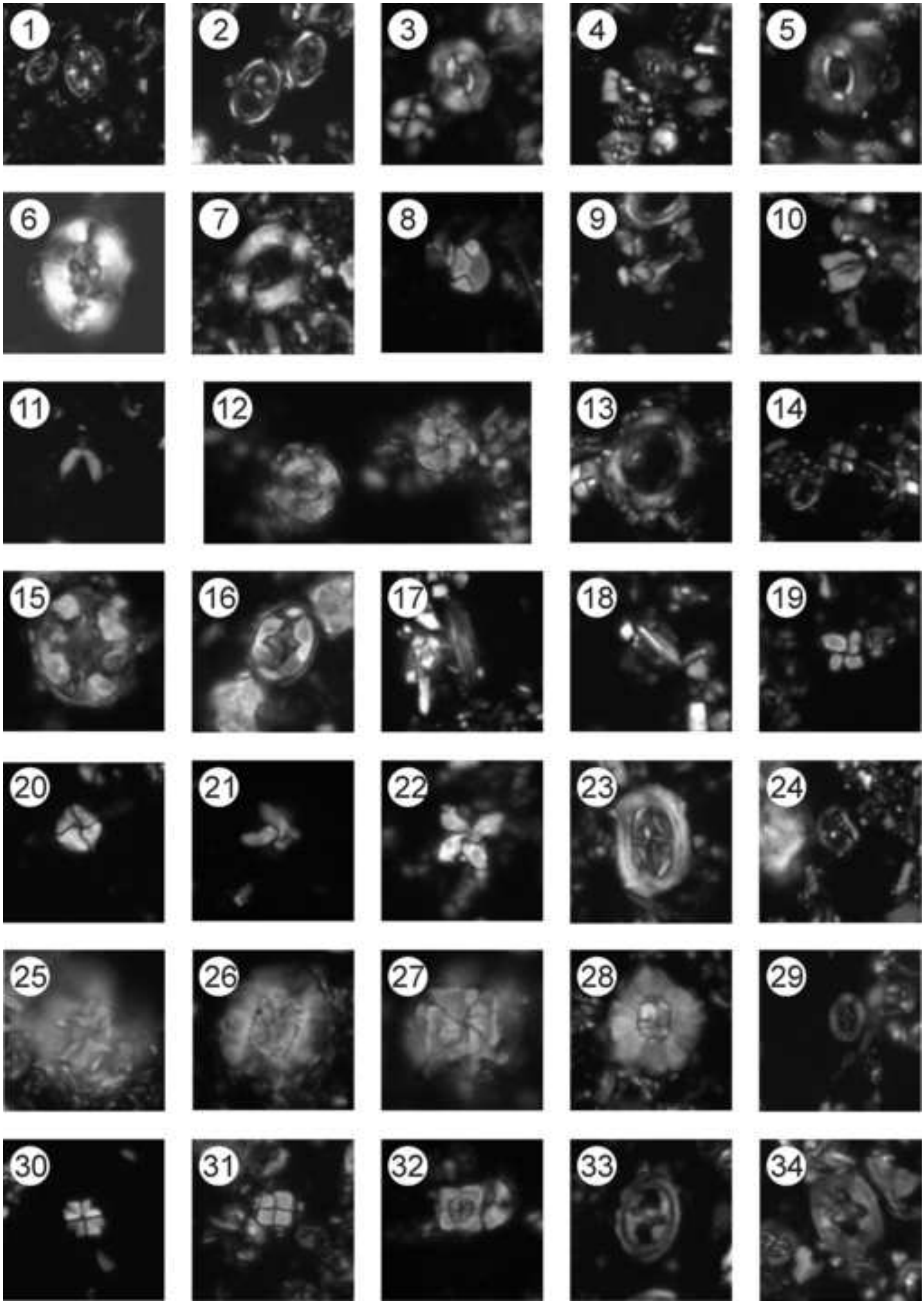

Plate2

Click here to download high resolution image

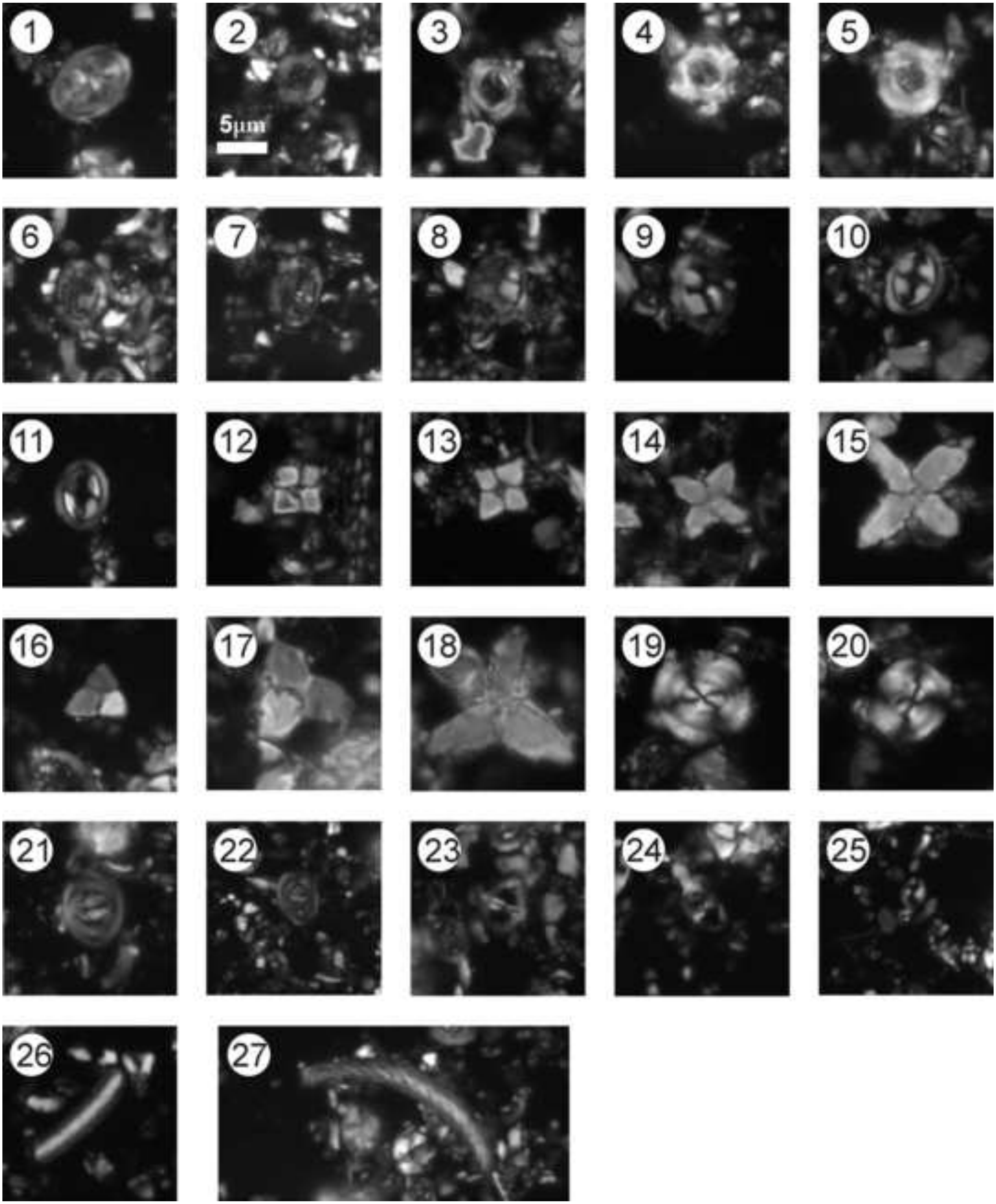

Table1
Click here to download Table: Table1-biostrat events.xls

Events	Top depth (mbsf)	Bottom depth (mbsf)	Top depth (ambsf)	Bottom depth (ambsf)	Age (Ma) with K/Pg at 66 Ma	Uncertainty (Ma)
K-Pg boundary	554.80	554.80	556.03	556.03	66.00	-
Top Acme *M. murus*[a]	555.51	556.33	556.74	557.56	66.07	±0.06
Top Acme *C. gallica*[a]	558.16	559.08	559.39	560.31	66.24	±0.07
FO *M. prinsii*[a]	560.46	561.40	561.69	562.63	66.39	±0.07
Base Acme *C. gallica*[a]	560.46	561.40	561.69	562.63	66.39	±0.06
Top Acme *L. quadratus*[a] & *L. praequadratus*[a]	560.46	561.40	561.69	562.63	66.39	±0.06
LO *B. constans*[a]	561.40	564.14	562.63	565.37	66.49	±0.1
Base Acme *M. murus*[a]	564.14	564.42	565.37	565.65	66.56	±0.04
LO *C. indiensis*[a], *D. ignotus*[a]	569.60	570.80	570.83	572.03	66.87	±0.07
FO *C. kamptneri*[a]	571.70	572.78	572.93	574.01	66.98	±0.1
Base Acme *L. quadratus*[a] & *L. praequadratus*[a]	573.60	573.97	574.83	575.20	67.07	±0.05
FO *M. murus*[a]	576.99	577.83	578.54	579.38	67.33	±0.07
FO *R. fructicosa*[b], *C. contusa*[b]	579.30	584.00	580.85	585.55	67.66	±0.22
FO *L. quadratus*[a], LO *A. octoradiata*[a]	583.20	583.89	584.75	585.44	67.79	±0.06
LO *P. vietus*[a]	583.20	583.89	584.75	585.44	67.79	±0.06
FO *P. quadrata*[a]	586.10	587.21	587.65	588.76	68.02	±0.08
FO *P. palpebra*[b], *G. angulata*[b], *R. powelli*[b]	587.20	593.60	588.75	595.15	68.18	±0.18
FO *M. praemurus*[a]	587.55	588.15	589.10	589.70	68.07	±0.05
FO *L. praequadratus*[a], *C. gallica*[a]	588.15	592.59	589.70	594.14	68.18	±0.13
FO *P. acervulinoides*[b]	593.60	595.70	595.15	597.25	68.36	±0.08
LO *S. coangustatus*[a]	595.28	595.40	596.83	596.95	68.40	±0.04
LO *A. brooksii*[a]	595.65	595.90	597.20	597.45	68.95	±0.06
FO *G. stuarti*[b]	595.70	599.60	597.25	601.15	69.30	±0.12
LO *B. parca constricta*[a]	599.09	600.23	600.64	601.78	69.48	±0.1
FO *P. elegans*[b], *P. intermedia*[b], LO *S. pommerana*[c]	599.60	600.60	601.15	602.15	69.54	±0.09
LO *T. orionatus*[a]	600.23	600.66	601.78	602.21	69.56	±0.07
LO *R. levis*[a], *Z. bicrescenticus*[a]	600.83	602.04	602.44	603.65	69.75	±0.15
FO *A. mayaroensis*[b]	601.70	603.00	603.31	604.61	69.92	±0.15
LO *G. linneiana*[b]	603.00	604.40	604.61	606.01	70.13	±0.14
LO *Z. erectus*[a]	604.64	604.82	606.25	606.43	70.28	±0.05
FO *N. frequens*[a]	604.82	605.20	606.43	606.81	70.32	±0.06
FO *C. daniae*[a]	605.20	605.57	606.81	607.18	70.37	±0.06
LO *M. quaternarius*[a], *Z. diplogrammus*[a]	610.18	610.37	611.79	611.98	71.22	±0.05
LO *B. parca parca*[a]	610.54	610.67	612.15	612.28	71.28	±0.05
LO *P. copulatus*[a]	610.97	611.59	612.94	613.56	71.46	±0.09
FO *P. mgayae*[a]	611.59	611.79	613.56	613.76	71.54	±0.05
FO *G. cuvillieri*[d,] LO *C. fornicata*[d]	611.20	614.10	613.17	616.07	71.71	±0.3
LO *U. trifidus* short-rayed[a]	614.00	614.12	615.97	616.09	72.00	±0.05
LO *T. stemmeriki*[a], *U. gothicus*[a]	614.12	614.70	616.09	616.67	72.03	±0.07
Campanian-Maastrichtian boundary level	-	615.40	-	617.37	72.15	±0.05
FO *A. intermedius*[d]	614.10	624.00	616.07	625.97	72.48	±0.39
FO *P. vietus*[a]	618.82	618.85	620.79	620.82	72.47	±0.04
LO *U. trifidus* medium-rayed[a]	619.50	621.11	621.47	623.08	72.57	±0.09
LO *R. elegans*[a]	633.61	635.12	635.96	637.47	73.80	±0.06
LO *E. eximius*[a], curved spine[a]	635.12	636.60	637.47	638.95	73.90	±0.09
LO *H. semicostata*[d]	637.10	642.50	639.45	645.12	74.20	±0.23
LO *E. angustus*[a]	638.36	640.11	640.71	642.46	74.15	±0.06
W. manivitae[a] s.l. C/F	648.35	649.63	650.97	652.25	74.83	±0.4
LO *B. coronum*[a]	655.91	657.19	658.53	659.81	75.36	±0.4
LO *W. manivitae*[a] s.s.	658.52	659.77	661.14	662.39	75.54	±0.4
FO curved spine[a]	659.77	660.39	662.39	663.01	75.60	±0.4
LO *R. anthophorus*[a]	660.39	661.72	663.01	664.34	75.67	±0.4
FO *H. rajagopalani*[d]	663.2	670.2	665.82	672.82	76.06	±0.4

Table 1

Table2
Click here to download Table: Table2-magnetostratigraphy.xls

Events	depth (mbsf)	ambsf	GTS2004	Husson et al. (2011)	
				Ref. Site	Option 2
K-Pg boundary	554.8	556.03	65.500	1267B	66±0.07
C29r/C30n	560.91+/-4.41	562.14	65.861	1267B	66.3±0.08
C30n/C30r	590.79 +/-2.15	592.34	67.696	1267B	68.2±0.08
C30r/C31n	594.72 +/-1.21	596.27	67.809	525A	68.32±0.07
C31n/C31r	598.16 +/-0.04	599.71	68.732	525A	69.22±0.07
C31r/C32n1n	611.46 +/-0.06	613.07	70.961	762C	71.4±0.08
C32n1n/C32n1r	612.37 +/-0.18	614.34	71.225	762C	71.64±0.07
C32n1r/C32n2n	612.975 +/-0.075	614.95	71.474	762C	71.72±0.07
C32n2n/C32r1r	631.475 +/-0.395	633.83	72.929	762C	73.6±0.08
C32r1r/C32r1n	635.885 +/-0.465	638.24	73.231	762C	73.9±0.09
C32r1n/C32r2r	637.39 +/-0.45	639.74	73.318	762C	74±0.08
C32r2r/C33n	638.78 +/-0.35	641.13	73.577	762C	74.1±0.08

Table 2a

Magnetochron	Duration in this study (Ma)	Husson et al. (2011)	GTS2004
C29r (Cretaceous)	0.397+/-0.22	0.3+/-0.02	0.361
C30n	1.798+/-0.16	1.9+/-0.03	1.835
C30r	0.173+/-0.07*	~0.12	0.113
C31n	-	~0.9	0.923
C31r	2.18+/-0.03	*id.*	2.229
C32n1n	0.240+/-0.06	*id.*	0.264
C32n1r	0.08+/- 0.03	*id.*	0.249
C32n2n	1.88 +/- 0.03	*id.*	1.456
C32r1r	0.3+/-0.06	*id.*	0.301
C32r1n	0.1+/-0.03	*id.*	0.087
C32r2r	0.1 +/- 0.04	*id.*	0.259

Table 2b

Table3
Click here to download Table: Table3-description of 13C events.xls

Carbon-isotope events	Stratigraphic interval	Top depth (mbsf)	Bottom depth (mbsf)	Description
M5+	upper Maastrichtian	554.80	557.36	Rapid 0.2‰ increase up to values around 2.6‰
M4-(b)	upper Maastrichtian	557.36	565.27	Sharp 0.4‰ negative decrease reaching a minimum value of 2.38‰
M4+	upper Maastrichtian	565.27	573.79	Positive 0.25‰ rebound with values fluctuating around 2.77‰
M4-(a)	upper Maastrichtian	573.79	579.93	Fluctuating values resulting in a progressive 0.55‰ decrease from 3.1 to 2.55‰
Exmouth Plateau event	upper Maastrichtian	579.93	583.20	Sharp 0.4‰ positive excursion up to values of 3.1‰
M3-(b)	upper Maastrichtian	583.20	588.75	Short-lived 0.1‰ negative excursion from values around 2.8 to values around 2.7‰
M3+	lower Maastrichtian	598.48	600.89	Rapid 0.3‰ increase up to 2.85‰
M2+	lower Maastrichtian	602.05	604.43	short-lived 0.1‰ positive excursion with values fluctuating around 2.55‰
M1-	lower Maastrichtian	604.43	609.45	Slight 0.1‰ negative excursion with values fluctuating gently around 2.45‰
M1+	lower Maastrichtian	609.45	612.11	Values increase from 2.45 to 2.7‰
CMB c	CMB	613.84	615.66	Third step of CMBE characterized by a 0.3‰ negative shift from 2.6 to 2.3‰
CMB b	upper Campanian	615.66	619.50	Second step of CMBE characterized by rapid fluctuations between 2.4 and 2.6‰
CMB a	upper Campanian	619.50	625.34	First step of CMBE characterized by a 0.3‰ negative shift from 2.7 to 2.4‰
C1-	upper Campanian	628.50	631.70	0.25‰ negative excursion from 2.75 to 2.5‰, immediataly followed by a 0.15‰ positive rebound
late Campanian event ?	upper Campanian	650.80	658.05	long-lasting 0.2‰ negative excursion with values shifting from an average of 2.8‰ to c. 2.6‰

Table 3

Table4
Click here to download Table: Table4-age of C13 events.xls

Carbon isotope Events	Top depth (mbsf)	Base depth (mbsf)	Top depth (ambsf)	Base depth (ambsf)	Age (Ma), K-Pg at 66		Duration (Ma)
					Top	Base	
M5+	554.80	557.36	556.03	558.59	66.00	66.16	0.16
M4-(b)	557.36	565.27	558.59	566.50	66.16	66.60	0.44
M4+	565.27	573.79	566.50	575.34	66.60	67.11	0.51
M4-(a)	573.79	579.93	575.34	581.48	67.11	67.54	0.43
Exmouth Plateau event	579.93	583.20	581.48	584.75	67.54	67.77	0.23
M3-(b)	583.20	588.75	584.75	590.30	67.77	68.11	0.34
M3+	598.48	600.89	600.03	602.44	69.34	69.64	0.30
M2+	602.05	604.43	603.66	606.04	69.87	70.24	0.38
M1-	604.43	609.45	606.04	611.06	70.24	71.04	0.80
M1+	609.45	612.11	611.06	614.08	71.04	71.62	0.57
CMBc	613.84	615.66	615.81	617.63	71.94	72.16	0.22
CMBb	615.66	619.50	617.63	621.47	72.16	72.52	0.35
CMBa	619.50	625.34	621.47	627.31	72.52	72.95	0.43
C1-	628.50	631.70	630.47	633.67	73.28	73.57	0.29
late Campanian event ?	650.80	658.05	653.42	660.67	74.96	75.40	0.44

Table 4

Samples	Depth mbsf	Inclination (°)	Chrons	Paleomagnetic Interpretation	Remarks	ambsf
ODP Leg 122 Hole 762C						
42X4, 80	550.3	-58		C29n		
42X5, 75	551.76	-2		?		
42X5, 130	552.3	11				
42X6, 25	552.75	6				
42X6, 136	553.86	29		**C29r**		
43X1, 41	554.91	41			**K-Pg at 554.8 mbsf**	
43X1, 100	555.5	53				
43X2, 50	556.5	20	C29r base of Galbrun (1992) does not fit with the FO of *M. prinsii*			557.73
43X2, 110	557.1	-40	weak			558.33
43X3, 42	557.92	-55	?			
43X3, 141	558.91	-18	weak			
43X4, 20	559.2	-12	weak			
43X4, 113	560.13	-22	weak	?	FO *Micula prinsii* at 560.46 mbsf	
43X5, 22	560.72	3	weak			
43X5, 96	561.46	-23	weak			
44X1, 51	564.51	-59	?			
44X1, 132	565.32	52	C29r larger uncertainty			566.55
44X2, 52	566.02	-56	C30n			567.25
44X2, 132	566.83	-76				
44X3, 126	568.26	-46				
44X4, 95	569.45	-49				
44X5, 102	571.02	-62				
44X6, 67	572.17	-44				
45X1, 29	573.79	-61				
45X2, 112	576.12	-58				
45X3, 86	577.36	-65				
45X4, 60	578.6	-23		**C30n**		
45X4, 111	579.11	-32				
45X5, 24	579.74	-13				
45X5, 110	580.6	-64				
46X1, 44	583.44	-61				
46X1, 120	584.2	-9				
46X2, 41	584.91	34				
46X2, 117	585.67	-42				
46X3, 45	586.45	-44				
46X3, 117	587.17	-52				
46X4, 38	587.88	-49				
46X4, 114	588.64	-57	C30n		No recovery interval between 589.5 and 592.5 mbsf	590.19
47X1, 44	592.94	55	C30r	**C30r**		594.49
47X2, 101	593.51	18	C30r		~500 kyr gap around 595.45 mbsf	595.06
47X3, 43	595.93	-16	C31n			597.48
47X3, 95	596.45	-73				
47X4, 48	597.48	-34		**C31n**		
47X4, 89,5	597.89	-48				
47X4, 112	598.12	-62	C31n			599.67
47X4, 120	598.2	57	C31r			599.75
47X4, 140	598.4	75				
47X5, 4	598.54	48				
47X5, 19	598.69	52				
47X5, 32	598.82	70				
47X5, 39,5	598.89	64				
47X5, 46	598.96	75				
47X5, 101	599.51	63				
47X6, 40	600.4	83		**C31r**		
48X1, 54	602.54	80				
48X2, 36	603.86	58				
48X3, 30	605.3	67				
48X4, 65	607.15	67				
48X5, 131	609.31	63				
48X6, 47	609.97	63				
48X7, 30	611.31	66				
48XCC, 6	611.4	57	C31r			613.01
48XCC, 18	611.52	-42	C32n1n			613.13
49X1, 10	611.6	-25				

49X1, 26,5	**611.76**	**-14**			
49X1, 37	**611.87**	**-45**		**C32n1n**	
49X1, 48	611.98	-24			
49X1, 58	**612.08**	**-40**			
49X1, 78	**612.28**	**-48**	C32n1n		614.25
49X1, 96	**612.46**	**31**	C32n1r		614.43
49X1, 118	612.68	52		**C32n1r**	
49X1, 122	**612.72**	**56**			
49X1, 142,5	**612.92**	**56**	C32n1r		614.89
49X2, 3,5	**613.03**	**-70**	C32n2n		615
49X2, 20,5	**613.2**	**-45**			
49X2, 49,5	**613.42**	**-55**			
49X2, 45	613.45	-51			
49X2, 117	614.17	-40			
49X3, 46	614.96	53		very small reverse within C32n2n ?	
49X3, 109	615.59	-54			
49X4, 50	616.5	-49			
49X4, 111	617.11	-59			
49X5, 41	617.91	-63		**C32n2n**	
49X5, 108	618.58	-59			
50X1, 47	621.47	-15			
40X1, 113	622.14	-44			
50X2, 102	623.52	-58			
50X3, 98	624.98	-55			
50X4, 104	626.54	-59			
50X5, 47	627.47	-56			
50X6, 121	629.71	-66			
50X7, 37	630.38	-69			
51X1, 58	631.08	-46	C32n2n		633.43
51X1, 135	631.87	38	C32r1r		634.22
51X2, 141	633.41	41		**C32r1r**	
51X3, 117	634.67	68			
51X4, 42	635.42	70	C32r1r		637.77
51X4, 135	636.35	-30	C32r1n	**C32r1n**	638.7
51X5, 44	636.94	-23	C32r1n		639.29
51X5, 133	637.84	8	C32r2r	**C32r2r**	640.19
51X6, 43	638.43	8	C32r2r		640.78
51X6, 112	639.13	-32	C33n		641.48
52X1, 117	641.17	-75			
52X2, 122	642.72	-54		**C33n**	
52X3, 114	644.14	-54			
52X4, 141	645.91	-71			

...and so on until 704.72 mbsf for base C33n

In black, samples from Galbrun (1992)

In bold grey, additional samples analysed by Galbrun in 2008

Appendix 1

Appendix 2: Alphabetical list of calcareous nannofossil species. All references prior to 1998 can be found in Perch-Nielsen (1985) and Bown (1998). Others are given in the reference list below.

Ahmuellerella octoradiata (Gorkà, 1957) Reinhardt, 1966

Amphizygus brooksii Bukry, 1969

Biscutum constans (Gorkà, 1957) Black *in* Black and Barnes, 1959

Biscutum coronum Wind and Wise *in* Wise and Wind, 1977

Biscutum magnum Wind and Wise *in* Wise and Wind, 1977

Broinsonia parca constricta Hattner et al., 1980

Broinsonia parca parca Hattner et al., 1980

Calculites obscurus (Deflandre, 1959) Prins and Sissingh *in* Sissingh, 1977

Ceratolithoides aculeus (Stradner, 1961) Prins and Sissingh *in* Sissingh, 1977

Ceratolithoides indiensis Burnett, 1997a

Ceratolithoides kamptneri Bramlette and Martini, 1964

Cribrocorona gallica (Stradner, 1963) Perch-Nielsen, 1973

Cribrosphaerella daniae Perch-Nielsen, 1973

Discorhabdus ignotus (Gorkà, 1957) Perch-Nielsen, 1968

Eiffellithus angustus (Bukry, 1969) Shamrock and Watkins, 2009

Eiffellithus eximius (Stover, 1966) Perch-Nielsen, 1968

Lithraphidites praequadratus Roth, 1978

Lithraphidites quadratus Bramlette and Martini, 1964

Micula murus (Martini, 1961) Bukry, 1973

Micula praemurus (Bukry, 1973) Stradner and Steinmetz, 1984

Micula prinsii Perch-Nielsen, 1979

Monomarginatus quaternarius Wind and Wise *in* Wise and Wind, 1977

Nephrolithus frequens Gorkà, 1957

Petrarhabdus copulatus (Deflandre, 1959) Wind and Wise *in* Wise, 1983

Petrarhabdus vietus Burnett, 1997b

Prediscosphaera mgayae Lees, 2007

Pseudomicula quadrata Perch-Nielsen in Perch-Nielsen et al., 1978

Quadrum gartneri Prins and Perch-Nielsen in Manivit et al., 1977

Quadrum svabenickae Burnett, 1997b

Reinhardtites anthophorus (Deflandre, 1959) Perch-Nielsen, 1968

Reinhardtites elegans (Gartner, 1968) Wise, 1983

Reinhardtites levis Prins and Sissingh *in* Sissingh, 1977

Rotelapillus laffittei (Noël, 1956) Howe, Bergen and Campbell *in* Howe et al., 2003

Stoverius achylosus (Stover, 1966) Perch-Nielsen, 1986

Stoverius coangustatus Howe, Bergen and Campbell *in* Howe et al., 2003

Tortolithus hallii (Bukry, 1969) Crux *in* Crux et al., 1982

Tranolithus orionatus (Reinhardt, 1966a) Reinhardt, 1966b

Tranolithus stemmerikii Thibault and Sheldon *in* Thibault, 2010

Uniplanarius gothicus (Deflandre, 1959) Prins and Perch-Nielsen *in* Manivit et al., 1977

Uniplanarius trifidus (Stradner *in* Stradner and Papp, 1961) Hattner and Wise, 1980

Watznaueria manivitiae Bukry, 1973

Zeugrhabdotus bicrescenticus (Stover, 1966) Burnett *in* Gale et al., 1996

Zeugrhabdotus diplogrammus (Deflandre in Deflandre and Fert, 1954) Burnett *in* Gale et al., 1996

Zeugrhabdotus erectus (Deflandre in Deflandre and Fert, 1954) Reinhardt, 1965

References

Burnett, J.A., 1997a. New species and conjectured evolutionary trends of Ceratholithoides Bramlette and Martini, 1964 from the Campanian and Maastricthian of the Indian Ocean. Journal of Nannoplankton Research 19, 123–131.

Burnett, J.A., 1997b. New species and new combinations of Cretaceous nannofossils, and a note on the origin of Petrarhabdus (Deflandre) Wind and Wise. Journal of Nannoplankton Research 19, 133–146.

Howe, R.W., Campbell, R.J., Rexilius, J.P., 2003. Integrated uppermost Campanian–Maastrichtian calcareous nannofossil and foraminiferal biostratigraphic zonation of the northwestern margin of Australia. Journal of Micropalaeontology 22, 29–62.

Lees, J.A., 2007. New and rarely reported calcareous nannofossils from the Late Cretaceous of coastal Tanzania: outcrop samples and Tanzania Drilling Project Sites 5, 9 and 15. Journal of Nannoplankton Research 29, 39–65.

Thibault, N., 2010. Calcareous nannofossils from the boreal Upper Campanian – Maastrichtian chalk of Denmark. Journal of Nannoplankton Research 31, 39–56.

Leg 122, Hole 762C, core, section, interval (cm)	profondeur (mbsf)	Preservation	Ahmuellerella octoradiata	Amphizygus brooksii	Biscutum coronum	Biscutum constans	Biscutum magnum	Broinsonia parca constricta	Broinsonia parca parca	Calculites obscurus	Ceratolithoides aculeus	Ceratolithoides indiensis	Ceratolithoides kamptneri	Cribrocorona gallica	Cribrosphaerella daniae	Cylindralithus? nieliae	Discorhabdus ignotus	Eiffellithus angustus	Eiffellithus eximius	Eiffellithus parallelus	Lithraphidites praequadratus	Lithraphidites quadratus	Lucianorhabdus cayeuxii	Micula murus	Micula praemurus	Micula prinsii	Monomarginatus quaternarius	Nephrolithus corystus	Nephrolithus frequens	Petrarhabdus copulatus	Petrarhabdus vietus	Prediscosphaera mgayae	Pseudomicula quadrata	Quadrum gartneri	Quadrum svabenickae	Reinhardtites anthophorus	Reinhardtites elegans	Reinhardtites levis	Stoverius coangustatus	Tortolithus hallii	Tranolithus orionatus	Tranolithus stemmerikii	Uniplanarius gothicus	Uniplanarius trifidus short-rayed	Uniplanarius trifidus medium-rayed	Watznaueria manivitae s.s.	Watznaueria manivitae s.l.	Zeugrhabdotus bicrescenticus sma	Zeugrhabdotus bicrescenticus big	Zeugrhabdotus diplogrammus	Zeugrhabdotus erectus	curved spine
43X-1, 33-34	554.83	M									R			F	R		R			R	F	F	F	R		R			F					R									S				F					
43X-1, 101-102	555.51	M				S					R			F	R		R			R	F	F	F	R	R	R			R						S												F					
43X-2, 33-34	556.33	M												F						R	F	F	R	F	R				F																		F					
43X-2, 83-84	556.83	P												F						R	R	R	R	F	F	R			R				S	R													F					
43X-3, 4-5	557.54	M												F						R	F	R	R	F	R				R																		F					
43X-3, 66-67	558.16	P												F							R	R	R	F	R	R			R				R														F					
43X-4, 8-9	559.08	M												C						R	F	R	R	C	R	R			F																		F					
43X-4, 145-146	560.46	P											R	F							R	R		F		R							R														F					
43X-5, 90-91	561.4	M												C	R					R	F	F	R	F					F																		F					
44X-1, 14-15	564.14	M				R								R	R					R	F	F		F																							F					
44X-1, 42-43	564.42	M				F								R						F	F	F		R					F																		F					
44X-2, 25-26	565.75	M				C								R	R					F	F	F		R					R																		F					
44X-2, 95-96	566.45	M				F								R						F	R	F																									F					
44X-2, 148-149	566.98	M				C							R	F						R	F	F		R					R																		F					
44X-3, 9-10	567.09	M				C								R	R					F	F	F		F					F																		F					
44X-3, 108-109	568.08	M				F							R		R					R	F	F		R					R																		F					
44X-4, 5-6	568.55	M				F								R						R	F	F		R					S																		F					
44X-4, 110-111	569.6	M				C								F	R					F	F	C		R	R																						F					
44X-5, 8-9	570.08	M				R						R					R			R	R	F											S														F					
44X-5, 119-120	571.19	M				F						F		R			R			C	F	F		R																							F					
44X-6, 20-21	571.7	M				F						R	R	R						F	F	F		R																							F					
44X-6, 128-129	572.78	M				F						F		R	R					F	F	C							R																		F					
44X-7, 14-15	573.14	P				F						F		R						F	R	F		R					R																		F					
45X-1, 10-11	573.6	M				C						R		R			R			F	F	F							R				R														F					
45X-1, 47-48	573.97	P				F						R		R			R			R	R	R											R														F					
45X-1, 145-146	574.95	M				C						F		F			F			F	F	F		F					C																		F					
45X-2, 25-26	575.25	P				F						R		R						F	R	R			R				R				F														F					
45X-2, 113-114	576.13	M				F						R		R						F		F							F																		F	S				
45X-3, 49-50	576.99	P				F						F		R			R			R		R		R	R																						F					
45X-3, 88-89	577.38	M				C						F		R						F	R	F																									F					
45X-3, 131-132	577.81	P				F					S	R		R						R	R	R																									F					
45X-4, 5-6	578.05	M				F						R		R			R			F	R	F							R																		F					
45X-4, 74-75	578.74	P				F						R		F						R		R							R				R														F					
45X-5, 4-5	579.54	M				C						F		R			R			F	R	R							R																		F					
45X-5, 80-81	580.3	P				C						F		F								F																									F					
45X-5, 143-144	580.93	M				C					R	R		R			R			F	R	F	R						R																		F					
46X-1, 20-21	583.2	M	R			C						R		R	R		R			F	F	R							R																		F					
46X-1, 89-90	583.89	P				C					R	R		R							R										R																F					
46X-2, 8-9	584.58	M	F			C						F		R			R			F	R								R																		F					
46X-2, 109-110	585.59	P	R			F						F		R						R	R				R						R																F					
46X-3, 10-11	586.1	M	F			C						F		R			R			F	F				R				F		R		R														F					
46X-3, 121-122	587.21	P				F					R	F		R							R		R						R		R																F					
46X-4, 5-6	587.55	M	F			C						R		R	R		R			F	F				R				R		F																F					
46X-4, 65-66	588.15	P	R			F						R		R			R			R	R																										F					
47X-1, 9-10	592.59	M	R			C					R	R								F			R						R		R																F					
47X-1, 95-96	593.35	M	F			F						R			F	R	R			C									F		F																F					
47X-2, 81-82	594.81	M	R			C						R								F											R																F					
47X-2, 128-129	595.28	M	F			C					R	R					R			F									F		F										S						F					
47X-2, 140-141	595.4	M	R			F						R				R	R			R										S	R								R								F					
47X-3, 16-17	595.65	M				F					R	F					R			F									R										R		S						F					
47X-3, 40-41	595.9	M	R	R		F						R			R		R			R									R										R								F					
47X-4, 40-41	597.4	M	F			F						R			R		F			F									R		R								R								F					
47X-4, 106-107	598.06	M	R	R		F						R			R	R	R			R									R									S	F								F					
47X-5, 23-24	598.73	M	R			F										R	R			F											R								R								F					
47X-5, 59-60	599.09	M	R			C					R	R				R	R			F									R										R								F					
47X-6, 23-24	600.23	P				C		R				R					R			F											R								R								F					
47X-6, 66-67	600.66	M	R			C						R			R		F			F									R										F		R						F					
47X-6, 85-86	600.83	M	R	R		C										R	R			C									R										R		R						F					
48X-1, 4-5	602.04	M	R	R		C		F			R	R					R			F									R									F	R		R						F	R				
48X-1, 40-41	602.4	M						F				R								R																		F	F								F	R				
48X-1, 100-101	603	M	R			F		F				R					R			R									R									R	F								F	R				
48X-2, 19-20	603.69	M	F	R		F		R									R			F																		F			R						F	F				
48X-2, 35-36	603.85	M	R	R		F		R									R			F																		F	R								F	R				
48X-2, 45-46	603.95	P				F		R				R					R			R																		R	R		R						F	R				
48X-2, 60-61	604.11	M	R			F		R							R					R																		R	R		R						F	F				
48X-2, 71-72	604.21	M	R	R		F		R				R			R		R			R									R									R			R						F	F				
48X-2, 80-81	604.3	P	R			F	S	R												R																		R	R								F	F				
48X-2, 93-94	604.43	M	F			F		R								R	F			R																		R	R		R						F	F				
48X-2, 105-106	604.55	M	F	R		F		R									F			F																		F	R		R						F	F				
48X-2, 114-115	604.64	M	R			F		R				R					F			R									S			S						R	R		R						F	F				
48X-2, 132-133	604.82	M	R			C		F									R			F									R		R							R									F	R			R	
48X-3, 21-22	605.2	M	F	R		C		R				R			R		F			F							S											R	R		R						F	F			F	
48X-3, 57-58	605.57	M	R			C		F				R					F			C											R							R									F	F				
48X-3, 74-75	605.74	M	F			F		R				R				R	F			F																		F	F		R						F	R			R	
48X-3, 94-95	605.94	M	R			C		R									F			C							S											F	R		R						F	R				
48X-3, 129-130	606.29	M	R			F		R				R					C			R														R				F	R		R						F	R				
48X-4, 10-11	606.6	M	R	R		C		R				R					C			F																		R	F		R						F				R	
48X-4, 17-18	606.67	M	F			C						R					C			F																			F		R						F	R			F	
48X-4, 30-31	606.8	M				C		R									F			F																		R	R								F	R			R	
48X-4, 39-40	606.89	M	F	R		C		F									F			C												S		R				R	R		R						F	F			R	
48X-4, 54-55	607.04	M	R	R		C		F									F			F											R			R				F	F		R						F	R				
48X-4, 73-74	607.23	M	R	R		C		R				R					C			C																		R	R		R						F	F			R	
48X-4, 85-86	607.35	M	R			C		R								R	F			F																		R	R								F	R				
48X-4, 103-104	607.53	M				F		R				R					F			F																		R	R		R						F	R			R	
48X-4, 120-121	607.7	M	R			C		R				R					F			C																		R	R		R						F	F				
48X-4, 138-139	607.88	M	S	R		R					R	R					R			F																		R	R		S						F	R				
48X-5, 55-56	608.55	M		R		F		R												C																	S	F									F	F				
48X-5, 78-79	608.78	M		R		F						R					F			F														R				R	R		R						F	R				
48X-5, 111-112	609.11	M				F														R			S								R							R	R								F	R				
48X-5, 122-123	609.22	M				C	R					R				R	C			C											R							R	R		R						F	F			R	
48X-5, 145-146	609.45	M	F	R		C											F			C																		F	R		R						F	F			R	
48X-6, 68-69	610.18	M				C											F			F																		F	F		R						F	R			R	
48X-6, 87-88	610.37	M				C						R				R	F			F							R											F	R		R						F	R		R	R	
48X-6, 97-98	610.47	M	R	R		C											C			C																		F			R						F	F			R	
48X-6, 104-105	610.54	M	R			C		R								R	C			F							R							R				R	R								F	R				
48X-6, 117-118	610.67	M	R	R		C		R	R								C			F												S						F	R		R						F	R			R	
48X-6, 147-148	610.97	M	R	R		C											C			F																		F	R		F						F	F			R	
49X-1, 9-10	611.59	M	R	R		C		R	R								F			F							R			R	R	R						F	R		R						F	F		R		
49X-1, 23-24	611.75	M	R			C		R	R											F			R				R				R							F	F								F	R				
49X-1, 61-62	612.11	M	R			C	R	R	R								F			F			R				F				R							R	R		F						F	F				
49X-1, 95-96	612.45	M	F	R		C											F			F							R				R							R	R		R						F	F		R		
49X-1, 116-117	612.66	M	R	R		F											F			R			R							R	R							F	R		R						F	R			S	
49X-2, 20-21	613.2	P				F		S				S					R			R			S							R	R			R				F	R		R						F	S				
49X-2, 82-83	613.82	M	R	R		C		R									F			R			R				R			R	R							F	R		R						F	R		R		
49X-2, 100-101	614	M	F			C						R					F			F			R							R	R							F	R		F						F	R			R	
49X-2, 112-113	614.12	M	R			F	R	R									R			R							R			R	R			R				F			R			S			F	R			S	
49X-3, 20-21	614.7	M	R			C		F			R						R			F											R						R	F	R		R	F	R				F	F		R	R	
49X-3, 38-39	614.88	M	R			C		R	R						S?		F			F							R				R			R				F	F		R	R	R	R			F	R			F	
49X-3, 55-56	615.05	M				C		F	R								R			F							R				F			R			R	C	R		F	R	R				F	R		R	R	
49X-3, 65-66	615.15	M	R			C		F	R			S					F			R							R			F	R			R			R	F	R		R	R	R	R			F	R			R	
49X-3, 78-79	615.28	M				C		F	R		S	S								R							S				R			R			S	R	R		R	R	R	S			F	R			S	

Leg 122, Hole 762C, core, section, interval (cm)	profondeur (mbsf)	Preservation	Ahmuellerella octoradiata	Amphizygus brooksii	Biscutum coronum	Biscutum constans	Biscutum magnum	Broinsonia parca constricta	Broinsonia parca parca	Calculites obscurus	Ceratolithoides aculeus	Ceratolithoides indiensis	Ceratolithoides kamptneri	Cribrocorona gallica	Cribrosphaerella daniae	Cylindralithus? nieliae	Discorhabdus ignotus	Eiffellithus angustus	Eiffellithus eximius	Eiffellithus parallelus	Lithraphidites praequadratus	Lithraphidites quadratus	Lucianorhabdus cayeuxii	Micula murus	Micula praemurus	Micula prinsii	Monomarginatus quaternarius	Nephrolithus corystus	Nephrolithus frequens s.l.	Petrarhabdus copulatus	Petrarhabdus vietus	Prediscosphaera mgayae	Pseudomicula quadrata	Quadrum gartneri	Quadrum svabenickae	Reinhardtites anthophorus	Reinhardtites elegans	Reinhardtites levis	Stoverius coangustatus	Tortolithus hallii	Tranolithus orionatus	Tranolithus stemmerikii	Uniplanarius gothicus	Uniplanarius trifidus short-rayed	Uniplanarius trifidus medium-rayed	Watznaueria manivitae s.s.	Watznaueria manivitae s.l.	Zeughrabdotus bicrescenticus sma	Zeughrabdotus bicrescenticus big	Zeughrabdotus diplogrammus	Zeughrabdotus erectus	curved spine
49X-3, 89-90	615.39	M		S		C		R	R								R			R										F	R			R				F	R		R	R	R	R			F	R		R		
49X-3, 104-105	615.55	P				C		F	R								R			F			R				R				F			R			R	F	R		R	R	R	R			F	R		R	R	
49X-3, 120-121	615.7	M				C		R	R		R						F			F			R				R			F	R			R				F	R		R	R	R				F	F			R	
49X-3, 130-131	615.8	M				C		R	R								R			R											R			R				R	S			R	R	R			F	R				
49X-4, 19-20	616.19	M				C	R	F	R								F			F			R				R				R							F	R		R	R					F	R		R	R	
49X-4, 93-94	616.93	M				F		R	R								F			R							R											R	R		R	R					F	R			R	
49X-4, 105-106	617.05	M	R	R		F	S	R	R								F			F							R	S		F				R				F	R		R	R	R	R			F	R			R	
49X-4, 117-118	617.17	P				F		R	R											F			S								R			R			S	F	R		R	R	R	R			F	R			S	
49X-4, 134-135	617.34	M				F		R	R							S	F			F																		F	S		R	R					F	R		S	S	
49X-5, 20-21	617.7	M	R			F		R	R								R			R											R			R				F	R		R	R	R	S			F	R			R	
49X-5, 35-36	617.85	M	R			F		R	R								F			R											R			R				F	R		R	R	R				F	R		R	R	
49X-5, 50-51	618	M				F		R	R								R			F														R				F	R		R	R	R	R			F	R				
49X-5, 80-81	618.3	M	R			F		R	R		R					R	F			F							R				R			R				F	R		R	R	R	R			F	R		R	R	
49X-5, 95-96	618.45	M	R			F		R	R								F			F														R				F	R		R	R	R	R			F	R				
49X-5, 124-125	618.74	M	R			F		R	R		S					R	F			R			S				R				R							F	R		R	R	R				F	R			R	
49X-5, 132-133	618.82	M	R			F		R	R		R						F			R			S								R			R				F	R		R	R	R	R			F	R				
49X-5, 135-136	618.85	M	F			F		F	R							R	F			F														R				F	R		R	F	R	R			F	R			R	
49X-CC, 20-21	619.5	M				F		R	R								R			C							R			C								F	F			F	F				F	R		S		
50X-1, 10-11	621.11	M	R	F		F		C	R								R			F							R											C	F			F			R		F			S		
50X-2, 11-12	622.62	M		R		C		C	C								F			F										R				R				F	F		R	R	R				F	R				
50X-3,10-11	624.11	M	F	R		F	S	F	F								F			R										R								F			R	R					F	F				
50X-3, 110-111	625.11	M				F		F	F							S	R			C							R			R								C	R		F	F	F		F		F					
50X-4, 101-102	626.52	M		R		F		R	F		R						R			F										F								F			R						F					
50X-5, 100-101	628.01	P	F			F		F		R							R			F			R							R								C	R		R	F	F				F	F				
50X-6, 110-111	629.61	P	F	R		F		F	F								F			R							R			F				R				C	F		F	R	R				F		R		S	
51X-1, 11-12	630.62	P	F	F		F		F	F	R							F			R			R							R					R			C	F		F		R		R		F		R			
51X-2, 10-11	632.11	M		F		F		F	F								F			F										R					R			C	F		F		F		R		F	R	F			
51X-3, 10-11	633.61	M	F			F		F	R								F			C										R				R	R			C	F		F	R	C	R			F		R			
51X-4, 11-12	635.12	M	F			F		F		R	R						F			F			F				R								R		R	C	R		F	F		F	F		F		F			
51X-5, 9-10	636.6	M	F			F		C									F		R	C							F							S			R	C	S		F	R					F	F				R
51X-6, 35-36	638.36	M	R			F		C	R								F		R	F										R				S			R	C	R	S	F		R	R			F	R	R	S		
52X-1, 10-11	640.11	M				F		F	F		R						F	R	R	F			R							R					R			C	F		C	R	F				F	F				R
52X-2, 4-5	641.55	M				C		F	R								F		R	R			F											S			R	C	F		F	F	R	R			F		F			F
52X-2, 112-113	642.63	M	F			C		F	R								F		R	R			R														R	C	F		F	F	F	F			F		F			R
52X-3, 77-78	643.78	M	R			F		F	R								F	R	R	R			F															C	F		C	F	R		R		F		F			F
52X-4, 10-11.5	644.62	M				C		F									F	R	R	F										F								F	F		F	F	R	F	F		F	R				R
52X-5, 10.5-11.5	646.12	M				C		F			R	R					F	R	R	F										F								F	F		F	F	R	F	F		F	R				
52X-6, 8-9	647.59	P				F		F	F								R	R	F	R			R															C	F		F			C	C		F	R	R			R
52X-6, 83-85	648.35	M				F		C	R								F	R	F	F			R				R			R				S			R	C	F		F	F	F				F	F				F
53X-1, 12-13	649.63	M				F		F									R		R				F							F				S			F	C	F		F		R	R	R		C					C
53X-1, 100-102	650.52	M	F			F		C									R						F											R			R	C	F		F	R	F	F	F		F	C	C			F
53X-2, 89-90	651.9	M	R	R		F		C	F								R	R	R	F			R														R	C	F		F	F	R	F	F		F	C	C			F
53X-3, 101-102	653.52	M		F		C		C	F							S	F	R	F	R			R														F	C	R	S	R				R		C	C	C			F
53X-4, 108-109	655.09	M	F			F		R									R	R	R	F			R											R			F	C	R			F					C	C	F			F
53X-5, 40-41	655.91	M	R			C					R						R	R	F	F			F							S							F	C	R	S	R	F	R		R		C	C	C		S	
53X-6, 18-19	657.19	M	F		R	C		F								S	F	R	F				F							S							F	C	F		F	F	R				C	F	F			
53X-7, 1-2	658.52	M	F	F		F		C	R								R	R	F	C																	R	C	F		F		F				C	F	F			
54X-1, 76-77	659.77	M	R	R	S	F											R		R				F							R							S	C	F		F		F			R	C	F	F			R
54X-1, 138-139	660.39	M	R			F		F									R		S				R											R				C	F		F	R	F		F	R	C	R	F		S	
54X-2, 121-122	661.72	M				F		C	F			S				R	F	R	F	F			F											F		R	F	F	F		F		F	F		R	C	R				
54X-3, 111-112	663.12	M		F		F		C	F		R						R			F																R	R	F			F		F	R	R	R	C					
54X-4, 120-121	664.71	M		F		F	R	F	F								R		R	F										S						R	R	F	R		F		F			R	C	R				
54X-5, 95-96	665.96	M		F	F	F		F	F			R					F	R	S	F			C														F	F	F		R	R	F		F	F	C					
54X-6, 60-62	667.12	M	F	F	S	F		F	R								R			R			C													R	R	F	R		R	F	R			R	C	R				
54X-7, 20-21	668.21	P	S	R	R	F		F	R								R	R	F	R			C											R				F	R	S	F		F			R	C	F			R	
55X-1, 66-67	669.17	P	F	R	R	F		F	R			R				R	R		R	R			R											F	F		R	F	F		F	F	C			R	C	F			R	

Leg 122, Hole 762C, core, section, interval (cm)	Samples numbers	depth (mbsf)	adjusted depth (ambsf)	13C standardized (‰ V-PDB)	Age (Ma) based on K/Pg at 65.59	Age (Ma) based on K/Pg at 66	100 kyr cycles
42X-5, 95-96	post-doc-1	551.95	552.98	1.40			
42X-CC, 35.5-35.5	post-doc-2	554.50	555.73	1.43			
43X-1, 33-34	PhD-129	554.83	556.06	2.55	65.592	66.002	e1
43X-1, 34-35	post-doc-3	554.85	556.08	2.65	65.593	66.003	
43X-1, 50-52	post-doc-4	555.01	556.24	2.56	65.602	66.012	
43X-1, 101-102	PhD-128	555.51	556.74	2.61	65.632	66.042	
43X-2, 33-34	PhD-127	556.33	557.56	2.49	65.680	66.090	
43X-2, 83-84	PhD-126	556.83	558.06	2.61	65.720	66.130	e2
43X-2, 103-104	post-doc-5	557.04	558.27	2.64	65.739	66.149	
43X-3, 4-5	PhD-125	557.54	558.77	2.44	65.784	66.194	
43X-3, 66-67	PhD-124	558.16	559.39	2.50	65.819	66.229	e3
43X-3, 147-148	post-doc-6	558.98	560.21	2.46	65.862	66.272	
43X-4, 8-9	PhD-123	559.08	560.31	2.38	65.867	66.277	
43X-4, 145-146	PhD-122	560.46	561.69	2.49	65.958	66.368	e4
43X-5, 47-48	post-doc-7	560.98	562.21	2.47	65.995	66.405	e5
43X-5, 90-91	PhD-121	561.40	562.63	2.48	66.019	66.429	
44X-1, 14-15	PhD-120	564.14	565.37	2.56	66.170	66.580	e6
44X-1, 42-43	PhD-119	564.42	565.65	2.60	66.185	66.595	
44X1-47-48	post-doc-8	564.48	565.71	2.64	66.188	66.598	
44X-2, 25-26	PhD-118	565.75	566.98	2.80	66.255	66.665	e7
44X-2, 95-96	PhD-117	566.45	567.68	2.75	66.292	66.702	e8
44X-2, 98-99	post-doc-9	566.48	567.71	2.77	66.293	66.703	
44X-2, 148-149	PhD-116	566.98	568.21	2.67	66.313	66.723	
44X-3, 9-10	PhD-115	567.09	568.32	2.68	66.317	66.727	
44X-3, 108-109	PhD-114	568.08	569.31	2.79	66.356	66.766	
44X-3, 147-148	post-doc-10	568.48	569.71	2.78	66.372	66.782	
44X-4, 5-6	PhD-113	568.55	569.78	2.76	66.368	66.778	e9
44X-4, 110-111	PhD-112	569.60	570.83	2.82	66.426	66.836	
44X-5, 8-9	PhD-111	570.08	571.31	2.85	66.453	66.863	
44X-5, 45-46	post-doc-11	570.45	571.68	2.85	66.474	66.884	
44X-5, 119-120	PhD-110	571.19	572.42	2.72	66.522	66.932	e10
44X-6, 95-96	post-doc-12	572.45	573.68	2.74	66.603	67.013	e11
44X-6, 128-129	PhD-108	572.78	574.01	2.71	66.618	67.028	
44X-7, 14-15	PhD-107	573.14	574.37	2.80	66.634	67.044	
45X-1, 10-11	PhD-106	573.60	575.15	2.87	66.655	67.065	
45X-1, 47-48	PhD-105	573.97	575.52	2.78	66.672	67.082	
45X-1, 50-51	post-doc-13	574.00	575.55	2.78	66.673	67.083	
45X-1, 145-146	PhD-104	574.95	576.50	*2.55*	66.732	67.142	e12
45X-2, 25-26	PhD-103	575.25	576.80	*2.65*	66.754	67.164	
45X-2, 113-114	PhD-102	576.13	577.68	*2.66*	66.814	67.224	e13
45X-3, 49-50	PhD-101	576.99	578.54	*2.67*	66.869	67.279	
45X-2, 100-102	post-doc-14	577.01	578.56	2.82	66.870	67.280	
45X-3, 88-89	PhD-100	577.38	578.93	*2.69*	66.895	67.305	e14
45X-3, 131-132	PhD-99	577.81	579.36	*2.84*	66.927	67.337	
45X-3, 149-150	post-doc-15	577.99	579.54	2.97	66.941	67.351	
45X-4, 5-6	PhD-98	578.05	579.60	*2.80*	66.946	67.356	
45X-4, 74-75	PhD-97	578.74	580.29	*2.73*	66.999	67.409	e15
45X-5, 4-5	PhD-96	579.54	581.09	2.94	67.065	67.475	
45X-5, 44-45	post-doc-16	579.95	581.50	2.87	67.101	67.511	e16
45X-5, 80-81	PhD-95	580.30	581.85	3.01	67.136	67.546	
45X-5, 143-144	PhD-94	580.93	582.48	3.09	67.197	67.607	e17
45X-CC, 40-42	post-doc-17	581.41	582.96	3.03	67.239	67.649	
46X-1, 20-21	PhD-93	583.20	584.75	2.74	67.373	67.783	e18
46X-1, 45-46	post-doc-18	583.45	585.00	2.74	67.391	67.801	e19
46X-1, 89-90	PhD-92	583.89	585.44	2.70	67.422	67.832	
46X-2, 8-9	PhD-91	584.58	586.13	2.66	67.472	67.882	
46X-2, 99-100	post-doc-19	585.50	587.05	2.76	67.535	67.945	e20
46X-2, 109-110	PhD-90	585.59	587.14	2.67	67.541	67.951	
46X-3, 10-11	PhD-89	586.10	587.65	2.66	67.575	67.985	
46X-3, 121-122	PhD-88	587.21	588.76	2.69	67.651	68.061	e21
46X-3, 147-148	post-doc-20	587.48	589.03	2.70	67.670	68.080	
46X-4, 5-6	PhD-87	587.55	589.10	2.71	67.674	68.084	

46X-4, 65-66	PhD-86	588.15	589.70	2.59	67.715	68.125	e22
46X-4, 125-126	post-doc-21	588.75	590.30	2.80	67.756	68.166	
46X-CC, 33-34	post-doc-22	589.30	590.85	2.83	67.791	68.201	e23
47X-1, 9-10	PhD-85	592.59	594.14	2.69	67.868	68.278	
47X-1, 23-24	post-doc-23	592.74	594.29	2.66	67.871	68.281	
47X-1, 95-96	PhD-84	593.35	594.90	2.81	67.886	68.296	
47X-2, 46-47	post-doc-24	594.46	596.01	2.67	67.957	68.367	e24
47X-2, 81-82	PhD-83	594.81	596.36	2.65	67.982	68.392	
47X-2, 128-129	PhD-82	595.28	596.83	2.70	68.024	68.434	e24,5
47X-2, 140-141	PhD-81	595.40	596.95	2.68	68.489	68.899	e29,5
47X-3, 16-17	PhD-80	595.65	597.20	2.74	68.557	68.967	e30
47X-3, 40-41	PhD-79	595.90	597.45	2.71	68.577	68.987	
47X-3, 111-112	post-doc-25	596.62	598.17	2.66	68.688	69.098	e31
47X-4, 40-41	PhD-78	597.40	598.95	2.69	68.808	69.218	e33
47X-4, 106-107	PhD-77	598.06	599.61	2.77	68.904	69.314	e34
47X-4, 147-148	post-doc-26	598.48	600.03	2.72	68.962	69.372	
47X-5, 23-24	PhD-76	598.73	600.28	2.77	68.995	69.405	e35
47X-5, 59-60	PhD-75	599.09	600.64	2.85	69.035	69.445	
47X-6, 23-24	PhD-74	600.23	601.78	2.60	69.157	69.567	e36
47X-6, 85-86	PhD-72	600.83	602.38	2.55	69.227	69.637	e37
47X-6, 88-89	post-doc-27	600.89	602.44	2.63	69.235	69.645	
48X-1, 4-5	PhD-71	602.04	603.65	2.37	69.469	69.879	e39
47X-CC, 28-29	post-doc-28	602.05	603.66	2.54	69.471	69.881	
48X-1, 10-11	post-doc-29	602.11	603.72	2.44	69.482	69.892	
48X-1, 40-41	PhD-70	602.40	604.01	2.57	69.531	69.941	e40
48X-1, 100-101	PhD-69	603.00	604.61	2.45	69.640	70.050	e41
48X-2, 19-20	PhD-68	603.69	605.30	2.59	69.778	70.188	e42
48X-2, 60-61	PhD-65	604.11	605.72	2.50	69.828	70.238	e43
48X-2, 69-70	post-doc-30	604.20	605.81	2.46	69.838	70.248	
48X-2, 93-94	PhD-62	604.43	606.04	2.49	69.862	70.272	
48X-2, 132-133	PhD-59	604.82	606.43	2.41	69.906	70.316	e44
48X-3, 74-75	PhD-56	605.74	607.35	2.50	70.024	70.434	e45
48X-3, 125-126	post-doc-31	606.26	607.87	2.46	70.103	70.513	e46
48X-3, 129-130	PhD-54	606.29	607.90	2.39	70.107	70.517	
48X-4, 30-31	PhD-51	606.80	608.41	2.48	70.173	70.583	
48X-4, 73-74	PhD-48	607.23	608.84	2.50	70.239	70.649	e47
48X-4, 120-121	PhD-45	607.70	609.31	2.38	70.311	70.721	e48
48X-5, 26-27	post-doc-32	608.27	609.88	2.52	70.391	70.801	e49
48X-5, 78-79	PhD-42	608.78	610.39	2.51	70.481	70.891	
48X-5, 145-146	PhD-39	609.45	611.06	2.54	70.586	70.996	e50
48X-6, 68-69	PhD-38	610.18	611.79	2.59	70.863	71.273	e53
48X-6, 71-72	post-doc-33	610.22	611.83	2.59	70.871	71.281	
48X-6, 87-88	PhD-37	610.37	611.98	2.61	70.898	71.308	e54
48X-6, 117-118	PhD-34	610.67	612.28	2.66	70.943	71.353	
48X-6, 147-148	PhD-33	610.97	612.58	2.56	70.988	71.398	
49X-1, 10-12	post-doc-34	611.62	613.59	2.43	71.120	71.530	e56
49X-1, 23-24	PhD-30	611.75	613.72	2.60	71.141	71.551	
49X-1, 61-62	PhD-29	612.11	614.08	2.43	71.197	71.607	e57
49X-1, 116-117	PhD-27	612.66	614.63	2.45	71.281	71.691	
49X-2, 11-12	post-doc-35	613.12	615.09	2.44	71.351	71.761	e58
49X-2, 20-21	PhD-26	613.20	615.17	2.44	71.364	71.774	
49X-2, 82-84	post-doc-36	613.84	615.81	2.42	71.493	71.903	e60
49X-2, 112-113	PhD-23	614.12	616.09	2.34	71.587	71.997	
49X-3, 10-11	post-doc-37	614.61	616.58	2.42	71.653	72.063	e61
49X-3, 20-21	PhD-22	614.70	616.67	2.40	71.665	72.075	
49X-3, 65-66	PhD-19	615.15	617.12	2.39	71.716	72.126	e62
49X-3, 104-105	PhD-16	615.55	617.52	2.34	71.756	72.166	
49X-3, 115-116	post-doc-38	615.66	617.63	2.54	71.767	72.177	
49X-4, 11-12	post-doc-39	616.12	618.09	2.48	71.814	72.224	e63
49X-4, 19-20	PhD-13	616.19	618.16	2.59	71.822	72.232	
49X-4, 93-94	PhD-12	616.93	618.90	2.44	71.900	72.310	e64
49X-4, 101-102	post-doc-40	617.02	618.99	2.45	71.908	72.318	
49X-5, 11-12	post-doc-41	617.62	619.59	2.38	71.965	72.375	
49X-5, 20-21	PhD-8	617.70	619.67	2.37	71.973	72.383	
49X-5, 80-81	PhD-5	618.30	620.27	2.45	72.039	72.449	e65
49X-5, 105-106	post-doc-42	618.56	620.53	2.65	72.070	72.480	
49X-5, 135-136	PhD-1	618.85	620.82	2.49	72.097	72.507	e66
49X-6, 10-11	post-doc-43	619.11	621.08	2.49	72.111	72.521	
49X-CC, 20-21	post-doc-44	619.50	621.47	2.44	72.133	72.543	

50X-1, 10-11	post-doc-45	621.11	623.08	2.42	72.233	72.643	e67
50X-1, 93-94	post-doc-46	621.94	623.91	2.47	72.295	72.705	e68
50X-2, 11-12	post-doc-47	622.62	624.59	2.55	72.338	72.748	
50X-2, 101-102	post-doc-48	623.53	625.50	2.52	72.399	72.809	e69
50X-3,10-11	post-doc-49	624.11	626.08	2.59	72.458	72.868	
50X-3, 110-111	post-doc-50	625.11	627.08	2.71	72.556	72.966	e70
50X-4, 10-11.5	post-doc-51	625.62	627.59	2.62	72.604	73.014	e71
50X-4, 101-102	post-doc-52	626.52	628.49	2.57	72.687	73.097	
50X-5, 11-12	post-doc-53	627.12	629.09	2.63	72.728	73.138	e72
50X-5, 100-101	post-doc-54	628.01	629.98	2.59	72.789	73.199	
50X-6, 16-17	post-doc-55	628.67	630.64	2.62	72.877	73.287	e73
50X-6, 110-111	post-doc-56	629.61	631.58	2.48	72.982	73.392	e74
50X-7, 10.5-11.5	post-doc-57	630.12	632.09	2.58	73.051	73.461	e75
50X-CC, 28.5-30	post-doc-58	630.50	632.85	2.60	73.100	73.510	e76
51X-1, 11-12	post-doc-59	630.62	632.97	2.53	73.110	73.520	
51X-1, 101.5-102.5	post-doc-60	631.53	633.88	2.71	73.191	73.601	e77
51X-2, 10-11	post-doc-61	632.11	634.46	2.73	73.222	73.632	
51X-2, 80-81	post-doc-62	632.81	635.16	2.70	73.259	73.669	
51X-3, 10-11	post-doc-63	633.61	635.96	2.80	73.308	73.718	e78
51X-3, 121.5-122.5	post-doc-64	634.73	637.08	2.71	73.396	73.806	e79
51X-4, 11-12	post-doc-65	635.12	637.47	2.64	73.431	73.841	
51X-4, 101-102	post-doc-66	636.02	638.37	2.76	73.505	73.915	e80
51X-5, 9-10	post-doc-67	636.60	638.95	2.77	73.544	73.954	
51X-5, 84-85	post-doc-68	637.35	639.70	2.69	73.594	74.004	e81
51X-6, 35-36	post-doc-69	638.36	640.71	2.66	73.656	74.066	
51X-6, 130-131	post-doc-70	639.31	641.66	2.72	73.713	74.123	e82
52X-1, 10-11	post-doc-71	640.11	642.46	2.68	73.759	74.169	
52X-1, 65-67	post-doc-72	640.67	643.02	2.63	73.791	74.201	e83
52X-2, 4-5	post-doc-73	641.55	643.90	2.62	73.838	74.248	
52X-2, 112-113	post-doc-74	642.63	644.98	2.76	73.896	74.306	e84
52X-3, 10-12	post-doc-75	643.12	645.47	2.66	73.924	74.334	
52X-3, 77-78	post-doc-76	643.78	646.13	2.67	73.970	74.380	
52X-4, 10-11.5	post-doc-77	644.62	646.97	2.67	74.028	74.438	
52X-4, 109-110.5	post-doc-78	645.61	647.96	2.55	74.097	74.507	
52X-5, 10.5-11.5	post-doc-79	646.12	648.47	2.66	74.132	74.542	
52X-5, 98-99	post-doc-80	646.99	649.34	2.58	74.193	74.603	
52X-6, 8-9	post-doc-81	647.59	649.94	2.57	74.235	74.645	
52X-6, 83-85	post-doc-82	648.35	650.70	2.56	74.288	74.698	
52X-7, 11-12	post-doc-83	649.12	651.47	2.56	74.341	74.751	
52X-CC, 5-6	post-doc-84	649.38	651.73	2.58	74.360	74.770	
53X-1, 12-13	post-doc-85	649.63	652.25	2.64	74.396	74.806	
53X-1, 100-102	post-doc-86	650.52	653.14	2.67	74.458	74.868	
53X-2, 1-2	post-doc-87	651.02	653.64	2.57	74.492	74.902	
53X-2, 89-90	post-doc-88	651.90	654.52	2.65	74.554	74.964	
53X-3, 9-10	post-doc-89	652.60	655.22	2.52	74.602	75.012	
53X-3, 101-102	post-doc-90	653.52	656.14	2.54	74.666	75.076	
53X-4, 15-16	post-doc-91	654.16	656.78	2.65	74.711	75.121	
53X-4, 108-109	post-doc-92	655.09	657.71	2.58	74.776	75.186	
53X-5, 40-41	post-doc-93	655.91	658.53	2.51	74.833	75.243	
53X-5, 148-149	post-doc-94	656.99	659.61	2.62	74.908	75.318	
53X-6, 18-19	post-doc-95	657.19	659.81	2.51	74.922	75.332	
53X-6, 101-102	post-doc-96	658.02	660.64	2.66	74.979	75.389	
53X-7, 1-2	post-doc-97	658.52	661.14	2.88	75.014	75.424	
53X-CC, 14-15	post-doc-98	658.75	661.37	2.71	75.030	75.440	
54X-1, 76-77	post-doc-99	659.77	662.39	2.76	75.101	75.511	
54X-1, 138-139	post-doc-100	660.39	663.01	2.74	75.144	75.554	
54X-2, 58-59	post-doc-101	661.09	663.71	2.62	75.193	75.603	
54X-2, 121-122	post-doc-102	661.72	664.34	2.64	75.237	75.647	
54X-3, 15-16	post-doc-103	662.16	664.78	2.66	75.267	75.677	
54X-3, 111-112	post-doc-104	663.12	665.74	2.80	75.334	75.744	
54X-4, 46-47	post-doc-105	663.97	666.59	2.69	75.393	75.803	
54X-4, 120-121	post-doc-106	664.71	667.33	2.71	75.445	75.855	
54X-5, 95-96	post-doc-107	665.96	668.58	2.89	75.532	75.942	
54X-6, 60-62	post-doc-108	667.12	669.74	2.87	75.612	76.022	
54X-6, 128-129	post-doc-109	667.79	670.41	2.80	75.659	76.069	
54X-7, 20-21	post-doc-110	668.21	670.83	2.57	75.688	76.098	
54X-CC, 25-26	post-doc-111	668.50	671.91	2.69	75.763	76.173	
55X-1, 11-12	post-doc-112	668.62	672.03	2.84	75.772	76.182	
55X-1, 66-67	post-doc-113	669.17	672.58	2.84	75.810	76.220	

Based on an average sedimentation of 14.5 m/Ma

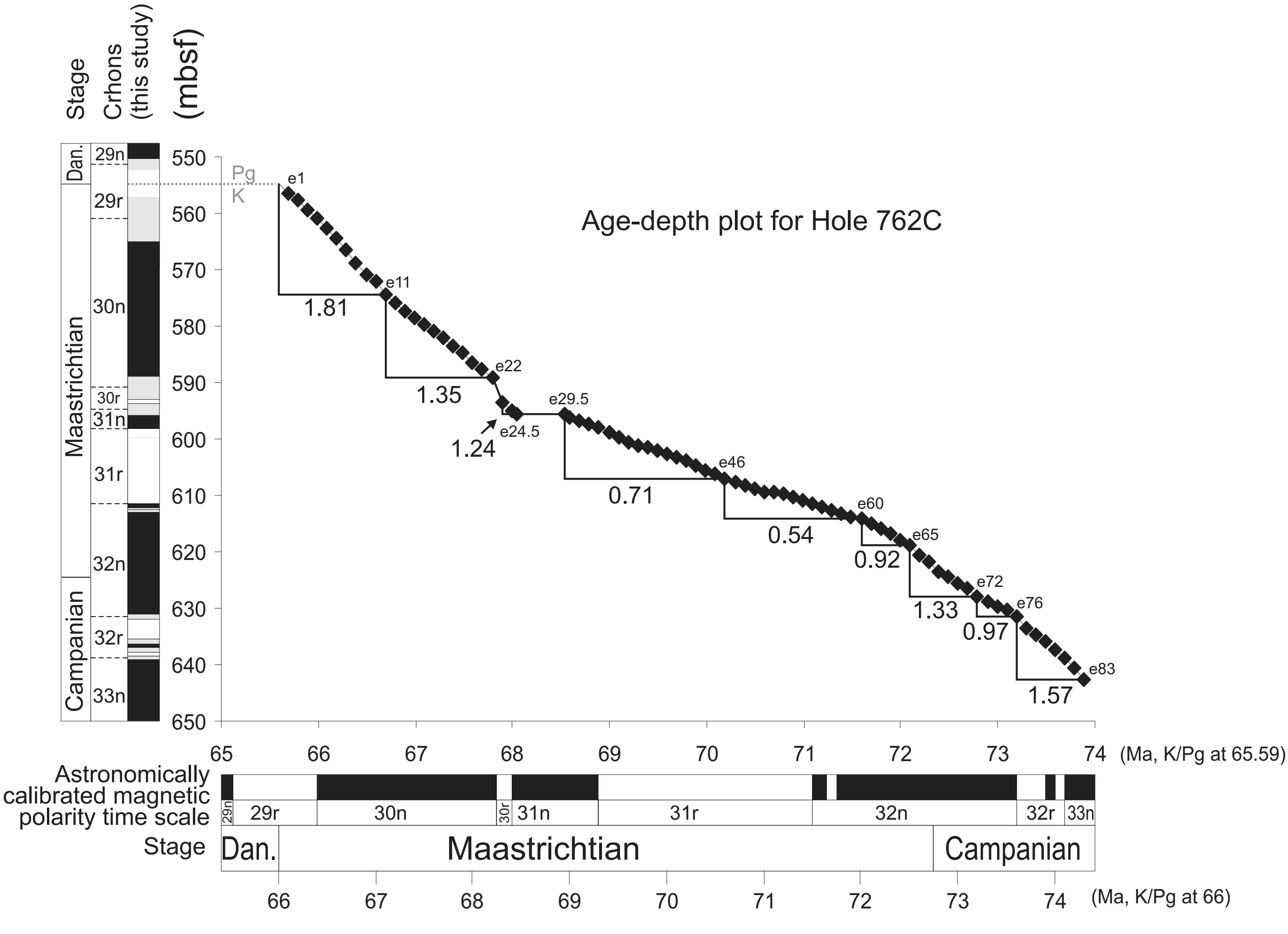

Stage
Crhons (this study)
(mbsf)
Dan.
Maastrichtian
Campanian
29n
29r
30n
30r
31n
31r
32n
32r
33n
550
560
570
580
590
600
610
620
630
640
650
Pg
K
Age-depth plot for Hole 762C
e1
e11
e22
e24.5
e29.5
e46
e60
e65
e72
e76
e83
1.81
1.35
1.24
0.71
0.54
0.92
1.33
0.97
1.57
65
66
67
68
69
70
71
72
73
74
(Ma, K/Pg at 65.59)
Astronomically calibrated magnetic polarity time scale
29n
29r
30n
30r
31n
31r
32n
32r
33n
Stage
Dan.
Maastrichtian
Campanian
66
67
68
69
70
71
72
73
74
(Ma, K/Pg at 66)

Appendix 6

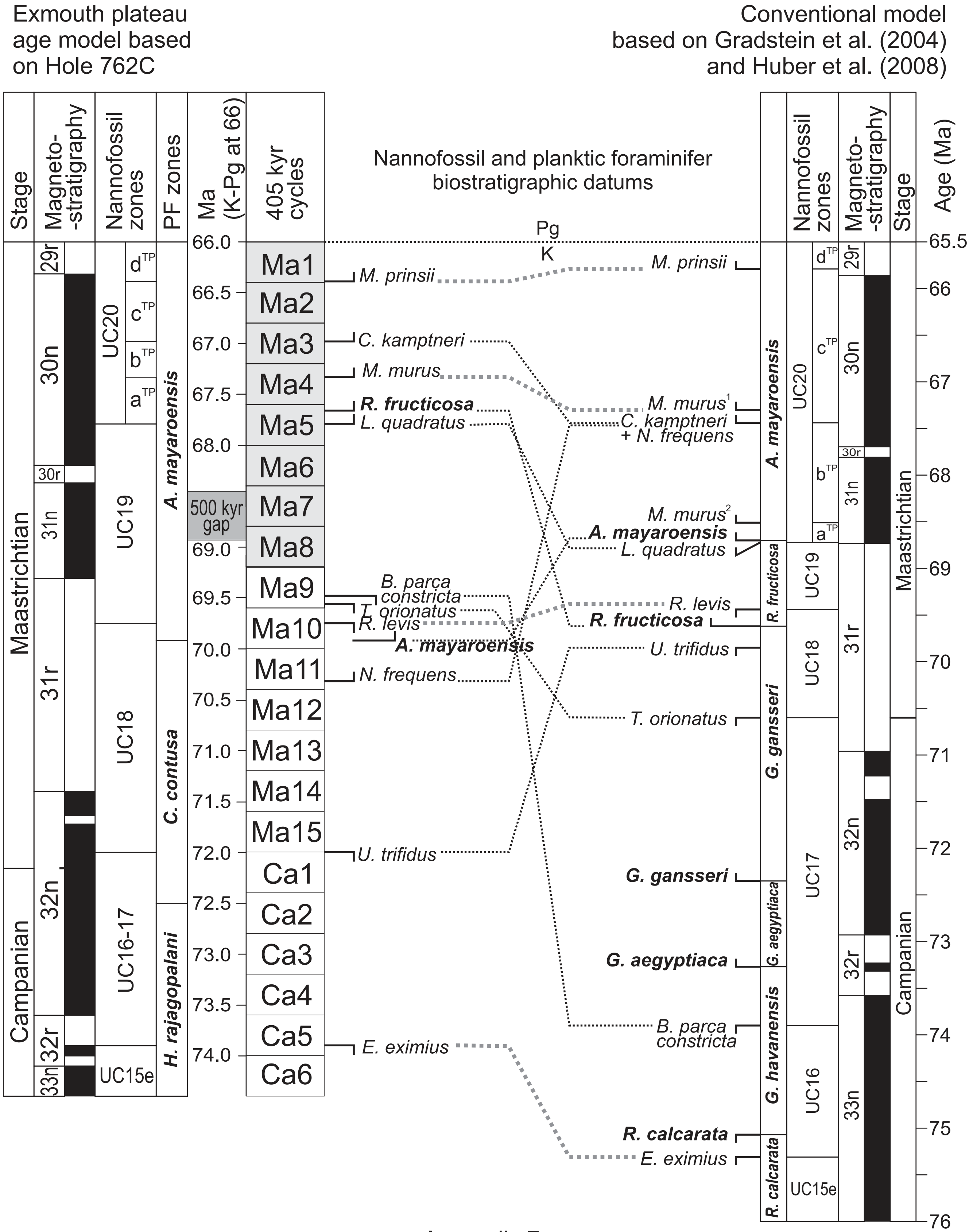

Exmouth plateau age model based on Hole 762C
Conventional model based on Gradstein et al. (2004) and Huber et al. (2008)
Stage
Magneto--stratigraphy
Nannofossil zones
PF zones
Ma (K-Pg at 66)
405 kyr cycles
Nannofossil and planktic foraminifer biostratigraphic datums
Age (Ma)
Pg
K
Maastrichtian
Campanian
A. mayaroensis
C. contusa
H. rajagopalani
UC20
UC19
UC18
UC16-17
UC15e
500 kyr gap
Ma1
Ma2
Ma3
Ma4
Ma5
Ma6
Ma7
Ma8
Ma9
Ma10
Ma11
Ma12
Ma13
Ma14
Ma15
Ca1
Ca2
Ca3
Ca4
Ca5
Ca6
M. prinsii
C. kamptneri
M. murus
R. fructicosa
L. quadratus
B. parca constricta
T. orionatus
R. levis
A. mayaroensis
N. frequens
U. trifidus
E. eximius
C. kamptneri + N. frequens
G. gansseri
G. aegyptiaca
R. calcarata
G. havanensis
UC17
UC16

Appendix 7